Extented Systems in Electrostatic Fields

Dissertation
zur Erlangung des Grades des
Doctors des Naturwissenschaften
der Naturwissenschaftlich-Technischen Fakultät III
Chemie, Pharmazie, Bio- und Werkstoffwissenschaften
der Universität des Saarlandes

von

Jorge Alberto Vargas Tellez

Saarbrücken
Dezember 2013

Tag des Kolloquiums:	20.12.2013
Dekan:	Prof. Dr. Volkhard Helms
Berichterstatter:	Prof. Dr. Michael Springborg Prof. Dr. Gregor Jung
Vorsitz:	Prof. Dr. David Scheschkewitz
Akad. Mitarbeiter:	Dr. Bernd Morgenstern

To my father, who awoke in me the appetite to know more.

Acknowledgements

This work would not have been possible without the support of the Mexican Consejo Nacional de Ciencia y Tecnologia (CONACYT) and the German Deutscher Akademischer Austauschdienst (DAAD) through the fellowship A0972597.

It gives me great pleasure in acknowledging the guidance, help, understanding and sympathy of Professor Michael Springborg. He is a good leader who ecourages, at the same time, the independent work and the collaboration in a pleasant environment. I am also thankful with all the group members, Valeri, Yi, Oha, Violina, Sahar, Nico, Yong, Stefan, Nathalie and Silvia for their support and friendly treatment. I specially appreciate the many fruitful discussions with Mohammad and Max.

I wish to thank my parents for their love and comprehension. I am indebted with them for all I am. They have been there whenever I have needed them and will remain in my heart forever.

Last but not least at all, I owe so much to my beloved wife and children for being the headlight and the motor of my effort. Arely thank you for your patience, your undying support and your unwavering belief that I can achieve it.

Contents

Abstract

The present work deals with the electronic response of one-dimensional extended systems to a spatially uniform electric field. This interaction is introduced via the scalar potential for the finite chain, but for the infinite peridic system, we use the vector potential approach (VPA) [1], specifically, the efficient method presented by Springborg and Kirtman [2, 3]. On this basis, simple models were developed to address two fundamental issues.

We explore whether the calculations for the finite system can be used to determine uniquely the band structure of the periodic system. For this aim, we present and compare three methods to extract the band structure of the finite system. When the field is included they lead to small differences, which can be ascribed to distortions of the spatial extensions of the orbitals generated by the field. We found that, at least with this procedure, it is not possible to determine uniquely the orbital phases, but their main effect is not seen in the band structure but in the calculated polarization, where the boundary condition of the phases can be used to model a quantized charge transfer between the ends of the finite system.

The overestimation of the response properties, found with density-functional methods (DFT), is extensively analyzed in comparison with the results obtained with the Hartree-Fock (HF) formalism. The results of the infinite periodic system are also studied and compared. We observed that the part of the responses attributable to the terminations in the finite system changes into delocalized current contributions in the corresponding infinite periodic system. In all the cases, the DFT method led to a larger electron delocalization along the whole chain increasing the response to the electric field. Finally, it was confirmed that a range-separated functional can improve the DFT results.

Zusammenfassung

Die vorliegende Arbeit beschäftigt sich mit der elektronische Antwort von eindimensionalen ausgedehnten Systemen auf ein räumlich gleichförmiges, elektrisches Feld. Diese Interaktion wird über das skalare Potential für die endliche Kette eingeführt, während für das unendliche periodische System, ein Vektor Potential Ansatz (VPA) [1] verwendet wird. Im Besonderen, benutzen wir die effizienteste Methode, die bei Springborg und Kirtman [2, 3] vorgestellt wurde. Auf dieser Grundlage, wurden einfache Modelle entwickelt, um zwei wesentliche Probleme zu lösen.

Wir untersuchen, ob die Berechnungen für das endliche System helfen können, um die Bandstruktur des unendlichen Systems einzigartig festzustellen. Für dieses Ziel, präsentieren und vergleichen wir drei Methoden um die Bandstruktur des endlichen Systems zu berechnen. In Anwesenheit des Feldes, führen die Methoden zu kleine Unterschiede. Dies kann auf Verzerrungen der räumlichen Ausgedehnung der Orbitale durch das elektrische Feld zurückgeführt werden. Bei diesem Verfahren, war es nicht möglich, die Orbitalphasen eindeutig zu bestimmen. Jedoch, wird der größte Einfluss nicht in der Bandstruktur gesehen, sondern in der berechneten Polarisation, wobei die Randbedingung der Phasen verwendet werden können, um eine quantisierten Ladungsübertragung zwischen den Enden der endlichen System zu modellieren.

Die Überschätzungen der Antworteigenschaften, die sich mit den Dichte-funktionale Methoden (DFT) ergeben, werden im Vergleich mit den erhaltenen Ergebnissen der Hartree-Fock (HF) Formalismus ausführlich analysiert. Die Ergebnisse der unendlichen periodischen Systemen werden ebenfalls untersucht und verglichen. Wir beobachteten, dass der Teil der Eigenshaften der durch den Terminierung im endlichen System entsteht, sich in delokalisierten Strömungsbeiträge in dem entsprechenden unendlichen Periodensystem verwandelt. In allen Fällen führte die DFT-Methode zu einer größeren Elektronendelokalisierung entlang der gesamten Kette, was zu einer Erhöhung der Reaktion auf das elektrische Feld führt. Schließlich konnte es gezeigt werden, dass ein *Bereich-getrenntes* Funktional die DFT Ergebnisse verbessern kann.

Introduction

An adequate description of the response of materials to electromagnetic fields is necessary for interpretative purposes and provides, in addition, a useful tool for identifying materials with optimal properties for applications in a large variety of disciplines. These include spectroscopy, for material characterization; non-linear optics, for manipulating the electromagnetic fields; piezoelectricity, where the coupling between electric and mechanical responses are exploited; the multiferroics, where the coupling between electric and magnetic responses opens up interesting fundamental physical issues as well as applications in spintronics; and conduction, where presently much attention is focused on conduction of chain compounds and single molecules.

In all cases, a proper theoretical treatment that goes beyond that of phenomenological model requires that the quantum-mechanical behavior of the electrons in the presence of the external electromagnetic field is determined. Moreover, when the frequency of the external field is small, also the response of the nuclei / phonons / structure to the field needs to be determined.

For finite systems the theory has been developed and applied for several decades and most fundamental problems have been solved. Although all the systems are finite, when the system is crystalline, it is very helpful for the study of macroscopic materials to assume that the system is infinite and periodic. These cases include polymers, chain compounds, films, surfaces and crystals. When studying the materials properties in the absence of external electromagnetic fields, the use of the periodic boundary conditions has many advantages, but when such fields are included the theory has become surprisingly difficult and complicated. Particularly, for the response to spatially uniform electric field, the scalar interaction potential is proportional to the operator $\vec{r}$ (the electronic position), which is nonperiodic and unbounded.

For an external electrostatic field the carrier of information is, for a finite system, the dipole moment, which for an infinite, periodic system translates into the polarization. For this, first during the 1990s a proper definition was presented [4, 5], the so-called

Modern Theory of Polarization (MTP) based on a discretized Berry phase treatment. It took another decade before methods were presented that, in principle, allows for the direct inclusion of external electrostatic fields in an electronic-structure calculation [6, 7], although these were numerically very demanding.

Instead of dealing with the scalar potential or the Berry phase, Kirtman et al. [1],[8] developed the so-called Vector Potential Approach (VPA). This approach has the virtue that it does not destroy the translational symmetry leaving the concept of band structures meaningful even when the system is in presence of a uniform electrostatic field. It also allows the introduction of frequency-dependent fields and can be applied to materials extended in one, two or three dimensions. But here, we restrict ourselves to the treatment of one-dimensional systems in electrostatic fields. Based on this formalism, Springborg and Kirtman [2, 3] presented a numerically stable and efficient method for calculating electronic and structural responses to electrostatic fields. The present work is mainly based on that approach.

Here, we deal with extended regular systems, meaning that the systems contain a reapeated set of identical units for which the regularity may be violated only at the boundaries of the sample. Ultimately, the goal is to be able to calculate the (electronic and structural) responses of these systems to electrostatic fields using accurate, parameter-free, electronic-structure methods. However, in order to develop, check, and understand the theoretical methodologies outlined above, we have found it extremely useful to apply the approach to simple model systems. By constructing the model carefully it is possible to simulate a realistic electronic-structure calculation and perform many calculations both on large, finite systems and on infinite, periodic systems using the same model. The advantage of studying a model, instead of a real system, is that one can eliminate truncation errors due to summations in real and reciprocal spaces and to basis set expansions. Furthermore, it becomes possible to study large finite systems without prohibitive computational demands. Nevertheless, we emphasize that model calculations can never provide an ultimate test of the theoretical treatment.

This work is organized in the following manner. In the first chapter the basic methods and concepts are briefly explained, starting from the Schrödinder equation and then, the approximations made to solve it within both the Hartree-Fock (HF) and Density Functional Theory (DFT) methodologies. The treatment considering the system infinite and periodic is also presented along with other important concepts as the Bloch functions and the Born von Kármán zone. This theoretical background is mainly based on Springborg's book for electronic-structure calculations [9]. In chapter

2, the dipole moment per unit as a bulk property is introduced as well as the definition of the field-induced responses. Different expresions for polarization are assessed within the framework of the MTP. Then, the self-consistent equations for the inclusion of an external electrostaic field are presented for both finite and periodic systems. In the latter case, the Vector Potential Approach is used including an efficient and numerically stable protocol [3] to solve the resulting single-particle equations. We present our approach and the results in the last two chapters. First, the attempt to extract the information from the calculations for long finite systems to adequately choose the phase factors involved in the calculations for infinite periodic systems in the presence of field using the dipole moment per unit as the relating property. Finally, the DFT overshoot in electronic responses is extensively analyzed with a simple model focussing on the different treatment of the exchange interactions between HF and DFT. The models used in chapters 3 and 4 are very similar but differ in the hopping integrals that define the Hamiltonian.

Chapter 1

Theoretical Background

1.1 The Schrödinger Equation

In quantum mechanics, all the information of a physical system is contained or can be extracted from the wavefunction Ψ, also called state vector. To determine it, in the non-relativistic case, one has to solve the Schrödinger equation,

$$\hat{H}\Psi = i\hbar\frac{\partial}{\partial t}\Psi, \tag{1.1}$$

where $\hat{H}$ is the Hamilton operator or Hamiltonian. This is the most general time-dependent Schrödinger equation. It predicts that the wavefunctions can form standing waves, called stationary states, which are essential for atomic, molecular or crystal systems. These stationary states are describe by the time-independent Schrödinger equation,

$$\hat{H}\Psi = E\Psi, \tag{1.2}$$

obtained through a factorization of the wavefunction into time-dependent and time-independent terms and assuming that the Hamiltonian does not depend explicitly on time. The expression (1.2) is, in fact, an eigenvalue equation, where the wavefunction is the eigenvector and the total energy E is eigenvalue associated to the Hamilton operator.

Within the position-space representation, the non-relativistic Hamiltonian is written as the sum of kinetic and potential energies for the system of interest with the help of position and moment variables. The kinetic energy of a particle of mass m is $\vec{p}^2/2m$, but here the momentum $\vec{p}$ is replaced by the operator $-i\hbar\nabla$. For the total

kinetic-energy operator of a system consisting of M nuclei and N electrons, we just have to add all the individual contributions,

$$\hat{H}_{\mathrm{k,n}} + \hat{H}_{\mathrm{k,e}} = -\sum_{i}^{M} \frac{\hbar^2}{2M_i}\nabla_i^2 - \sum_{j}^{N} \frac{\hbar^2}{2m_e}\nabla_j^2. \tag{1.3}$$

where we are distinguishing between the nuclei and the electron terms. The potential energy is calculated in the same manner as the classical electrostatic energy due to the Coulomb interactions,

$$\begin{aligned}\hat{H}_{\mathrm{p,n-n}} + \hat{H}_{\mathrm{p,n-e}} + \hat{H}_{\mathrm{p,e-e}} = &\frac{1}{2}\sum_{i_1\neq i_2=1}^{M} \frac{1}{4\pi\epsilon_0}\frac{e^2 Z_{i_1} Z_{i_2}}{|\vec{R}_{i_1} - \vec{R}_{i_2}|} - \sum_{i=1}^{M}\sum_{j=1}^{N} \frac{1}{4\pi\epsilon_0}\frac{e^2 Z_i}{|\vec{R}_i - \vec{r}_j|} \\ &+ \frac{1}{2}\sum_{j_1\neq j_2=1}^{N} \frac{1}{4\pi\epsilon_0}\frac{e^2}{|\vec{r}_{j_1} - \vec{r}_{j_2}|},\end{aligned} \tag{1.4}$$

with eZ_i and $\vec{R}_i$ being the charge and position of the i'th nucleus, whereas e and $\vec{r}_j$ are the charge and position of the j'th electron. ϵ_0 is the vacuum permitivity and the $1/2$ factor is included because in the summations all the pairs are counted twice in the first and third terms. Accordingly, we have now three terms describing each one of the nucleus-nucleus, the nucleus-electron and the electron-electron interactions. The total Hamiltonian is then,

$$\hat{H} = \hat{H}_{\mathrm{k,n}} + \hat{H}_{\mathrm{k,e}} + \hat{H}_{\mathrm{p,n-n}} + \hat{H}_{\mathrm{p,n-e}} + \hat{H}_{\mathrm{p,e-e}}, \tag{1.5}$$

where the first and third terms depend only on the nuclei positions $\vec{R}_i$. Hereafter we adopt the atomic units defined by setting the fundamental constants e, m_e, $\hbar$ and $4\pi\epsilon_0$ equal to 1. In this way, the energies are meassured in hartrees (1 hartree = 27.21 eV) and lengths in bohrs (1 bohr = 0.5295 Å).

Because of the sizeable difference in their masses, the nuclei move much more slowly than the electrons and are much more localized in space. We can think that for a given position of the nuclei, the electrons adjust their positions 'immediatly' to these before the nuclei move. This is the idea behind the *Born-Oppenheimer approximation*, in which the kinetic energy of the nuclei is neglected. In basic terms, within this approximation the wavefuntion is factorized into its electronic and nuclear components

leading to the Schrödinger equation for the electrons,

$$\hat{H}_e \Psi_e = E_e \Psi_e, \tag{1.6}$$

where the Hamilton operator $\hat{H}_e$ is composed by the second, forth and fifth terms of equation (1.5), so the dependence of Ψ_e on the nuclear coordinates is only through the electrostatic interactions between the electrons and the nuclei. This means that the nuclei generate an 'external' potential, in which the electrons move. For later purposes this potential is referred as

$$V_{\mathrm{n}}(\vec{r}) = -\sum_{i=1}^{M} \frac{Z_i}{|\vec{R}_i - \vec{r}|}. \tag{1.7}$$

In this manner, the electronic Hamiltonian can be written as

$$\hat{H}_e = -\sum_{j=1}^{N} \frac{1}{2}\nabla_j^2 + \sum_{j=1}^{N} V_{\mathrm{n}}(\vec{r}_j) + \frac{1}{2} \sum_{j_1 \neq j_2 = 1}^{N} \frac{1}{|\vec{r}_{j_1} - \vec{r}_{j_2}|}. \tag{1.8}$$

We observe that the first two terms are the sum of identical single-particle operators acting on different electrons, while the last one is a sum of double-particle operators.

Finally, once the Schrödinger equation for the electrons (1.6) is solved, the total energy is calculated adding the nucleus-nucleus potential to the electronic energy,

$$E = E_e + \frac{1}{2} \sum_{i_1 \neq i_2 = 1}^{M} \frac{Z_{i_1} Z_{i_2}}{|\vec{R}_{i_1} - \vec{R}_{i_2}|}. \tag{1.9}$$

If one is interested in a relaxed structure, the total energy has to be minimized varying the nuclear coordinates.

1.2 The Hartree-Fock Method

Since the beginning of the quantum theory there have been attempts to solve the electronic Schrödinger equation (1.6) for molecular systems, but it can not be exactly solved whenever more than 2 particles are involved. For that reason one has to do approximations. We may apply the variational principle to find an approximate solution $\Psi' \approx \Psi_e$, which minimizes the expectation value of the Hamilton operator $\hat{H}_e$, i.e., find the gound state of the electronic energy. One of the first proposals was to construct the

many-body wavefunction Ψ' as a multiplication of single-particle functions ψ_i called orbitals. In this way, we imagine the system of N electrons as particles occupying N different orbitals that can each accomodate one electron. In order to be consistent with the Pauli's exclusion principle, it was proposed not to use a simple multiplication but rather the so-called *Slater determinant*,

$$\Psi'(\vec{x}_1, \vec{x}_2, \ldots, \vec{x}_N) = \frac{1}{\sqrt{N!}} \begin{vmatrix} \psi_1(\vec{x}_1) & \psi_2(\vec{x}_1) & \ldots & \psi_N(\vec{x}_1) \\ \psi_1(\vec{x}_2) & \psi_2(\vec{x}_2) & \ldots & \psi_N(\vec{x}_2) \\ \vdots & \vdots & \ddots & \vdots \\ \psi_1(\vec{x}_N) & \psi_2(\vec{x}_N) & \ldots & \psi_N(\vec{x}_N) \end{vmatrix} \tag{1.10}$$

where the components of $\vec{x}_i$ are the generalized coordinates (position and spin) of the ith electron and the $1/\sqrt{N!}$ factor is introduced to normalize the wavefuntion. In this sense, the Slater determinant is antisymmetric with respect to the exchange of two electrons.

With the help of the Lagrange multipliers, one can seek to minimize $\langle\Psi'|\hat{H}_e|\Psi'\rangle$ under the constraints that all the individual orbitals are orthonormal by considering the quantity

$$F = \langle\Psi'|\hat{H}_e|\Psi'\rangle - \sum_{i,j} \lambda_{ij}[\langle\psi_i|\psi_j\rangle - \delta_{ij}], \tag{1.11}$$

and imposing the condition $\delta F = 0$, where δF is the change in F upon changing any of the orbitals $\psi_i \to \psi_i + \delta\psi_i$.

Developing these ideas one ends up to the *Hartree-Fock equations*,

$$\hat{F}\psi_j = \varepsilon_j\psi_j. \tag{1.12}$$

The Fock operator $\hat{F}$ is defined as

$$\hat{F} = -\sum_{i=1}^{N} \frac{1}{2}\nabla_i^2 + \sum_{i=1}^{N} V_{\mathrm{n}}(\vec{r}_i) + \sum_{i=1}^{N} (\hat{J}_i - \hat{K}_i) \tag{1.13}$$

where the operators $\hat{J}_i$ and $\hat{K}_i$ arise from the electron-electron interactions,

$$\begin{aligned} \hat{J}_i|\psi_j(\vec{x}_1)\rangle &= \int \frac{|\psi_i(\vec{x}_2)|^2\psi_j(\vec{x}_1)}{|\vec{r}_2 - \vec{r}_1|}\mathrm{d}\vec{x}_2 \\ \hat{K}_i|\psi_j(\vec{x}_1)\rangle &= \int \frac{\psi_i^*(\vec{x}_2)\psi_j(\vec{x}_2)\psi_i(\vec{x}_1)}{|\vec{r}_2 - \vec{r}_1|}\mathrm{d}\vec{x}_2, \end{aligned} \tag{1.14}$$

and are known as the Coulomb and exchange operators respectively. The Coulomb operator describes the classical electrostatic interactions between two charge distributions, whereas the exchange operators have no classical analogue and their existence is a direct consequence of the quantum-mechanical requirement of the wavefunction antisymmetry.

The Hartree-Fock equations (1.12) seems very similar to the Schrödinger equation, but unlike the Hamilton operator, the Fock operator is for single electrons and not for all the N particles. The effects of all the other electrons are included in $\hat{F}$ which, accordingly, depends on the solutions themselves through the $\hat{J}_i$ and $\hat{K}_i$ operators. For this reason, the equations can only be solved using a self-consistent procedure and the Hartree-Fock method is also known as a *self-consistence field* (SCF) method.

The total electronic energy $E_{\mathrm{HF}} \equiv \langle \Psi' | \hat{H}_e | \Psi' \rangle$ can be calculated from the solutions and eigenvalues of the Hartree-Fock equations,

$$E_{\mathrm{HF}} = \sum_{j=1}^{N} \varepsilon_j - \frac{1}{2} \sum_{j,k=1}^{N} \left[\langle \psi_j \psi_k | \hat{h}_2 | \psi_j \psi_k \rangle - \langle \psi_j \psi_k | \hat{h}_2 | \psi_k \psi_j \rangle \right], \tag{1.15}$$

where $\hat{h}_2$ is the two-electron operator,

$$\hat{h}_2 | \psi_j \psi_k \rangle = \frac{\psi_j(\vec{x}_2)\psi_k(\vec{x}_1)}{|\vec{r}_j - \vec{r}_k|}. \tag{1.16}$$

Thanks to the *Koopmans' theorem*, the eigenvalues ε_j can be interpreted as orbital energies that are related to the electronic transition energies.

Solving the Hartree-Fock equations would result in calculating the value of every single orbital in every single point in the space. It is computationally not possible to determine so much information. Instead, a finite variation is carried out by expanding the orbitals in a set of fixed basis functions,

$$\psi_j(\vec{x}) = \sum_{p=1}^{N_b} c_{pj} \chi_p(\vec{x}), \tag{1.17}$$

where the basis functions χ_p as well as their number N_b have been chosen in advance and only the expansion coefficients c_{pj} are varied. Inserting this expansion in the Hartree-Fock equations (1.12) leads to a generalized matrix eigenvalue equation, which can be written as

$$\underline{\underline{F}} \cdot \underline{c}_j = \varepsilon_j \, \underline{\underline{O}} \cdot \underline{c}_j, \tag{1.18}$$

where $\underline{\underline{F}}$ contains the Fock matrix elements,

$$F_{pq} = \left\langle \chi_p \left| -\tfrac{1}{2}\nabla^2 + V_{\mathrm{n}}(\vec{r}) \right| \chi_q \right\rangle + \sum_{j=1}^{N} \sum_{p',q'=1}^{N_b} c^*_{p'j} c_{q'j} \left[\langle \chi_p \chi_{p'} | \hat{h}_2 | \chi_q \chi_{q'} \rangle - \langle \chi_p \chi_{p'} | \hat{h}_2 | \chi_{q'} \chi_q \rangle \right], \tag{1.19}$$

$\underline{\underline{O}}$ is the overlap matrix,

$$O_{pq} = \langle \chi_p | \chi_q \rangle. \tag{1.20}$$

and the sought coefficients are arranged in column vectors,

$$\underline{c}_j = \begin{pmatrix} c_{1j} \\ c_{2j} \\ \vdots \\ c_{N_b j} \end{pmatrix}. \tag{1.21}$$

The equation (1.18) is just the matrix form of the *Hartree-Fock-Roothaan equations* that have made the Hartree-Fock method so widely used. However, the quality of a given calculation depends heavily on the quality of the basis functions and, therefore, it is important to use basis sets that are adequate for the problem at hand.

In the *restricted Hartree-Fock* (RHF) approximation no spin polarizations is considered and, accordingly, it is assumed that every pair of orbitals differing only in the spin have equivalent position dependence. In this manner the Hartree-Fock-Roothaan equations can be simplified by performing all spin integrations halving the number of terms in the double-particle summation, so that the Fock matrix elements become,

$$F_{pq} = \left\langle \chi_p \left| -\tfrac{1}{2}\nabla^2 + V_{\mathrm{n}}(\vec{r}) \right| \chi_q \right\rangle + \sum_{j=1}^{N/2} \sum_{p',q'=1}^{N_b} c^*_{p'j} c_{q'j} \left[2\langle \chi_p \chi_{p'} | \hat{h}_2 | \chi_q \chi_{q'} \rangle - \langle \chi_p \chi_{p'} | \hat{h}_2 | \chi_{q'} \chi_q \rangle \right], \tag{1.22}$$

where the basis functions $\chi(\vec{r})$ are now assumed to depend only on position coordinates. In other words, there are only $N/2$ different orbitals $\psi_j(\vec{r})$ each one for two electrons.

Summarizing, in addition to the Born-Oppenheimer approximation and a non-relativistic treatment, the Hartree-Fock method is based on the assumption that the electronic wavefunction can be approximated by a single Slater determinant containing single-electron orbitals, which are optimized, using the variational principle, by linear

combinations of certain set of basis functions. The electron exchange interaction is fully accounted for and the equations have to be solve self-consistently.

1.3 Density Funtional Theory

Once the Schrödinger equation is (approximately) solved and the wavefunction Ψ_e found, in principle, it is possible to calculate any physical observable, but the wavefunction is much more complicated than needed when calculating experimental observables and the practical limitations and approximations hinder the accuracy. Instead, one alternative is to solve another equation that determines directly the electron density $\rho(\vec{r})$. Although this proposal has its roots in the *Thomas-Fermi model*, the firm theoretical background was given by the two *Hohenberg-Kohn theorems*. The first demonstrates that the ground-state properties of a many-electron system are uniquely determined by the electron density in position space $\rho(\vec{r})$. In other words, any ground-state property is a functional of the electron density, $F[\rho(\vec{r})]$, however, the explicit functional is in most cases unknown. The second theorem states that the correct electron density minimizes the total electron energy, thus if the functional that relates them is known, one can use the variational principle to approach the total energy by varying an approximete electron density.

The *Kohn-Sham approach* provides a practical scheme to take advantage of the Hohenberg-Kohn theorems. Although the complete electonic-energy functional $F[\rho]$ is unknown, there are some terms that should be present like kinetic energy $T[\rho]$, the contribution due to the potential generated by the nuclei $V_{\mathrm{n}}(\vec{r})$ and that due to the classical Coulomb interaction between electrons $V_{\mathrm{C}}(\vec{r})$. All further terms are included via the *exchange-correlation* (xc) energy E'_{xc}. Therefore, in total we have

$$E_e = T[\rho(\vec{r})] + \int V_{\mathrm{n}}(\vec{r})\rho(\vec{r})\mathrm{d}\vec{r} + \frac{1}{2}\int V_{\mathrm{C}}(\vec{r})\rho(\vec{r})\mathrm{d}\vec{r} + E'_{\mathrm{xc}}[\rho(\vec{r})], \tag{1.23}$$

where the second and third terms are

$$\int V_{\mathrm{n}}(\vec{r})\rho(\vec{r})\mathrm{d}\vec{r} = -\int \sum_{j=1}^{M} \frac{Z_j\rho(\vec{r})}{|\vec{R}_j - \vec{r}\,|}\mathrm{d}\vec{r}, \tag{1.24}$$

$$\frac{1}{2}\int V_{\mathrm{C}}(\vec{r})\rho(\vec{r})\mathrm{d}\vec{r} = \frac{1}{2}\iint \frac{\rho(\vec{r}_1)\rho(\vec{r}_2)}{|\vec{r}_1 - \vec{r}_2|}\mathrm{d}\vec{r}_1\mathrm{d}\vec{r}_2. \tag{1.25}$$

The variational principle is applied over the electron energy E_e with help of a Lagrange

multiplier λ, varying the electron density under the constraint that the total number of electrons remains equal to N,

$$\delta\left\{E_e[\rho(\vec{r})] - \lambda\left[\int \rho(\vec{r})\mathrm{d}\vec{r} - N\right]\right\} = 0. \tag{1.26}$$

Thus, using the functional derivatives with respect to $\rho(\vec{r})$ and substituting E_e from equation (1.23), the requirement $\frac{\delta E_e}{\delta\rho} = 0$ leads to

$$\frac{\delta T}{\delta\rho} + V_{\mathrm{n}}(\vec{r}) + V_{\mathrm{C}}(\vec{r}) + \frac{\delta E'_{\mathrm{xc}}}{\delta\rho} = \lambda. \tag{1.27}$$

Now, the crucial assumption is that it is possible to construct a fictitious system of *non-interacting* particles, which has the same electron density and energy as the real system. To ensure that, these particles are assumed moving in some external potential V_{eff}. In this case the total-energy expression is considerably simpler,

$$E_e = T_0[\rho(\vec{r})] + \int V_{\mathrm{eff}}(\vec{r})\rho(\vec{r})\mathrm{d}\vec{r}. \tag{1.28}$$

Since these particles are different, their kinetic energy is not identical to that of equation (1.23). Thus, similarly as above,

$$\frac{\delta T_0}{\delta\rho} + V_{\mathrm{eff}}(\vec{r}) = \lambda. \tag{1.29}$$

The effective potential $V_{\mathrm{eff}}(\vec{r})$ can be written in the expressed terms by comparing equations (1.27) and (1.29), but by grouping all the unknown terms in a single one,

$$\frac{\delta T}{\delta\rho} - \frac{\delta T_0}{\delta\rho} + \frac{\delta E'_{\mathrm{xc}}}{\delta\rho} \equiv \frac{\delta E_{\mathrm{xc}}}{\delta\rho} \equiv V_{\mathrm{xc}}(\vec{r}), \tag{1.30}$$

the so-called exchange-correlation energy and potential are thereby defined and

$$V_{\mathrm{eff}}(\vec{r}) = V_{\mathrm{n}}(\vec{r}) + V_{\mathrm{C}}(\vec{r}) + V_{\mathrm{xc}}(\vec{r}). \tag{1.31}$$

In this manner, the Hamilton operator for the model system is particularly simple,

$$\hat{H} = \sum_{i=1}^{N}\left[-\frac{1}{2}\nabla^2 + V_{\mathrm{eff}}(\vec{r}_i)\right] \equiv \sum_{i=1}^{N}\hat{h}_{\mathrm{KS}}(i). \tag{1.32}$$

Accordingly, there are only single-particle operators. The solution to the Schrödinger equation for this system can, therefore, be written exactly as a single Slater determinant composed by single-particle orbitals ψ_i determined by the *Kohn-Sham equations*,

$$\hat{h}_{\mathrm{KS}}\psi_i = \varepsilon_i\psi_i, \tag{1.33}$$

which are very similar to the Hartree-Fock equations (1.15), but with the important simplification that there are not two-particle operators.

Moreover, the electron density is

$$\rho(\vec{r}) = \sum_{i=1}^{N} |\psi_i(\vec{r})|^2, \tag{1.34}$$

where the summations runs over the N orbitals with the lowest eigenvalues ε_i, i.e., those which are occupied.

The Kohn-Sham equations (1.33) are also solved by expanding the solutions ψ_i in a set of fixed basis functions as in equation (1.17). In that case, the Kohn-Sham equations can be expressed in a matricial form

$$\underline{\underline{h}}^{\mathrm{KS}} \cdot \underline{c}_j = \varepsilon_j \, \underline{\underline{O}} \cdot \underline{c}_j, \tag{1.35}$$

analogously to equation (1.18), but here the $\underline{\underline{h}}^{\mathrm{KS}}$ contains the Kohn-Sham matrix elements,

$$h_{qp}^{\mathrm{KS}} = \langle\chi_q| -\tfrac{1}{2}\nabla^2 + V_{\mathrm{n}} + V_{\mathrm{C}} + V_{\mathrm{xc}}|\chi_p\rangle \tag{1.36}$$

The main problem of this methodology is that we do not know the exchange-correlation energy and potential. One of the first was suggested by Slater [10], even before the Hohenberg-Kohn theorems, which corresponds to neglecting the correlation effects and only including those of the exchange. He arrived to an expression propotional to $-\rho^{1/3}$, which was shortly later corrected as

$$V_{\mathrm{x}}(\vec{r}) = -\left[\frac{3}{\pi}\rho(\vec{r})\right]^{1/3}. \tag{1.37}$$

Of course, there has been proposed many other good approaches for many cases, with the *local-* or *non-local-density* aproximations, but we will not discuss them here. The Kohn-Sham operator $\hat{h}_{\mathrm{KS}}$ (as the Fock operator $\hat{F}$) depends on the solutions and, therefore, has to be solved with a self-consistent procedure too. The general advantages

of the density functional theory (DFT) is that the correlation effects can be included and that, particularly for larger systems, the calculations do not become prohibitively involved to apply.

When comparing the results obtained within Hartree-Fock or Kohn-Sham methods, one often finds that the energy gap separating occupied and unoccupied orbitals in Hartree-Fock calculations is significantly overestimated and in density-functional calculations significantly underestimated. Similarly, Hartree-Fock calculations have the tendency to underestimate the binding energies, while the opposite trend is found in the local-density calculations.

1.4 Periodicity and Band Structures

The symmetry of a system can be used to reduce or simplify the eigenvalue problem posed by the Hartree-Fock or Kohn-Sham equations, here generically referred as single-particle equations,

$$\hat{h}\psi_j = \varepsilon_j \psi_j. \tag{1.38}$$

In both cases the Hamilton-like single-particle operators possess the full symmetry of the system. When the system is considered to be a perfect crystal, i.e., an infinite and periodic array of atoms, the translational symmetry is fundamental for this simplification. First of all, the potential generated by the ions is periodic and it is possible to write the orbitals in terms of symmetry-addapted basis functions. To explain the basics of these ideas and concepts we will consider here only the one-dimensional case, which in turn, is the case of study throughout the present work.

Let us consider a ring molecule of K identical atoms like that of the figure 1.1. We assumed, accordingly, that the solutions of equation (1.38) can be written as a sum of functions centered on the different atoms. We will also assume that we have only one function per atom. Thus, we have

$$\psi_j(\vec{r}) = \sum_{n=1}^{K} c_{nj}\chi_n(\vec{r}), \tag{1.39}$$

where χ_n is the basis function of the nth atom. One of the symmetry elements in the ring molucule is the C_K axis passing through the center of the ring perpendicularly to the plane of the molecule, which describes the fact that rotating the molecule any angle defined by $m(2\pi/K)$ (being m an integer) maps the molecule onto itself. Therefore,

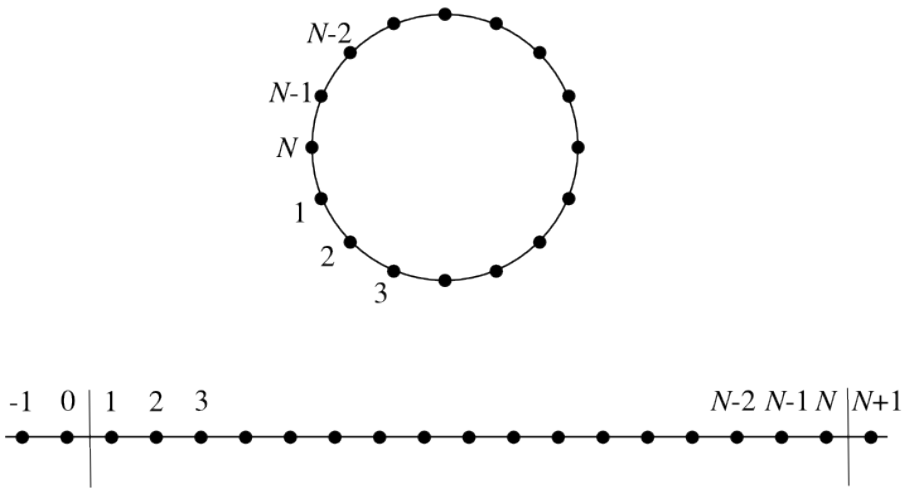

Figure 1.1: A ring molecule consisting of K identical atoms and the BvK zone defined for an infinite linear chain.

the single-electron Hamiltonian does not change under this symmetry operator and the solutions ψ_i can be classified according to the irreductible representations of the symmetry-group operations. In this manner, we may construct the symmetry-addapted basis functions as a linear combination of atomic orbitals (LCAO),

$$\chi_{\tilde{k}}(\vec{r}) = \frac{1}{\sqrt{K}} \sum_{n=1}^{K} e^{i\tilde{k}n} \chi_n(\vec{r}). \tag{1.40}$$

Here, $\tilde{k}$ is the label of the irreductible representation, but its values are determined by the fact that rotating the molecule K times any allowed angle $m(2\pi/K)$ the system is mapped identically onto itself. This leads to the condition $e^{i\tilde{k}K} = 1$, which is satisfied with

$$\tilde{k} = 0, \pm\frac{2\pi}{K}, \ldots, \begin{cases} \pm\frac{(K-3)\pi}{K}, \pm\frac{(K-1)\pi}{K} & \text{for } K \text{ odd} \\ \pm\frac{(K-2)\pi}{K}, \pi & \text{for } K \text{ even} \end{cases} \tag{1.41}$$

Then, from group theory it is known that functions belonging to different representations do not mix. In our case, it means that the overlap and Hamilton matrix elements between them vanish,

$$\begin{aligned} \langle \chi_{\tilde{k}_1} | \chi_{\tilde{k}_2} \rangle &= 0 \quad \text{for} \quad \tilde{k}_1 \neq \tilde{k}_2 \\ \langle \chi_{\tilde{k}_1} | \hat{h} | \chi_{\tilde{k}_2} \rangle &= 0 \quad \text{for} \quad \tilde{k}_1 \neq \tilde{k}_2. \end{aligned} \tag{1.42}$$

Considering the definition of equation (1.40), for functions of the same representation we have,

$$\begin{aligned}\langle\chi_{\tilde{k}}|\chi_{\tilde{k}}\rangle &= \frac{1}{K}\sum_{n,m=1}^{K} e^{i\tilde{k}(n-m)}\langle\chi_m|\chi_n\rangle \\ &= \frac{1}{K}\sum_{n,m=1}^{K} e^{i\tilde{k}(n-m)}\langle\chi_1|\chi_{n-m+1}\rangle \\ &= \sum_{n=1}^{K} e^{i\tilde{k}(n-1)}\langle\chi_1|\chi_n\rangle, \end{aligned} \tag{1.43}$$

where we have used that $\langle\chi_m|\chi_n\rangle = \langle\chi_{m+1}|\chi_{n+1}\rangle = \ldots$ Thus, considering the site $n-m+1$ equivalent to $K+n-m+1$, the overlap depends only on the number of units (including the sign) separating the two functions. The same is valid for the exponential, since $e^{i\tilde{k}(n-m)} = e^{i\tilde{k}(K+n-m)}$. As a consecuence, we can replace the double summation over n and m by a single summation over n holding $m = 1$ fixed and multiply by K, thereby, the factor $1/\sqrt{K}$ introduced in the expression (1.40) is justified. The Hamilton matrix elements can be calculated similarly,

$$\langle\chi_{\tilde{k}}|\hat{h}|\chi_{\tilde{k}}\rangle = \sum_{n=1}^{K} e^{i\tilde{k}(n-1)}\langle\chi_1|\hat{h}|\chi_n\rangle \tag{1.44}$$

These formulae (1.42-1.44) are independent of the type of approach. These equations are the same if, instead of a ring molecule, we have an infinite chain and we require that the symmetry-addapted orbitals map onto themselves when the system is translated K units. Thereby, for all practical effects, the site $K+1$ is identical to the site 1 as in the ring. These are the so-called periodic boundary conditions (PBC). Formally,

$$\psi_j(\vec{r}+\vec{T}) = \psi_j(\vec{r}), \tag{1.45}$$

with $\vec{T}$ being a defined lattice translation vector. In one dimension, the system consists of an infinite succession of identical units in one direction, e.g. $\hat{z}$. Thus, if the length of each unit is a, the lattice translation can be expressed as $\vec{T} = Ka\hat{z}$. In this sense, the size of the ring molecule defines a fragment of the infinite linear chain. This fragment is known as the *Born-von Kármán* (BvK) zone.

Instead of using the dimensionless $\tilde{k}$, it is custom to define $k = \tilde{k}/a$, which can

be seen as the one-dimensional analogue of the *reciprocal lattice* vectors defined for three-dimensional systems. k is known as the wavenumber and has the dimension of lenght^{-1}. The condition that the translation $\vec{T}$ maps the system onto itself leads to the condition $e^{ikaK} = 1$. Therefore, replacing $k \to k + 2\pi/a$ generates no changes and we can choose to restrict k to

$$-\frac{\pi}{a} < k \leq \frac{\pi}{a}, \tag{1.46}$$

by taking any value out of the set of K values written in the expression (1.41). The interval (1.46) defines the *first Brillouin zone* (BZ), where all the information of the system is contained. Additionally, if $\psi_j(k, \vec{r})$ is an eigenfunction of $\hat{h}$ with the eigenvalue $\varepsilon_j(k)$, then $\psi_j^*(k, \vec{r}) = \psi_j(-k, \vec{r})$ is also an eigenfunction for $\hat{h}$ with the same eigenvalue,

$$\varepsilon_j(-k) = \varepsilon_j(k). \tag{1.47}$$

This means that for the band structures we do not need $\varepsilon_j(k)$ in the full interval $[-\pi/a, \pi/a]$ but only in $[0, \pi/a]$.

In the case of real one-dimensional systems the number of basis functions per repeated unit may be large, but we can still construct symmetry-addapted linear combinations from the equivalent atom-centered ones of different units. They are called *Bloch functions* or *Bloch waves* and can be written in a similar way as in expression (1.40),

$$\chi_p(k, \vec{r}) = \frac{1}{\sqrt{K}} \sum_{n=1}^{K} e^{ikan} \chi_{pn}(\vec{r}), \tag{1.48}$$

where $p = 1, 2, \ldots, N_b$ denotes the different basis function per unit (possibly centered on different atoms) and n is the unit index. In this manner, omitting the $\vec{r}$ dependence, the generalization of equations (1.42-1.44) would be

$$\begin{aligned} \langle \chi_p(k) | \hat{h} | \chi_q(k') \rangle &= \delta_{kk'} \frac{1}{K} \sum_{m,n=1}^{K} e^{ika(n-m)} \langle \chi_{pm} | \hat{h} | \chi_{qn} \rangle \\ &= \delta_{kk'} \sum_{n=0}^{K-1} e^{ikan} \langle \chi_{p0} | \hat{h} | \chi_{qn} \rangle, \end{aligned} \tag{1.49}$$

using that $\chi_{p0} \equiv \chi_{pK}$. In the same manner the origin of the BvK zone can be set at $n = 0$. This result is valid for any single-particle operator including the identity or even the Fock or the Kohn-Sham operators.

The single-particle wavefunctions written in terms of Bloch waves become k-depen-

dent,

$$\psi_j(k) = \sum_{p=1}^{N_b} C_{pj}(k)\chi_p(k), \tag{1.50}$$

which inserted in equation (1.38) lead to the also k-dependent secular equation,

$$\underline{\underline{h}}(k) \cdot \underline{C}_j(k) = \varepsilon_j(k)\, \underline{\underline{O}}(k) \cdot \underline{C}_j(k), \tag{1.51}$$

similar to equations (1.18) and (1.35). Here, the Hamilton $\underline{\underline{h}}(k)$ and overlap $\underline{\underline{O}}(k)$ matrices have the size $N_b \times N_b$ and we make use of equations (1.49) to define them,

$$\begin{aligned} O_{pq}(k) &= \sum_n e^{ikan} \langle \chi_{p0} | \chi_{qn} \rangle \\ h_{pq}(k) &= \sum_n e^{ikan} \langle \chi_{p0} | \hat{h} | \chi_{qn} \rangle. \end{aligned} \tag{1.52}$$

In this way we have reduced the problem of solving the single $(KN_b \times KN_b)$ eigenvalue problem for real expansion coefficients of equation (1.18) to solve K eigenvalue equations of size $(N_b \times N_b)$ for complex expansion coefficients. This reduction may have an overwhelming effect on the required computational time.

Moreover, the eigenvalues $\varepsilon_j(k)$ define in total N_b bands. For each band we have K (the size of the BvK zone) orbitals meaning that, if we do not consider spin polarization, each band can accommodate two electrons per unit. The set of N_b bands arisen from plotting ε_j against k form the so-called *band structure*. In the ground state, the lowest-energy orbitals are filled with the available electrons. The *Fermi energy* is the midpoint between the energies of the so called highest occupied molecular orbital (HOMO) and the lowest unoccupied molecular orbital (LUMO). In the semiconductors and insulators there is an energy range, which is not crossed by any of the bands, between the HOMO and LUMO leaving only completly filled and completly empty bands. This range of forbidden energy is called the *band gap* and, in that case, the Fermi energy lies in the middle of the gap.

Chapter 2

Including an External Electric Field

2.1 The Dipole Moment

The response of any system to electric fields can be described through the *dipole moment*, which determines linear and non-linear optical properties, as well as piezoelectricity, pyroelectricity, etc. Let us discuss some of its fundamental properties.

The dipole moment of a finite molecule with M nuclei and an electron density $\rho(\vec{r})$ is given through

$$\vec{\mu} = \sum_{i=1}^{M} Z_i \vec{R}_i - \int \vec{r}\rho(\vec{r})\mathrm{d}\vec{r} = \vec{\mu}_\mathrm{n} + \vec{\mu}_e, \tag{2.1}$$

where, Z_i and $\vec{R}_i$ are the charge and position of the ith nucleus, respectively. Thereby, the nuclear and the electronic contributions are defined too.

If the total system is neutral,

$$\sum_{i=1}^{M} Z_i - \int \rho(\vec{r})\mathrm{d}\vec{r} = 0, \tag{2.2}$$

the dipole moment is independent of the choice of the origin of the coordinate system, because by shifting it,

$$\vec{R}_i \longrightarrow \vec{R}_i + \vec{X}$$
$$\vec{r} \longrightarrow \vec{r} + \vec{X},$$

the 'new' dipole moment would be

$$\begin{aligned}\vec{\mu}\,' &= \sum_{i=1}^{M} Z_i(\vec{R}_i + \vec{X}) - \int (\vec{r} + \vec{X})\rho(\vec{r})\mathrm{d}\vec{r} \\ &= \left[\sum_{i=1}^{M} Z_i - \int \rho(\vec{r})\mathrm{d}\vec{r}\right]\vec{X} + \vec{\mu} = \vec{\mu}.\end{aligned}$$

2.1.1 A Quantized Bulk Property

The dipole moment is an extensive property, which depends on the number of units of the system, N. However, in the termodynamic limit, we may define the intensive *dipole moment per unit* for any of its ($i = x, y, z$) components as

$$\bar{\mu}_i = \lim_{N\to\infty} \frac{\mu_i(N)}{N} = \lim_{N\to\infty} \frac{1}{\Delta N}[\mu_i(N) - \mu_i(N - \Delta N)]. \tag{2.3}$$

Both definitions are equivalent, but in the practice N is always finite and normally the definition of the right-hand side converges much faster for increasing N.

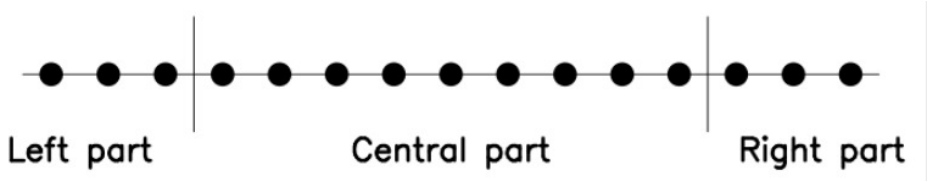

Figure 2.1: Schematic representation of a long, but finite, regular chain. Each black circule represents a building block containing one or more atoms, which is regularly along the chain axis (z). The separation into a central and two terminal regions is indicated by the vertical lines.

A schematic representation of a long, but finite, one-dimensional chain along the z axis is shown in figure 2.1. It is useful to split this system into three distinct spacial parts: a perfectly regular region in the center (C) where the electrons do not feel the finite size of the system, and two terminal regions (L and R). The fact that such a split can be made defines what we mean by 'long' chain. The units in the central region have to be neutral because, otherwise, there would be an extra charge not localized at the terminations that would change the charge per central unit when the chain length is increased with fixed terminations. This conflicts with being able to identify a central region with given properties.

The z component of the dipole moment of the system depicted in figure 2.1 can be written [11] as

$$\begin{aligned}\mu_z &= \int_L \rho_T(\vec{r}) z \mathrm{d}\vec{r} + \int_C \rho_T(\vec{r}) z \mathrm{d}\vec{r} + \int_R \rho_T(\vec{r}) z \mathrm{d}\vec{r} \\ &= N_C \mu_C + \left[Z_L \int_L \rho_T(\vec{r}) \mathrm{d}\vec{r} + Z_R \int_R \rho_T(\vec{r}) \mathrm{d}\vec{r} \right] \\ &\quad + \left[\int_L \rho_T(\vec{r})(z - Z_L) \mathrm{d}\vec{r} + \int_R \rho_T(\vec{r})(z - Z_R) \mathrm{d}\vec{r} \right], \end{aligned} \tag{2.4}$$

in which $\rho_T(\vec{r})$ is the total charge density, μ_C is the z component of the dipole moment of a central unit, N_C is the number of units in C, while Z_L and Z_R are the average of nuclear positions in the L and R regions, respectively. Assuming that the entire system is neutral, the charge at the terminations is

$$Q_L = \int_L \rho_T(\vec{r}) \mathrm{d}\vec{r} = -\int_R \rho_T(\vec{r}) \mathrm{d}\vec{r} = -Q_R, \tag{2.5}$$

then, the first term in square brackets of equation (2.4) becomes

$$Z_L \int_L \rho_T(\vec{r}) \mathrm{d}\vec{r} + Z_R \int_R \rho_T(\vec{r}) \mathrm{d}\vec{r} = (Z_R - Z_L) Q_R. \tag{2.6}$$

For fixed terminations, increasing the chain length means that ΔN units are added in C, hence, the total chain length and, in particular, the distance $Z_R - Z_L$ are increased by $\Delta N a$, with a being the lattice constant in the C region. Additionally, it is important to note that the last term in square brackets of equation (2.4) describes the local dipole moments that arise from the charge distribution within the two terminal region. Thus, for fixed terminations, it is the only term in this equation that does not vary when the chain length is enlarged and, therefore, it does not contribute to the dipole moment per unit as defined in equation (2.3). Consecuently, we have

$$\bar{\mu}_z = \mu_C + Q_R \, a. \tag{2.7}$$

According to this expression, the dipole moment per unit depends on the charge accumulated in the terminal regions, which at first glance, can vary widely. However, there are restrictions on the these charges as Vanderbilt and King-Smith [12] have shown. They write the electronic part of the dipole moment in terms of localized orthonormal functions obtained by a unitary transformation of the occupied canonical orbitals.

In terms of these functions, the density matrix consists of three diagonal blocks [13], one for each region in figure 2.1, whereas the remaining elements are exponentially vanishing. Since the complete matrix is idempotent, each of the three blocks will be idempotent as well. This implies that the number of electrons associated with each block can change only by an integer and, therefore, that Q_R can vary only by an integer.

On this basis, the dipole moment per unit is essentially a bulk property with quantized values that differ from one another only by lattice vectors [11, 14]. It follows that this property is accessible (modulo a lattice vector) through a conventional band-structure calculation on an infinite periodic system, even though, per construction, there are no terminations in the latter case.

2.1.2 Polarizability and Hyperpolarizabilities

When a molecule is exposed to a static (DC) field,

$$\vec{E} = (E_x, E_y, E_z) = \sum_i E_i \hat{\imath}, \tag{2.8}$$

its electronic and structural properties may change. In the general case, we can quantify the changes through the changes of the dipole moment, which may contain both linear and non-linear dependences on $\vec{E}$,

$$\mu_i = \mu_{0i} + \sum_j \alpha_{ij} E_j + \frac{1}{2!} \sum_{jk} \beta_{ijk} E_j E_k + \frac{1}{3!} \sum_{jkl} \gamma_{ijkl} E_j E_k E_l + \dots \tag{2.9}$$

Here, $\vec{\mu}_0$ is the dipole moment of the system in the absence of external electrostatic fields also called the *permanent dipole moment*, α is the (linear) *polarizability*, while β and γ are the *first* and *second hyperpolarizabilities*.

When a neutral system has additionally the special feature of being centrosymmetric, the replacement $\vec{r} \to -\vec{r}$ leaves the system unchanged. For this system the permanent dipole moment vanishes ($\vec{\mu}_0 = 0$) while turning the field on may lead to a non-vanishing dipole moment $\vec{\mu}$. Thus, replacing $\vec{E} \to -\vec{E}$ leads to $\vec{\mu} \to -\vec{\mu}$, which can be fulfilled only if all the components of the first hyperpolarizability vanish, $\beta_{ijk} = 0$.

When the system is in the presence of a weak electric field $\vec{E}$ we can expand the energy in terms of the field according to

$$E(\vec{E}) = E(0) + \sum_i \mu_{0i} E_i + \frac{1}{2!} \sum_{ij} \alpha_{ij} E_i E_j$$

$$+\frac{1}{3!}\sum_{ijk}\beta_{ijk}E_iE_jE_k+\frac{1}{4!}\sum_{ijkl}\gamma_{ijkl}E_iE_jE_kE_l+\ldots, \tag{2.10}$$

where $E(0)$ is the energy without the electric field. Therefore, the dipole moment, the polarizability and the hyperpolarizabilities can be also obtained thourgh energy derivatives with respect to the field strength. However, very often the derivation entails an approximation which is less accurate for higher orders. In this sense, it is advisable to use the expansion (2.9) instead.

Both the nuclei and the electrons contribute to the response of the system, but to take into account the part due to the nuclei, we have to allow the system to relax or to analyze the vibrations. On the other hand, there are mainly two different approaches to calculate the electronic contribution. One consists of including the effects of the extra field perturbatively. That needs third-order perturbed equations to relate the polarizability and hyperpolarizabilities to the different terms in the pertubation expansion.

The other approach amounts to perform different calculations for different directions and strengths of the field $\vec{E}$, and subsequently to fit the results with an expression of the form of equation (2.9) or (2.10). This is the method used in the present work, which in the case of a one-dimensional system in a uniform electrostatic field is drastically simplified. Thus, placing the chain along the z direction with a uniform electrostaic field parallel to it,

$$\vec{E}=(0,0,E_{\mathrm{DC}}), \tag{2.11}$$

the only relevant component of the response will be the z component, which from the expansion (2.9) becomes

$$\mu_z=\mu_{0z}+\alpha_{zz}E_{\mathrm{DC}}+\frac{1}{2}\beta_{zzz}E_{\mathrm{DC}}+\frac{1}{6}\gamma_{zzzz}E_{\mathrm{DC}}+\ldots. \tag{2.12}$$

Hereafter we will omit the z subindices.

2.2 The Polarization

For macroscopic systems, one considers instead of the dipole moment, the polarization $\vec{P}$, defined as the dipole moment per unit volume [5], thus similar to equation (2.1),

$$\vec{P}=\frac{1}{V}\left[\sum_{i=1}^{M}Z_i\vec{R}_i-\int\vec{r}\rho(\vec{r})\mathrm{d}\vec{r}\right]=\vec{P}_{\mathrm{n}}+\vec{P}_e. \tag{2.13}$$

So expressed, the polarization is not a bulk property because it depends on the shape and truncation of the sample, but the variations of $\vec{P}$ are measured as bulk material properties in several circumtances. Some macroscopic physical properties are just derivatives of $\vec{P}$ with respect to suitably chosen perturbations. This is the case of the dielectic permitivity, piezoelectricity, effective charges and pyroelectricity, which are phenomenologically measured as bulk material tensors and, therefore, should be accessible through calculations considering the system as being infinite and periodic. In that case, using the periodic boundary conditions in a BvK zone of K unit cells, the relation between the dipole moment $\vec{\mu}$ and the polarization is

$$\vec{P} = \frac{\vec{\mu}}{K\Omega}. \tag{2.14}$$

Here, Ω is the volume of the unit cell, which turns out to be the area or the length of the unit for two-dimensional and one-dimensional periodic systems respectively. Thus, the polarization is closely related to the dipole moment per unit $\vec{\mu}/K$ and it can be split into nuclear and electronic contributions as well.

In the description provided here, we concentrate on a one-dimensional periodic system (chain) that lies parallel to the z axis and we will neglect the spin polarization. In the absence of an external electric field, the orbitals of interest are typically written as Bloch waves,

$$\psi(\vec{r}) = \psi_j(k, \vec{r}) = e^{ikz} u_j(k, \vec{r}), \tag{2.15}$$

with j being the band index, $u_j(k, \vec{r})$ a lattice-periodic function and k a continuous variable in the BZ, i.e., in the interval $(-\pi/a, \pi/a)$, where a is the unit cell length. In a practical calculation one considers only a finite set of K equidistant k values separated by

$$\Delta k = \frac{2\pi}{Ka}. \tag{2.16}$$

Finally, we consider only systems with a gap between filled and empty bands.

Within either Hartree-Fock or Kohn-Sham theory, the Slater determinant wave function Ψ_e consists of $2B\,K$ occupied (non-spin-polarized) orbitals, with $2B$ being the number of electrons per unit.

When a uniform electrostatic field parallel to the chain is present ($E_z = E_{\mathrm{DC}}$), we seek the minimum of

$$G = \langle \Psi | \hat{H} | \Psi \rangle - E_{\mathrm{DC}}\, \mu_e - \sum_{i,j} \lambda_{ij} [\langle \psi_i | \psi_j \rangle - \delta_{ij}]. \tag{2.17}$$

The first suggestion for the definition of the z component of the electronic dipole moment μ_e is

$$\mu_e = (Ka)P_e \equiv -\langle \Psi_e | \hat{Z} | \Psi_e \rangle, \tag{2.18}$$

However, this expectation value cannot be evaluated if the wavefunctions obey the periodic boundary conditions. In fact, $\hat{Z}$ does not commute with a translation by Ka, and therefore is not a legitimate operator in the Hilbert space of Ψ_e. Thus, one must consider an alternative approach.

2.2.1 The Modern Theory of Polarization

About 20 years ago, there began to appear alternative formulations allowing for calculation of the dipole moment per unit cell based on an operator that has the BvK periodicity and approaches the position operator as the size of the BvK zone approaches infinity. Working expressions were initialy proposed within the so-called modern theory of polarization [4, 5, 12, 15] (MTP), based on a discretized Berry phase treatment. It was first applied to calculate the static polarization and then extended to include the effect of electric fields [6, 7, 16].

According to the MTP, there are at least three different ways of approching the electronic polarization of equation (2.18) (or the electronic dipole moment per unit $\bar{\mu}_e = \mu_e / K = aP_e$). The original form proposed by Resta [5] is

$$\bar{\mu}_e = \bar{\mu}_{\mathrm{R}} = -\frac{a}{\pi} \mathrm{Im} \ln \det \underline{\underline{S}}^{+} = \frac{a}{\pi} \mathrm{Im} \ln \det \underline{\underline{S}}^{-}, \tag{2.19}$$

where the dimension of the matrices $\underline{\underline{S}}^{\pm}$ is equal to the number of electrons per BvK zone (i.e., $2B\,K$) and the elements, considering the Bloch waves of the equation (2.15),

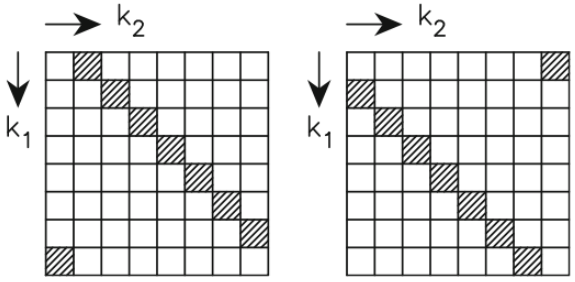

Figure 2.2: The structure of the $\underline{\underline{S}}^{\pm}$ matrices in a Bloch-function representation.

are

$$S^{\pm}_{j_1 j_2}(k_1,k_2) = \langle \psi_{j_1}(k_1,\vec{r})|e^{\pm \Delta k z}|\psi_{j_2}(k_2,\vec{r})\rangle$$
$$= \delta_{k_1 k_2 \pm \Delta k}\langle u_{j_1}(k_1,\vec{r})|u_{j_2}(k_2,\vec{r})\rangle. \tag{2.20}$$

Upon organizing the occupied Bloch waves in order of increasing k, the $\underline{\underline{S}}^{\pm}$ matrices have the simple structure shown in figure 2.2 with the shaded squares representing the non-vanishing terms above and below the $k_1 = k_2$ diagonal and one element in the opposite corner. Thus, the dipole moment per unit is non-diagonal in k.

Alternatively, one may consider an expression due to King-Smith and Vanderbilt [4], which can be obtained from $\bar{\mu}_{\mathrm{R}}$ by using the first-order Taylor series expansion,

$$u_j(k \pm \Delta k, \vec{r}) \simeq u_j(k,\vec{r}) \pm \Delta k \frac{\partial}{\partial k} u_j(k,\vec{r}), \tag{2.21}$$

which leads to

$$\bar{\mu}_e = \bar{\mu}_{\mathrm{KSV}} = -\frac{2i}{K}\sum_{k=1}^{K}\sum_{j=1}^{B}\left\langle u_j(k,\vec{r})\left|\frac{\partial}{\partial k}\right|u_j(k,\vec{r})\right\rangle$$
$$= -\frac{2i}{K}\sum_{k=1}^{K}\sum_{j=1}^{B}\left\langle \psi_j(k,\vec{r})\left|e^{ikz}\frac{\partial}{\partial k}e^{-ikz}\right|\psi_j(k,\vec{r})\right\rangle, \tag{2.22}$$

remembering that B is the number of occupied bands and we do not consider spin degeneracy. Finally, it can be shown [17] that equation (2.22) is equivalent to

$$\bar{\mu}_e = \bar{\mu}_{\mathcal{W}} = -\frac{2}{K}\sum_{n=1}^{K}\sum_{j=1}^{B}\langle \mathcal{W}_{jn}(\vec{r})|z|\mathcal{W}_{jn}(\vec{r})\rangle \tag{2.23}$$

where the $\mathcal{W}_{jn}$'s are the localized Wannier functions transformed from the delocalized Bloch waves according to

$$\mathcal{W}_{jn}(\vec{r}) = \frac{1}{\sqrt{K}}\sum_{k=1}^{K} e^{-ikan}\psi_j(k,\vec{r}). \tag{2.24}$$

Here the Wannier function $\mathcal{W}_{jn}$ of the jth band is more or less localized to the nth unit inside the BvK zone.

The equations (2.19), (2.22) and (2.23) are valid only for systems with an energy gap between occupied and unoccupied bands. These expressions were derived [18] for

an independent particle model and were later generalized [19] to the case of a multi-determinant electronic wavefunction.

On the other hand, instead of the expression (2.15) for the orbitals, we may consider the LCAO approach of equations (1.48) and (1.50), in which the single particle orbitals are written as linear combinations of localized basis functions centered on the atoms,

$$\begin{aligned}\psi_j(k,\vec{r}) &= \sum_{p=1}^{N_b} C_{pj}(k)\chi_p(k,\vec{r}) \\ \chi_p(k,\vec{r}) &= \frac{1}{\sqrt{K}}\sum_{n=1}^{K} e^{ikan}\chi_{pn}(\vec{r}),\end{aligned} \tag{2.25}$$

with χ_{pn} being the pth atomic basis function of the nth unit and N_b is number of basis functions per unit ($N_b > B$). Introducing this in expression (2.22) gives

$$\begin{aligned}\bar{\mu}_e =& -\frac{2i}{K^2}\sum_{k,j}\left\langle \sum_{p,m} C_{pj}(k)e^{-ik(z-ma)}\chi_{pm}\left|\frac{\partial}{\partial k}\right|\sum_{q,n} C_{qj}(k)e^{-ik(z-na)}\chi_{qn}\right\rangle \\ =& -\frac{2i}{K^2}\sum_{k,j}\sum_{p,q}\sum_{m,n} C^*_{pj}(k)e^{ika(n-m)}\left[-i\langle\chi_{pm}|z-na|\chi_{qn}\rangle + \langle\chi_{pm}|\chi_{qn}\rangle\frac{d}{dk}\right]C_{qj}(k) \\ =& -\frac{2}{K}\sum_{k,n=0}^{K-1} e^{ikan}\sum_{j=1}^{B}\sum_{p,q=1}^{N_b} C^*_{pj}(k)\left[\underbrace{\langle\chi_{p0}|z-na|\chi_{qn}\rangle}_{\text{charge}} + \underbrace{i\langle\chi_{pm}|\chi_{qn}\rangle\frac{d}{dk}}_{\text{current}}\right]C_{qj}(k)\end{aligned} \tag{2.26}$$

using the relation (1.49) to reduce the summation over m in the second step. Hereby, we have split $\bar{\mu}_e$ into so-called charge ($\bar{\mu}_Q$) and current ($\bar{\mu}_I$) contributions. The former is the expectation value for a function that resembles z but is piecewise linear with the periodicity of the lattice. If the atom-centered basis functions are orthonormal, this equation reduces to

$$\bar{\mu}_e = -\frac{2}{K}\sum_{j=1}^{B}\sum_{k}\sum_{p}\left[|C_{pj}(k)|^2 z_{p0} + iC^*_{pj}(k)\frac{dC_{pj}(k)}{dk}\right] = \bar{\mu}_Q + \bar{\mu}_I. \tag{2.27}$$

In order to complete the picture, the nuclear contribution to the z component of the dipole moment per unit cell may be obtained simply as

$$\bar{\mu}_{\mathrm{n}} = \frac{1}{K}\sum_{m=0}^{K-1}\sum_{p}(Z_{pm} - ma)Q_p = \sum_{p} Z_{p0}Q_p, \tag{2.28}$$

with Z_{pm} being the z component of the position of the pth nucleus in the mth unit cell of the BvK zone and Q_p is its nuclear charge. The nuclear contribution modifies only the charge term of $\bar{\mu}_e$.

2.2.2 Phase Factors and non Uniqueness

It is important to notice that each expression for the dipole moment per unit is not unique since it may contain an unknown integer multiple of the lattice constant. In the expression (2.19), the term $\mathrm{Im}\ln\det\underline{\underline{S}}^{\pm}$ is just the phase of the complex number $\det\underline{\underline{S}}^{\pm}$, which contains an unknown integer multiple of 2π. Thus, $\bar{\mu}_{\mathrm{R}}$ is only determined up to an integer times the lattice constant. Equivalently, in evaluating $\bar{\mu}_{\mathrm{KSV}}$ of equation (2.22) we may modify each electronic orbital by a phase factor,

$$\psi_j(k,\vec{r}) \longrightarrow \psi_j(k,\vec{r})e^{i\phi_j(k)}, \tag{2.29}$$

which is arbitrary except for requiring that

$$\phi_j\left(-\frac{\pi}{a}\right) = \phi_j\left(\frac{\pi}{a}\right) + 2\pi\,\tilde{n}_j, \tag{2.30}$$

with $\tilde{n}_j$ being an unknown integer. Adding the contributions from all bands, the dipole moment per unit is changed by an amount

$$\Delta\bar{\mu} = -a\sum_{j=1}^{B}\tilde{n}_j = -\tilde{n}\,a \tag{2.31}$$

This change modifies the current, but not the charge term in equation (2.26). Finally, since the assignment of the Wannier functions in equation (2.24) to the individual units is not unique, the expression (2.23) also contains an unknown integer multiple of the lattice constant.

Moreover, when the phase-modified orbitals of the expression (2.29) are inserted in the secular equation, the orbital energies are shifted by a term proportional to the field strength as we will see in the next chapter. Therefore, we can say that the band structure is not unique for the system is in the presence of an electric field.

2.3 The SCF Equations

2.3.1 For Finite Systems

When a finite system is in the presence of an electric field, the total Hamiltonian changes according to

$$\hat{H} \longrightarrow \hat{H} - \vec{\mu} \cdot \vec{E}. \tag{2.32}$$

In the case studied here, i.e., a one-dimensional system of repeating units along the z axis in a uniform elestrostatic field E_{DC} parallel to it, the second term adds simply

$$\hat{h}_{\mathrm{DC}} = E_{\mathrm{DC}}\, z, \tag{2.33}$$

to the Fock (or Kohn-Sham) operator. In ohter units system the elementary charge e should be included, distinguishing this from the scalar potential V_{DC} which determines the electric field,

$$\vec{E} = -\nabla V_{\mathrm{DC}} = -\nabla(-E_{\mathrm{DC}}\, z), \tag{2.34}$$

so we must be careful not to confuse them because here, they differ only in the sign.

To solve the single-particle equations,

$$\left(\hat{F} + E_{\mathrm{DC}}\, \hat{z}\right) \psi_j = \varepsilon_j \psi_j, \tag{2.35}$$

we expand the electronic orbitals in a set of atom centered basis functions considering that we have N units and N_b basis functions per unit,

$$\psi_j = \sum_{p=1}^{N_b} \sum_{m=1}^{N} c_{pmj} \chi_{pm}, \tag{2.36}$$

with χ_{pm} being the pth basis function of the mth unit. Then, the equations (2.35) can be expressed in matrix form including the term due to the field as

$$\left\{ \underline{\underline{F}} + E_{\mathrm{DC}} \cdot \underline{\underline{M}} \right\} \cdot \underline{c}_j = \varepsilon_j \cdot \underline{\underline{O}} \cdot \underline{c}_j \tag{2.37}$$

where $\underline{c}_j$ is the field-dependent jth column of the matrix $\underline{\underline{c}}$, whose rows are determined by the pm indices. In addition

$$O_{pm}^{qn} = \langle \chi_{pm} | \chi_{qn} \rangle$$

$$M^{qn}_{pm} = \langle \chi_{pm} | z | \chi_{qn} \rangle \qquad (2.38)$$
$$F^{qn}_{pm} = \langle \chi_{pm} | \hat{F} | \chi_{qn} \rangle$$

are the overlap, dipole moment, and Fock (or Kohn-Sham) matrix elements, respectively. Here $\hat{F}$ depends indirectly on the field through the orbital coefficients because the equation (2.37) is solved self-consistently. The matrices in equation (2.37) are all real and have a size of $(NN_b \times NN_b)$, but $\hat{F}$ only depends on the doubly occupied orbitals $N_O = NB$, with $2B$ being the number of electrons per unit.

2.3.2 For Periodic Systems

We have seen that, in the case of finite systems, the interaction of the electrons with the external field is introduced through the scalar potential V_{DC}. The analogous methodology for the infinite periodic system requires a different expression for the dipole moment per unit. All the expressions (2.19), (2.22) and (2.23) for $\bar{\mu}_e$ have been used to minimize the electric enthalpy of equation (2.17) [6, 7, 16], but those approaches are not based on solving a standard secular equation self-consistently and some of them lead to a computationally extensive and/or not particularly stable procedures.

Instead of dealing with the scalar potrential V_{DC}, one can make use of the vector potential approach (VPA), a completely different methodology recently developed [1, 8], where the effect of the field is included by using the time-dependent vector potential $\vec{A}(\vec{r}, t)$, which defines the electric field through

$$\vec{E}(\vec{r}, t) = -\frac{1}{c}\frac{\partial}{\partial t}\vec{A}(\vec{r}, t). \qquad (2.39)$$

Then, in presence of this electric field, the single-particle momentum operator is replaced by

$$\hat{p} = \hat{p} + \frac{1}{c}\vec{A}(\vec{r}, t), \qquad (2.40)$$

in the time-dependent Hartree-Fock (or Kohn-Sham) equation,

$$\left(\hat{F} - i\frac{\partial}{\partial t}\right)\psi_j(\vec{r}, t) = \sum_i \varepsilon_{ij}(t)\psi_i(\vec{r}, t). \qquad (2.41)$$

Using the LCAO expansion of equations (2.25),

$$\begin{aligned}\psi_j(k,\vec{r}) &= \sum_{p=1}^{N_b} C_{pj}(k)\chi_p(k,\vec{r}) \\ \chi_p(k,\vec{r}) &= \frac{1}{\sqrt{K}}\sum_{n=1}^{K} e^{ikan}\chi_{pn}(\vec{r}),\end{aligned} \tag{2.42}$$

and considering a uniform electric field $\vec{E}(\vec{r},t) = E(t)$, we obtain

$$\begin{aligned}\underline{\underline{F}}(k,t)\cdot\underline{\underline{C}}(k,t)+E(t)\left[\underline{\underline{M}}(k)\cdot\underline{\underline{C}}(k,t)+i\underline{\underline{O}}(k)\cdot\frac{\partial}{\partial k}\underline{\underline{C}}(k,t)\right]-i\underline{\underline{O}}(k)\frac{\partial}{\partial t}\underline{\underline{C}}(k,t) \\ = \underline{\underline{O}}(k)\cdot\underline{\underline{C}}(k,t)\cdot\underline{\underline{\varepsilon}}(k,t).\end{aligned} \tag{2.43}$$

Here,

$$\begin{aligned}O_{pq}(k) &= \sum_n e^{ikan}\langle\chi_{p0}|\chi_{qn}\rangle \\ M_{pq}(k) &= \sum_n e^{ikan}\langle\chi_{p0}|z-na|\chi_{qn}\rangle = \sum_n e^{-ikan}\langle\chi_{pn}|z|\chi_{q0}\rangle \\ F_{pq}(k) &= \sum_n e^{ikan}\langle\chi_{p0}|\hat{F}|\chi_{qn}\rangle,\end{aligned} \tag{2.44}$$

are the overlap, dipole moment and Fock (or Kohn-Sham) matrices, respectively. For the special case of an static field, $E(t) = E_{\mathrm{DC}}$, there is no time dependence. In addition, one may choose the Lagrange multipliers so that only diagonal elements are nonvanishing. Then, equation (2.43) becomes

$$\left\{\underline{\underline{F}}(k)+E_{\mathrm{DC}}\left[\underline{\underline{M}}(k)+i\underline{\underline{O}}(k)\frac{d}{dk}\right]\right\}\cdot\underline{C}_j(k) = \varepsilon(k)\,\underline{\underline{O}}(k)\cdot\underline{C}_j(k), \tag{2.45}$$

where $\underline{C}_j(k)$ is the jth column of $\underline{\underline{C}}(k)$. Due to the partial derivative with respect to k, this equation is not a standard matrix-eigenvalue problem. However, it can be recast by multiplying the term with the derivative on the left-hand side by $\underline{\underline{1}} = \underline{\underline{C}}^{\dagger}(k)\cdot\underline{\underline{O}}(k)\cdot\underline{\underline{C}}(k)$, which gives

$$\underline{\underline{O}}(k)\cdot\frac{d}{dk}\underline{\underline{C}}(k) = \left[\underline{\underline{O}}(k)\cdot\left(\frac{d}{dk}\underline{\underline{C}}(k)\right)\cdot\underline{\underline{C}}^{\dagger}(k)\cdot\underline{\underline{O}}(k)\right]\cdot\underline{\underline{C}}(k). \tag{2.46}$$

Then, the equation (2.45) takes the standard form

$$\left\{\underline{\underline{F}}(k) + E_{\mathrm{DC}}\left[\underline{\underline{M}}(k) + i\underline{\underline{Q}}(k)\cdot\left(\frac{d}{dk}\underline{\underline{C}}(k)\right)\cdot\underline{\underline{C}}^{\dagger}(k)\cdot\underline{\underline{Q}}(k)\right]\right\}\cdot\underline{C}_j(k) \tag{2.47}$$
$$= \varepsilon(k)\,\underline{\underline{Q}}(k)\cdot\underline{C}_j(k).$$

Here, the effective Hamiltonian (in curly brackets) remains Hermitian. This is the equation that is solved self-consistently for the complex expansion coefficients.

The equation (2.47) reduces simply to equation (1.51) in absence of electric field. Beyond resulting in a conventional eigenvalue equation, it is important to note that k remains as a good quantum number and thus, the translational symmetry is preserved. This equation differs fundamentally from equation (2.37) because of an additional current term (second term in square brackets), but this term gives a crutial contribution as we will see later on. On the other hand, for time-dependent fields, the VPA is the natural way to proceed, since the frequency dependence can be introduced in equation (2.43). Finally, under the considered conditions, the expression for the dipole moment per unit within the VPA coincides with that of equation (2.26), i.e., an identical formulation may be developed from the MTP point of view.

Having defined the dipole moment per unit in equation (2.26), we can write the electronic energy per unit as

$$\bar{E}_e(E_{\mathrm{DC}}) = \bar{E}_e(0) - E_{\mathrm{DC}}\,\bar{\mu}_e, \tag{2.48}$$

where $\bar{E}_e(0)$ is the field-free electronic energy per unit.

2.3.3 Solving the VPA Equation

Considering the VPA secular equation for infinite periodic systems in external electrostatic fields, equation (2.47), the key aspect for practical computational purposes involves differentiating the expansion coefficients $\{C_{pj}(k)\}$ with respect to k. For the finite field case, the derivatives must be determined numerically. However, the calculated coefficients contain an arbitrary k-dependent phase factor, so it is computationally of enourmous advantage to smooth the coefficients to ease the differentiation. Thus, an additional phase factor is introduced,

$$\tilde{C}_{pj}(k) = C_{pj}(k)e^{i\phi_j(k)}, \tag{2.49}$$

which is chosen so that the change in the coefficients from one k point to the next is minimized. According to numerous test calculations, a numerically stable and accurate *smoothing procedure* was developed [2, 3]. This multistep method starts with the field-free expansion coefficients obtained by solving the single-particle equation (1.51). Then we proceed as follows:

1. It is important to correctly join the band orbitals at different k points. Thus, we first identify band crossings. Assuming that orbitals for the same band have very similar expansion coefficients, we can identify band crossings from the relation

$$\sum_p C^*_{pj}(k)C_{pj}(k+\Delta k) \leq \delta, \tag{2.50}$$

   for each j band and k value. If the sum is smaller than a chosen threshold, δ, the orbitals are taken as belonging to two different crossing bands and the coefficients $C_{pj}(k+\Delta k)$ and $C_{pj+1}(k+\Delta k)$ are interchanged.

2. When two or more band orbitals are energetically degenerate at a given k point, we construct linear combinations that are maximally similar to those of the two neighboring k points.

3. After the resulting coefficients $\{C_{pj}(k)\}$ have been modified (or not) according to steps 1 and 2, we rotate all the coefficients at $k = 0$ on the complex plane by multiplying them by $e^{i\theta}$, so that they are all real. The multiplication by the complex number $e^{i\theta}$ is equivalent to a rotation on the complex plane an angle of θ. Thus, we can take the introduction of phase factors as rotations. However we have to stress that our coefficients are eigenvectors, so that whenever one coefficient $C_{pj}(k)$ is rotated, all the coefficients (for all $p = 1, 2, ..., N_b$) of the corresponding j eigenvector have to be rotated with the same angle.

4. Starting from $k = 0$ and $\phi_j(0) = 0$, we consider consecutive positive k points and rotate the N_b coefficients $C_{pj}(k+\Delta k)$ of the j'th orbital an angle given by

$$\phi_j(k+\Delta k) = \arg\left[\sum_p C^*_{pj}(k+\Delta k)C_{pj}(k)\right]. \tag{2.51}$$

   For negative k,

$$C_{pj}(-k)e^{i\phi_j(-k)} = C^*_{pj}(k)e^{-i\phi_j(k)}. \tag{2.52}$$

This transformation is readily carried through. It leads to coefficients that are smooth as a function of k for $-\pi/a < k < \pi/a$, however discontinuities may occur at the zone boundaries.

5. In order to remove discontinuities at $k = \pm\pi/a$, the quantity

$$Q_j = \sum_{k,p} |C_{pj}(k+\Delta k)e^{i\phi_j(k+\Delta k)} - C_{pj}(k)e^{i\phi_j(k)}|^2 + \lambda \sum_{k,p} |C_{pj}(k+2\Delta k)e^{i\phi_j(k+2\Delta k)} - C_{pj}(k)e^{i\phi_j(k)}|^2 \tag{2.53}$$

is minimized for each j band under the constraint,

$$\phi_j\left(-\frac{\pi}{a}\right) = \phi_j\left(\frac{\pi}{a}\right), \tag{2.54}$$

and with $\phi_j(0)$ fixed. The first term in equation (2.53) makes the coefficients between neighboring k points maximally similar. However, it can be useful to include a next-nearest neighbor term as well. This improves the numerical stability of the derivatives with respect to k. A reasonable value for that contribution is $\lambda = 0.1$. In this way, we arrive at a set of smooth coefficients for the field-free case, $\{\tilde{C}^0_{pj}(k)\}$. This is the time consuming step in the overall smoothing procedure, which increases with the number of k points. It involves a nonlinear optimization that is carried out using conjugate gradients explained in Appendix A. The four preceding steps are necessary just to provide a good initial guess. We emphasize that it is done only for zero field and, for a typical problem, will require just a small fraction of the overall computation time.

6. The smooth coefficients are used to evaluate the dipole moment per unit according to equation (2.26), where the numerically stable derivatives are obtained from a finite-difference approximation,

$$\frac{dC_{pj}(k)}{dk} \simeq \frac{1}{2\Delta k} \sum_{n=1}^{N_D} w_{n,N_D} \left[C_{pj}(k+n\Delta k) - C_{pj}(k-n\Delta k)\right], \tag{2.55}$$

with

$$C_{pj}\left(k + \frac{2\pi}{a}\right) = C_{pj}(k). \tag{2.56}$$

The most frequently used approximation is to take $N_D = 1$, $w_{11} = 1$. However, test calculations showed that an improved accuracy was obtained by using larger

N_D. In that event, the coefficients w_{n,N_D} are taken from Dvornikov [20],

$$w_{n,N_D} = \left[n \prod_{m \neq n}^{N_D} \left(1 - \frac{n^2}{m^2} \right) \right]^{-1} . \tag{2.57}$$

Typically, $N_D \simeq 5$ leads to accurate results.

7. The derivatives are substituted in equation (2.45), which is solved for $E_{\mathrm{DC}} \neq 0$ and with the obtained coefficients $\{C_{pj}(k)\}$ we repeat the steps 2 and 3 and, then, skip to step 8 below. It is thereby assumed that the weak field E_{DC} does not remove band crossings by lowering the symmetry and that does not change the orbitals significantly, as was found to be the case in all the tests.

8. The coefficients are made maximally similar to those of the field-free case, $\tilde{C}^0_{pj}(k)$, by rotating them with an angle given by

$$\phi_j(k) = \arg \left[\sum_p C^*_{pj}(k) \tilde{C}^0_{pj}(k) \right] , \tag{2.58}$$

so we get the smooth coefficients

$$\tilde{C}_{pj}(k) = C_{pj}(k) e^{i\phi_j(k)}, \tag{2.59}$$

which in turn are used to calculate $\bar{\mu}_e$ for $E_{\mathrm{DC}} \neq 0$ returning to step 6.

9. The equation (2.45) is solved self-consistently by repeating the steps 7 and 8 until the convergence threshold is reached.

Chapter 3

Searching for the Correct Band Structures

As discussed in the previous chapter, for an extended finite system, the dipole moment per unit is defined up to an integer times the lattice constant as expressed in equation (2.7),

$$\bar{\mu} = \mu_C + Q_R\, a, \tag{3.1}$$

where the charge Q_R can change only by an integer. This theoretical limitation on the terminal charge has been termed charge quatization [14].

On the other hand, for infinite periodic system, the introduction of phase factors in the orbital expansion coefficients,

$$C_{pj}(k) \longrightarrow C_{pj}(k)e^{i\phi_j(k)}, \tag{3.2}$$

may lead to a change in the dipole moment per unit [13],

$$\bar{\mu} \longrightarrow \bar{\mu} - \tilde{n}\, a, \tag{3.3}$$

with $\tilde{n}$ being the unknown integer described in equation (2.31). The arbitrariness of the phase factors leads to an arbitrariness in the crystal-orbital energies. Thus, upon making the substitution of equation (3.2) in equation (2.47), $\varepsilon_j(k)$ changes according to

$$\varepsilon_j(k) \longrightarrow \varepsilon_j(k) + E_{\mathrm{DC}}\frac{d}{dk}\phi_j(k). \tag{3.4}$$

Although the integral of the second term over the entire band will vanish, except for possible contributions from the undetermined $\tilde{n}_j$ in equation (2.30), the field-dependent

orbital energies may vary in a somewhat arbitrary fashion as one goes across the band. Despite appearing to be physically irrelevant, different values of $\tilde{n}$ will lead to different values of, for example, the piezoelectric coefficient.

A highly relevant question is whether the properties of the infinite periodic systems and those of the large finite systems coincide. In order to address that issue we have studied a simple model linear chain [13, 19, 21] parametrizing all the elements of the Fock and overlap matrices as described in the next section. In those studies, it has been found that the integer $\tilde{n}$ can be used to reproduce the results obtained for a long finite chain with a quantized charge transfer between the terminations.

Here, we explore the opposite problem, i.e., to determine if the results for the finite chain can be used to avoid the arbitrariness of the phase factors and, in this sense, obtain the 'correct' band structure. For this aim, first, we need to build the band structure of the finite chain. This is a simple task in the field-free case, however, in presence of an external field, the orbitals are distorted hindering the procedure. In section 3.2, we present and discuss three methods to do it. Then, with both band structures, we use the expression (3.4) to try to determine the phase factors in section 3.3. This study was published in [22].

For practical reasons we decided to use a model system. Care has been taken to introduce the most important features that would appear in an *ab initio* calculation, but other aspects, such as a more complicated band structure, could be of significance. In the following section we shall describe the main features of the model, and the details of how it is implemented in the program code are very similar to those exposed in the next chapter.

3.1 Model I

We consider a simple model system schematically represented in figure 3.1. It is a linear A-B chain with alternating bond lengths. For the infinite, periodic system, the structure is described through the lattice constant a, and a parameter u_0 that quantifies the alternating bond lengths $(a/2 - 2u_0)$ and $(a/2 + 2u_0)$. For the infinite periodic chain in the absence of the electrostatic field, the two structures differing in the sign of u_0 are energetically degenerate. We shall here study only the case that $u_0 < 0$. This corresponds to choosing the unit cell so that the shorter interatomic bonds are between atoms of the same unit cell and the longer ones are between atoms of neighboring unit cells.

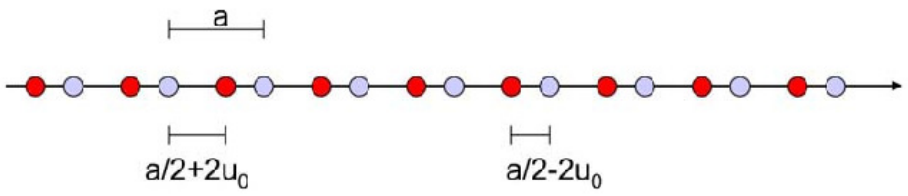

Figure 3.1: Schematic representation of the system used in our model studies. The system is a linear chain with two types of atom and alternating bond lengths. The lattice constant is denoted a, whereas u_0 is a bond-length-alternation parameter. We will denote the two types of atom as A and B.

There are 4 electrons per repeated unit and the nuclear charge on each atom is +2 a.u. We use a modified Hückel-type model for the Hartree-Fock Hamiltonian with a basis set that consists of four orthonormal functions per unit χ_{pm}, with $\{\chi_{1m}, \chi_{2m}\}$ centered on the atom A, and $\{\chi_{3m}, \chi_{4m}\}$ centered on the atom B in the mth unit. Although the field-free Hamiltonian matrix elements are parametrized, simple mathematical expressions for the basis functions are introduced to obtain a consistent treatment of the field-dependent terms. Thus, for the atom A placed at $z_m = z_{1m} = z_{2m}$ we use

$$\chi_{1m} = \begin{cases} \frac{1}{\sqrt{w_1}} & \text{for} \quad |z - z_m| \leq \frac{w_1}{2} \\ 0 & \text{otherwise} \end{cases}$$

$$\chi_{2m} = \begin{cases} \frac{1}{\sqrt{w_2}} & \text{for} \quad \frac{w_2}{4} < |z - z_m| \leq \frac{w_2}{2} \\ -\frac{1}{\sqrt{w_2}} & \text{for} \quad |z - z_m| \leq \frac{w_2}{4} \\ 0 & \text{otherwise} \end{cases} \tag{3.5}$$

and similar expressions for the functions centered on atom B. The widths, w (obeying $w_1 > w_2$), were kept sufficiently small so that functions on different atoms do not overlap.

We write the field-free many-body Hamiltonian as a sum of one- and two-electron operators,

$$\hat{H}_e = \sum_i \hat{h}_1(i) + \frac{1}{2} \sum_{i \neq j} \hat{h}_2(i, j). \tag{3.6}$$

The one-center one-electron term $\langle \chi_{pm} | \hat{h} | \chi_{qm} \rangle$ is taken to be non-zero only if $p = q$, defining the so-called *on-site energies*. Moreover, the two-center matrix elements are assumed to vanish except for those between functions that have the same spin and are located on neighboring atoms. These non-vanishing elements are taken to vary linearly

as a function of the interatomic distance. For each of four pairs of nearest-neighbor basis functions there are, accordingly, two parameters. Additionally, for simplicity, the only two-electron terms retained are those where all four indices are the same, i.e., $\langle \chi_{pm}\chi_{qn}|\hat{h}|\chi_{pm}\chi_{qn}\rangle$.

For the finite chain, the DC field is included in the electronic Hamiltonian through the operator $\hat{h}_{\mathrm{DC}}$, which modifies only the diagonal matrix elements,

$$\langle \chi_{pm}|\hat{h}_{\mathrm{DC}}|\chi_{qn}\rangle = E_{\mathrm{DC}} z_{pm}\, \delta_{pq}\delta_{mn}, \tag{3.7}$$

whereas, for the infinite periodic chains the static field is introduced by means of the VPA methodology explained in the previous chapter.

The dipole moment per unit of the infinite periodic system is calculated through the equation (2.27). As discussed, it will lie in a certain range of length a. In order to modify this range by an integer times a, the orbitals of one or more bands are given additional phase factors, $e^{ika\tilde{n}_j}$, with $\tilde{n}_j$ being an integer. Then, the phases become discontinuous across the boundary of the Brillouin zone, although the phase factors remain continuous. The model assumes a restricted Hartree-Fock approximation to be valid, so that the $\tilde{n}$ is even and, equivalently, only an even number of electrons can be transferred from one end to the other of the finite system. For the finite chain, the equation (2.3) is used to determine the dipole moment per unit. In this case, to obtain different terminations we modified the on-site energies only of the first and last atoms of the chain. This allows us to change the charge at the chain ends by ± 2 electrons.

Finally, for the purpose of having a pre-chosen minimum energy structure in the field-free case, we include an elastic term in the potential for nuclear motion, which contains 2nd and 4th order terms in nearest- and next-nearest-neighbor changes in the interatomic distance. However, since in the present work, we are interested solely in electronic properties, we do not carry out structure optimizations. In total, our model is very similar to a standard semi-empirical electronic structure method, except that we do not attempt to interpret the results as being those of specific systems.

3.1.1 The Periodic-System Band Structures

The band structures for two infinite periodic systems with different lattice constants, i.e., $a = 2.3$ and $a = 2.0$ are shown in figure 3.2. We shall now discuss these band in detail. As it can be seen in the left panel, the second and third bands are very flat compared to the first and fourth ones, meaning that the energies along those bands

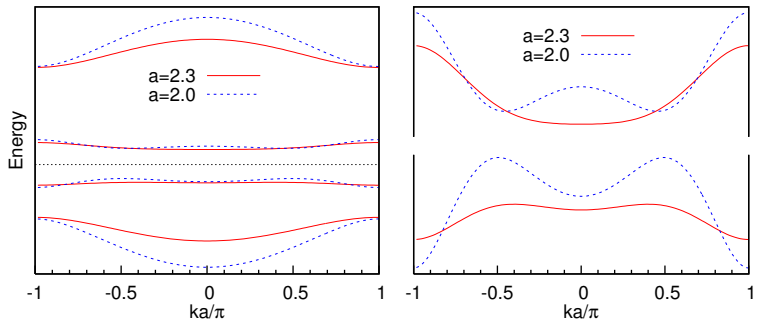

Figure 3.2: **Left:** Complete field-free band structures of the infinite periodic system with two different lattice constants. **Right:** Details of the valence and condution bands.

vary very little. For the smaller lattice constant the interaction between neighbouring atoms increases, giving wider bands, and, for our purpose, making the k assignment for the finite system easier.

The bands are even functions of k, so that we do not obtain additional information from the $k < 0$ part. Considering only the positive values of k, the first and fourth bands are monotonic functions of k. This is also the case for the third band with $a = 2.3$, which has its minimum (LUMO) at $k = 0$, but with $a = 2.0$ the minimum is found near $k = \pi/2a$. For $a = 2.3$, the maximum of the second band (HOMO) lies at $k = 2\pi/5a$, whereas it shifts to $k = \pi/2a$ when the lattice constant equals 2.0. Then, for the second band we have a situation, in which two orbitals with different k can have the same energy. Hereafter, we refer to this energy range as the "double-k region". In this sense, the third band with $a = 2.0$ also has a double-k region. This will become important below when the orbitals of the finite system are analyzed.

We considered both the field-free case for which the band structures are unique, as well as different non-vanishing fields. In the latter case, the band structures are not unique and, accordingly, it is also of fundamental interest to be able to identify a unique set of band structures, as discussed above.

3.2 Extracting the Band Structures

The calculation for the finite chain results only in the orbital energies but not in the k values. Thus, in order to construct the band structures from this information it is, at first, necessary to identify k for each orbital. One may suggest several procedures for

this purpose, and here we shall discuss three such methods.

We consider a long and finite chain that is separated into units. These units will become the unit cells when the chain is considered as being infinite and periodic. For the finite chain we write the jth orbital according to equation (2.36). For the long and finite chain, also in the presence of an electrostatic field, it is possible to choose C_{pnj} to be real. We will assume that this choice has been made. Therefore, for the model system with 4 basis functions per unit, if the chain has N units, the coefficients matrix consists of $(4N \times 4N)$ real numbers.

On the other hand, when the chain is treated as being infinite and periodic, the orbitals are the Bloch functions of the equation (2.42). In this case the orbital expansion coefficients are complex, so that if the size of the BvK zone is K, we have $K(4 \times 4)$ complex matrices.

3.2.1 Method 1: Expectation Value

Starting from the expansion (2.36), the set of atom-centered basis functions may be transformed into one of Bloch waves,

$$\psi_j(\vec{r}) = \sum_{p,m} c_{pmj}\chi_{pm}(\vec{r}) = \sum_{p} C_{pj}(k)\chi_p(k,\vec{r}), \tag{3.8}$$

where

$$\chi_p(k,\vec{r}) = \frac{1}{\sqrt{N}} \sum_{n} e^{ikan}\chi_{pn}(\vec{r}). \tag{3.9}$$

Here, we shall have exactly N equidistant k values in the range

$$-\frac{\pi}{a} < k \leq \frac{\pi}{a}. \tag{3.10}$$

Thus, including $k = 0$, the set of k values is

$$k_q = \Delta k\, q = \frac{2\pi}{Na}\, q, \tag{3.11}$$

with

$$q = 0, \pm 1, \pm 2, \ldots, \begin{cases} \pm\frac{N-1}{2} & \text{for } N \text{ odd} \\ \pm\frac{N-2}{2}, \frac{N}{2} & \text{for } N \text{ even} \end{cases} \tag{3.12}$$

We observe that the equation (3.9) is nothing but the discrete Fourier transform in

its unitary form. Thus, considering the inverse of this transform,

$$\chi_{pn}(\vec{r}) = \frac{1}{\sqrt{N}} \sum_k e^{-ikan} \chi_p(k, \vec{r}), \tag{3.13}$$

allows us to define 'crystal-orbital' expansion coefficients from the molecular ones,

$$C_{pj}(k) = \frac{1}{\sqrt{N}} \sum_n e^{-ikan} c_{pnj}. \tag{3.14}$$

If we apply the momentum operator on a pure Bloch function,

$$\psi(k, \vec{r}) = e^{ikz} u(k, \vec{r}), \tag{3.15}$$

we obtain

$$\begin{aligned} \hat{p} \left| \psi(k, \vec{r}) \right\rangle &= -i \frac{\partial}{\partial z} \left[e^{ikz} u(k, \vec{r}) \right] \\ &= k \left[e^{ikz} u(k, \vec{r}) \right] - i e^{ikz} \frac{\partial}{\partial z} u(k, \vec{r}) \\ &= k\psi(k, \vec{r}) - i e^{ikz} \frac{\partial}{\partial z} u(k, \vec{r}) \\ &\to k\psi(k, \vec{r}) \end{aligned} \tag{3.16}$$

when ignoring the second term in the second-last equation. This can also be used on the linear combination of Bloch waves of equation (3.8), giving

$$\hat{p} \left| \psi_j(k, \vec{r}) \right\rangle = \sum_p k C_{pj}(k) \chi_p(k, \vec{r}). \tag{3.17}$$

Then, the expectation value for the momentum of the jth orbital is

$$\begin{aligned} \left\langle \psi_j \right| \hat{p} \left| \psi_j \right\rangle &= \sum_{k_1, k_2} \sum_{p_1, p_2} C^*_{p_1 j}(k_1) C_{p_2 j}(k_2) \left\langle \chi_{p_1}(k_1, \vec{r}) \right| \hat{p} \left| \chi_{p_2}(k_2, \vec{r}) \right\rangle \\ &= \sum_{k_1, k_2} \sum_{p_1, p_2} C^*_{p_1 j}(k_1) C_{p_2 j}(k_2) k_2 \, \delta_{p_1 p_2} \delta_{k_1 k_2} \\ &= \sum_k \sum_p |C_{pj}(k)|^2 k. \end{aligned} \tag{3.18}$$

Similarly,

$$\left\langle \psi_j \right| \hat{p}^2 \left| \psi_j \right\rangle = \sum_k \sum_p |C_{pj}(k)|^2 k^2. \tag{3.19}$$

However, in the present case, the coefficients c_{pmj} of equation (3.14) are real, whereby

$$C_{pj}(-k) = C^*_{pj}(k), \tag{3.20}$$

and, accordingly, $\langle\psi_j|\,\hat{p}\,|\psi_j\rangle$ vanishes. Therefore, we instead consider

$$\langle\psi_j|\,|\hat{p}|\,|\psi_j\rangle = \sum_k \sum_p |C_{pj}(k)|^2 |k|, \tag{3.21}$$

and then ultimately define

$$\Delta|p_j| = \left[\langle\psi_j|\,\hat{p}^2\,|\psi_j\rangle - \langle\psi_j|\,|\hat{p}|\,|\psi_j\rangle^2\right]^{1/2}. \tag{3.22}$$

Accordingly, with the help of the expression (3.21) we can ascribe the jth orbital a k value, and with the standard daviation defined in equation (3.22) we can assess the quality of this assignment. This procedure may work well when the band of interest is monotonous as a function of $k > 0$, but if the band has a double-k region, the finite-chain calculations may lead to orbitals that contain arbitrary linear combinations of the energetically degenerate band orbitals with different k.

An alternative could be to study the coefficients $\{C_{pj}(k)\}$ themselves. This could be done with the help of the quantity

$$Q^I_j(k) = \sum_p |C_{pj}(k)|^2, \tag{3.23}$$

which simply gives the contribution of the k value to $|\hat{p}_j|$ in equation (3.18). Then, we may consider a k mesh defined by

$$k_q = \frac{\pi}{(N+1)a}\, q, \qquad \text{with} \quad q = 1, 2, \ldots, N. \tag{3.24}$$

With this set of k values, the transformation of equation (3.9) is no longer unitary, but since we do not calculate any expectation value this fact should not cause a problem. Instead, we will seek the major contribution to the momentum, i.e., the maximum of $Q^I_j(k_q)$. Often, $Q^I_j(k_q)$ has a narrow peak for k_q close to the expectation value of equation (3.21). However, when, for the infinite periodic system, more band orbitals with different k are energetically degenerate, Q^I_j may possess more peaks. When these peaks are of comparable height, a k assignment becomes difficult.

Our model calculations in the absence of the electrostatic field showed that the

band structures obtained by this method agreed well with those obtained from the periodic-system calculations, and even when a weak, non-vanishing field was included a realistic set of band structures was obtained. However, we observed some shifts of the assigned k values, mainly for the smallest values $k \to 0$ which caused some differences for the band structure between finite and infinite systems. Another problem that we observed was that some orbitals (with different energies) were associated to the same k_q value which in particular happened for the orbitals close to the HOMO and LUMO. In that case it was often possible to obtain smooth band structures by carefully selecting one of the k_q values, which, however, is a cumbersome and biased procedure. In other cases, a unique identification of the k was not possible, leaving some 'holes' in the band structures, which might be filled by interpolation. In total, this method was not optimal and often not able to automatically provide a 'good' set of band structures. One reason for the problems could be that some orbitals for the finite system was localized to the terminations and, accordingly, hardly resembled periodic-system orbitals. With this in mind we developed the method to be described in the subsequent subsection.

3.2.2 Method 2: Fitting the Contributions of the Central Region

As an alternative to transform the results for the finite-system one may instead study the periodic-system orbitals of equation (2.42). In this case, due to time-reversal symmetry, $\psi_j(k, \vec{r})$ and $\psi_j(-k, \vec{r})$ are energetically degenerate and, similarly that in equation (3.20), it is possible to choose

$$C_{pj}(-k) = C^*_{pj}(k). \tag{3.25}$$

Then, from the two energetically degenerate orbitals, we may construct new ones that have the same energy,

$$\begin{aligned} \tilde{\psi}_j(k, \vec{r}) &= a_1 \psi_j(k, \vec{r}) + a_2 \psi_j(-k, \vec{r}) \\ &= \sum_p \sum_n \frac{1}{\sqrt{N}} \left[a_1 C_{pj}(k) e^{ikan} + a_2 C_{pj}(-k) e^{-ikan} \right] \chi_{pn}(\vec{r}). \end{aligned} \tag{3.26}$$

In equation (3.8), the orbital expansion coefficients for the finite system, c_{pmj}, were chosen to be real. Thus, in order to establish a relation between the finite and the infinite system, it will be useful to require that the sum in the square brackets of

equation (3.26) is real, too. By writing

$$C_{pj}(k)e^{ikan} = x + iy, \tag{3.27}$$

we get

$$\begin{aligned} a_1 C_{pj}(k)e^{ikan} + a_2 C_{pj}(-k)e^{-ikan} &= a_1 C_{pj}(k)e^{ikan} + a_2 \left[C_{pj}(k)e^{ikan}\right]^* \\ &= a_1(x+iy) + a_2(x-iy) \\ &= (a_1+a_2)x + i(a_1-a_2)y. \end{aligned} \tag{3.28}$$

In this equation, n takes many different values, so that the expression can only then be real if the complex numbers a_1 and a_2 fulfill that $a_1 + a_2$ is real and $a_1 - a_2$ is imaginary, i.e., $a_2 = a_1^*$, or

$$\begin{aligned} a_1 &= ae^{i\phi} \\ a_2 &= ae^{-i\phi}. \end{aligned} \tag{3.29}$$

with $a = 1/\sqrt{2}$. By writing

$$\frac{1}{\sqrt{2}} e^{i\phi} C_{pj}(k) \equiv \tilde{C}_{pj}(k) \equiv \frac{1}{2}\left(A^k_{pj} - iB^k_{pj}\right), \tag{3.30}$$

the expression in Eq. (3.28) becomes

$$\tilde{C}_{pj}(k)e^{ikan} + \tilde{C}^*_{pj}(k)e^{-ikan} = A^k_{pj}\cos(kan) + B^k_{pj}\sin(kan). \tag{3.31}$$

This expression will be compared with the expression for the orbitals for the finite system, whereby we will consider only that part of the finite system (the central region) that is sufficiently far from the terminations. In that region, the expansion coefficients to the orbitals are sought written as

$$c_{pmj} = a_{pm}\cos(kam) + b_{pm}\sin(kam). \tag{3.32}$$

Our goal is to find the appropiate k for the obtained coefficients $\{c_{pmj}\}$. We notice that there is some arbitrariness in the choice of the unit-cell index, m. Thus, changing

$$m \to m + \Delta m$$

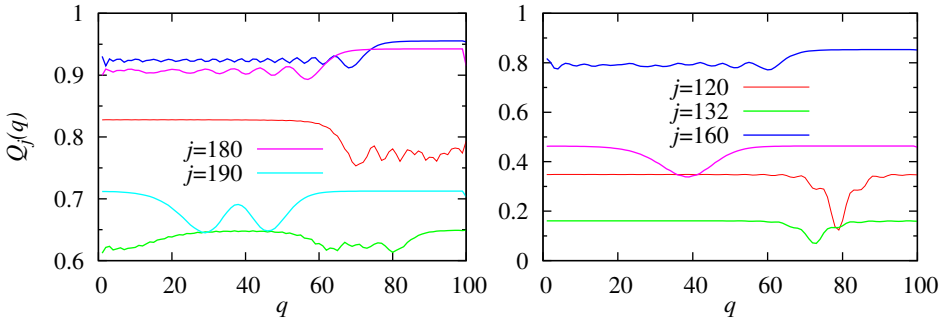

Figure 3.3: $Q_j^{II}(q)$ defined in equation (3.33) for different orbitals of the valence band with $t = 10$ (left) and $t = 30$ (right). The system is a 100-units chain, with $a = 2.3$ and an applied electrostatic field of strength $E_{\mathrm{DC}} = 0.0005$ a.u.

would change the values of the quantities in equation (3.32), but would not lead to a different k.

Accordingly, for each orbital, j, we seek that value of k_q for which

$$Q_j^{II}(k_q) = \sum_{m=t+1}^{N-t} \sum_{p} [c_{pmj} - x_{pj}(q)\cos(k_q am) - y_{pj}(q)\sin(k_q am)]^2 \tag{3.33}$$

has its minimum. The set of k_q values is given by equation (3.24). The t parameter is the number of units (at each termination) whose contribution is ruled out from the summation of equation (3.33), defining in this way a central region of $N - 2t$ units. The quantities $x_{pj}(q)$ and $y_{pj}(q)$ are fitting constants that for each k_q shall be adjusted in order to minimize $Q_j^{II}(k_q)$. We add that this approach can be considered a generalization of what was presented by Pomogaeva et al. [23].

In the ideal case, $Q_j^{II}(k_q)$ will lead to a narrow and single minimum with a value close to zero for each orbital j. In our model calculations, we did indeed find such a case for the first and fourth bands in the absence of an external field, similar to what we found in the previous subsection. However, the present approach becames less easy to apply for the valence and conduction bands. Even without the electrostatic field, the single peak of $Q_j^{II}(k_q)$ splits into two for orbitals whose energies are found in the double-k region. Moreover, in the presence of a field, the minimum of $Q_j^{II}(k_q)$ becomes much broader and the function shows an oscillatory behaviour. However, by varying the size of the central region, it became possible to change the shape of the Q_j^{II}-functions so that in most cases a single minimum could be identified.

This can be seen in figure 3.3 where Q_j^{II} for some orbitals of the second band is

plotted with $t = 10$ (left) and $t = 30$ (right). The system consists of 100 units and is exposed to an electrostatic field of strength 0.005 a.u. The overall effect of reducing the central region is a general shift downward of Q_j^{II}, decreasing also the oscillations until, eventually, the function has a well identifiable single (or double) minimum. Examples of that are the Q_j^{II}-functions for the orbitals $j = 120$, $j = 132$ and $j = 180$ (red, green and magenta lines respectively), that have a single minimum with $t = 30$ but not with $t = 10$. In fact, the orbital $j = 180$ has the wavenumber of the HOMO, but there are several orbitals with the same k_q. The orbital $j = 190$ (cyan line) has an energy in the double-k region, therefore its Q_j^{II}-function exhibits two similar minima with $t = 10$ (left), but it vanishes for $t = 30$ (right). The Q_j^{II}'s for different orbitals change differently as a function of t, whereby for some of them one obtains rapidly a single- or a double-minimum structure, while others, such as the orbital $j = 160$ (blue line), need a higher value of t to exhibit a simple minimum. It turned out that in some cases, a minimum of $Q_j^{II}(k_q)$ can be identified for a small t, whereas the function essentially vanishes for larger t. However, we found that each Q_j^{II}-function has a minimum close to zero for a certain t before the function vanishes. This gives us a reliable criterion to assign the k value to each finite-system orbital.

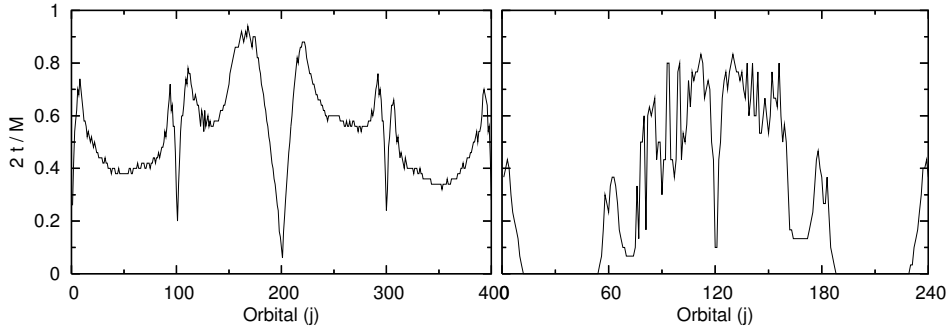

Figure 3.4: The optimized t-value as a function of orbital index. The system of left (right) panel is a chain of $N = 100$ (60) units with a lattice constant $a = 2.3$ ($a = 2.0$) in presence of an electrostatic field with a strength of $E_{DC} = 0.0005$ a.u. (both cases). The k-dependent orbitals are ordered according to increasing energy. The Fermi energy is between the second and third band.

By letting t to be a variable that is determined for each orbital separately so that a well-defined minimum is identified, we can uniquely determine the k value for each orbital. The resulting t values from this automatic procedure are shown in figure 3.4. The optimized t tends to be larger at the band edges, resulting in a smaller central region for those orbitals. A second finding is that some of the orbitals close to the band

edges have very widespread Q_j^{II}-functions that vanish for smaller t, without exhibiting an identifiable minimum. These orbitals can in the figure be identified as those for which pronounced drops occur at all the band edges in the left panel, but only at the band gap in the right panel. These orbitals are mainly localized to the termination regions of the finite chains, so that they hardly correspond to orbitals that can be recovered for the infinite, periodic system, and, therefore, can be excluded from our analysis. A third finding from figure 3.4 is that t is smaller in the middle of each band. Finally, the problem related to orbitals with energies in the double-k region is also manifested through the oscillating line around the band gap in the right panel.

The method of this subsection is based on the assumption that it is possible to reproduce the orbitals of the infinite and periodic chain by fitting the orbitals of the long but finite chain in a variable central region [equation (3.33)], which works well in the absence of an external electrostatic field. However, the inclusion of the field leads to some smaller but noticeable inconsistencies described in the previous paragraph, mainly because the orbitals are distorted and become more or less localized at the terminations. For this reason, we decided to study a third approach described below.

3.2.3 Method 3: Fourier Analysis

Given the results of the previous methods, we turned to directly analyze the spacial distribution of the orbitals along the chain. Since the used basis functions have the same (spherical) symmetry, the coefficients c_{pmj} with different p of the jth orbital for the finite chain show a very similar m-dependence. Therefore, we define for each j orbital the discrete function,

$$b_j(m) = \sum_p c_{pmj}. \tag{3.34}$$

In a first study we considered a chain with 60 units and $a = 2.0$ in the absence of an external field. For this, b_j could be accurately fitted by

$$b_j(m) \simeq A \sin\left(\frac{\pi q m}{N+1}\right) \qquad \text{with} \quad m = 1, 2, \ldots, N \tag{3.35}$$

The denominator in the argument to the sine function equals $N+1$ and not N so that the function does not vanish at the first and last unit, but (hypothetically) for $m = 0$ and $m = N+1$. Thus, the finite chain of N units gives orbitals similar to those of an infinite periodic chain with a Born von Kármán zone of $2(N+1)$ units. If some orbital has an energy in the double-k region, we find that $b_j(m)$ resembles a superposition of

two functions of the type of equation (3.35), i.e., sinusoidals with different frequencies. Therefore, a more general and useful approach is to perform a Fourier analysis on the b_j-functions.

We make accordingly a discrete Fourier transform of the coefficients $b_j(m)$,

$$\begin{aligned} B_j(q) &= \frac{1}{\sqrt{N+1}} \sum_{m=0}^{N} b_j(m) \exp\left(\frac{-i2\pi qm}{N+1}\right) \\ &= \frac{1}{\sqrt{N+1}} A_j(q) \exp[i\phi_j(q)] \end{aligned} \tag{3.36}$$

where we have included $b_j(0) = 0$ so that the periodicity becomes $N+1$. B_j is a complex number with amplitude $A_j(q)$ and phase $\phi_j(q)$. $A_j(q)$ is the contribution of the sinusoid with frequency $qm/(N+1)$ to $b_j(m)$. Therefore, that $q_j = q$ for which the amplitude is largest can be used in assigning a k value to the orbital of interest. Moreover, once the biggest contribution has been identified at q_j, we can compare only the corresponding sinusoid,

$$f_j(m) = b'_j \cos\left(\frac{2\pi q_j m}{N+1} + \phi_j(q_j)\right), \tag{3.37}$$

with the b_j-function of equation (3.34), and define the parameter

$$\Delta b_j = \left\{ \frac{\sum_m [b_j(m) - f_j(m)]^2}{N\, b'_j} \right\}^{1/2}, \tag{3.38}$$

to quantify the quality of the wavenumber assigment for each j-orbital. By defining the amplitud $b'_j = \max\{\text{abs}[b_j(m)]\}$ in equation (3.37), we can also identify, through the Δb_j, when the orbital is highly localized.

However, since $b_j(m)$ is real, we do not have N independent expansion coefficients, $B_j(q)$, but instead $B_j(q) = -B_j(N+1-q)$. In order to extract more information from the finite-system calculations we, therefore, decided to replace 2π by π in the arguments in equations (3.36) and (3.37). Thereby the transformation of equation (3.36) is no longer unitary which, however, for our purposes is not important. Hence, if $A_j(q)$ has its maximum at a certain q_j and Δb_j is lower than a pre-defined cutoff value, the wavenumber

$$k = \frac{\pi}{(N+1)a} \cdot q_j$$

is assigned to the jth orbital.

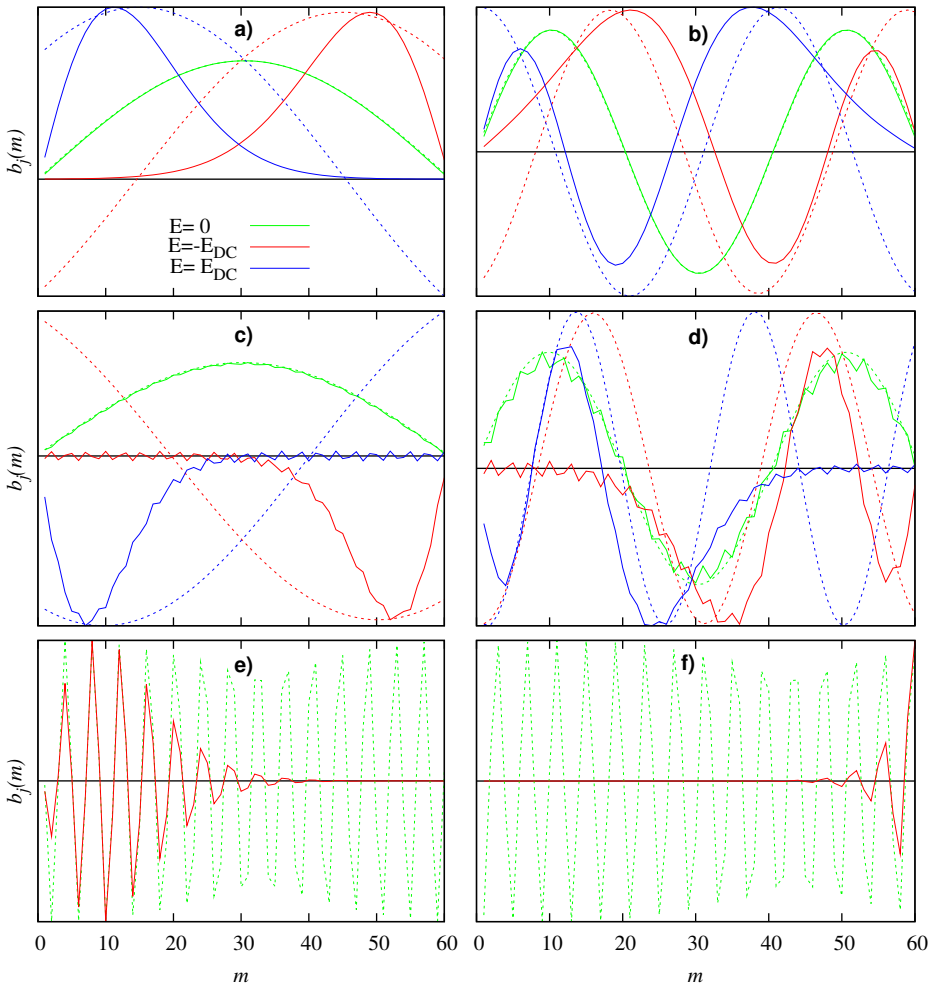

Figure 3.5: $b_j(m)$ in solid lines and $f_j(m)$ in dotted lines for the system in the absence as well as in the presence of an electrostatic field with strength of $E_{DC} = \pm 3 \times 10^{-4}$ a.u. for different orbitals: **a)** $q_j = j = 1$ and **b)** $q_j = j = 3$ belonging to the first band; **c)** $j = 77$, $q_j = 1$, **d)** $j = 79$, $q_j = 5$, **e)** $j = 118$ and **f)** $j = 120$ of the second band, both with $q_j = 30$.

We applied this method to a 60-units chain in the absence of an external field and found $q_j = j$ for $j = 1, 2, \cdots, 60$ for the energetically lowest band. Similarly, for the energetically highest (fourth) band (with j running from 181 to 240) we obtained $q_j = 241 - j$. The orbitals of the second and third bands in the double-k region exhibit some superposition of the functions of the type given in equation 3.35, so that the q_j's jump back and forth when orbitals of increasing energy are considered. Nevertheless, it was possible to assign a k value to almost all orbitals with the orbitals 120 and 121, i.e., the HOMO and LUMO, being the only exceptions. These were strongly localized at

the terminations (very similar to what is shown in figure 3.5 b) and were, accordingly, not relevant for the infinite and periodic system.

When the electric field is included, the orbitals are perturbed in different ways. This is exemplified in figure 3.5. In the four upper panels, $b_j(m)$ and the corresponding $f_j(m)$ are shown both without and with the inclusion of an electrostatic field. As can be seen, the orbitals change shape with the inclusion of the electric field although their overall structure (i.e., numbers of maxima and nodes) remains unchanged. This change in shape is more evident for small k and it is even larger for the second (figure 3.5 a and b) and third bands. However, the automated procedure to determine q_j seems to be adequate because $f_j(m)$ provides good approximations to $b_j(m)$. The values of q_j that are determined can be seen to correlate with the number of nodes of the dotted curves. However, there are some deviations from this general rule. Thus, whereas it is well fulfilled for the cases $q_j = 1$ and $q_j = 3$, deviations are seen in figure 3.5 d (i.e., for the 79th orbital) where the dotted line have 5 nodes. This means that the dominating contribution to the Fourier expansion of $b_{79}(m)$ in the presence of the electrostatic field originates from $q_{79} = 5$ although $b_{79}(m)$ has only 3 maximals as is the case for the orbital in the absence of the field (solid line). In cases like this, we correct by hand the automatically identified values of q_j, although we emphasize that this procedure was necessary for only few orbitals. In figure 3.5 c and d one may also observe a trend towards a superposition of sinusoidals with different q. This is a result that is found for orbitals whose energies are in the double-k region. Finally, in the bottom panels, two examples of orbitals ($j = 118$ and $j = 120$) with different degree of localization are shown. Their corresponding $f_j(m)$'s are both plotted for $q_j = 30$. The HOMO ($j = 120$) is practically unchanged from the field-free case, but the inclusion of the external field leads to a localization of those orbitals that have energies close to the band gap or the band edges.

3.2.4 The Finite-System Band Structures

Ultimately, the purpose of the present study is to reveal whether a finite-system calculation can provide results that are sufficiently accurate to extract a band structure for the infinite-system limit. As discussed above, this would ultimately mean that it would be possible to identify an optimal set of phase factors for the infinite-system orbitals. To this end, we used the three methods described in the previous section in order to extract the band structures for the finite chain.

It turned out that for all three methods it was uncomplicated to extract the band

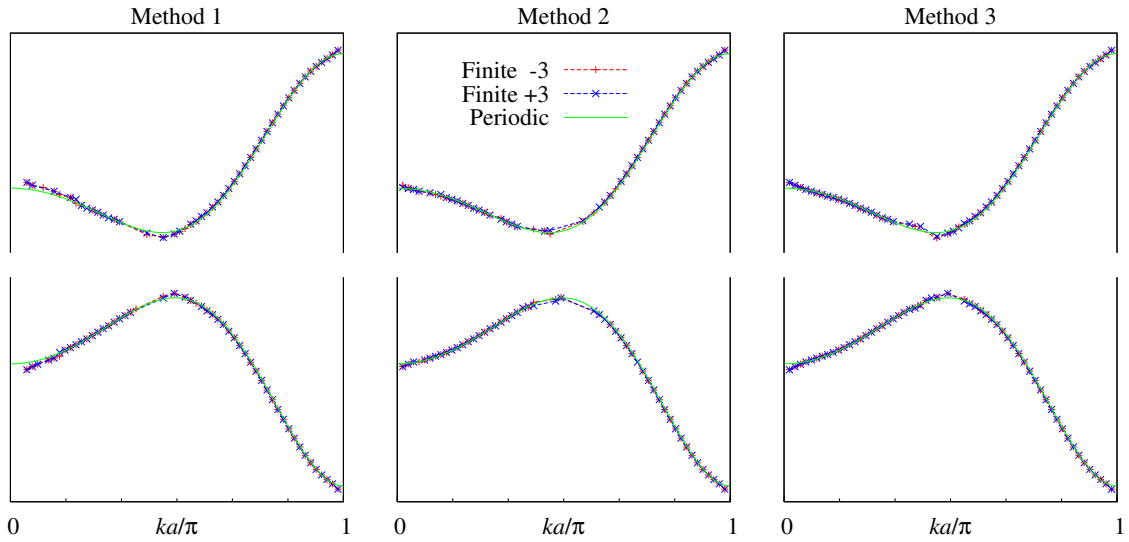

Figure 3.6: The calculated band structures for the infinite, periodic system in comparison with those extracted from the finite-chain results. Only the second and third bands are shown. The finite chain consists of 60 AB units with a lattice constant $a = 2.0$. The field strength was set equal to $E_{\mathrm{DC}} = \pm 0.0003$ a.u. $+$ and $\times$ mark finite-system results, whereas the solid curves mark the periodic-chain results. For the latter, the differences between the results for the two field strengths cannot be resolved in the figure.

structures in the absence of an electrostatic field, but with its inclusion, the k assignments of the different methods was non-trivial, whereby each method showed its own complications. Nevertheless, for all methods it was advantageous to consider only weak field strengths between -0.0003 and 0.0003 a.u. In figure 3.6 the resulting band structures are presented extracted from the results for a finite system consisting of 60 units both in the absence and in the presence of an external electrostatic field.

The problems related to the first method are evident in the left panel: in the region $k \to 0$ several orbitals were ruled out from the band structure by the algorithm and the points for the smallest values of k were shifted by a considerable amount. Moreover, for several orbitals in the regions close to the HOMO and LUMO, the method is not capable of identifying k. As mentioned in the previous sections, this region is the most problematic one, and the number of 'holes' increases with the field strength. The results obtained by the second method are slightly different in this region, giving lower energies for the orbitals of the second band and higher values for those of the third band. This difference is related to how the orbital (and its energy) is selected when two orbitals have been assigned the same k value. It is worth to emphasize that the orbital

energies of the finite system are the same for the three methods; the only difference lies in how the wavenumbers are assigned and which orbital energies are ruled out from the band structure. Often, those orbitals that are excluded are more localized than the others, as is the case in figure 3.5 e and f. Thus, they could be located in the band gap just between the considered HOMO and LUMO. Of the three methods, the third method appears to be the most adequate, and the problems found for the other two methods are here less pronounced.

3.3 The Phase Factors

As just mentioned, the ultimate goal is to obtain a unique set of band structures for an infinite, periodic system exposed to an electrostatic field, something that is not possible with present periodic-system approaches. Thus, once the band structures have been extracted from the finite-system results, we compare those with those of the infinite periodic system in the presence of an electrostatic field of the same strength,

$$\Delta\varepsilon_{jq} = \Delta\varepsilon_j(k_q) = \varepsilon_j^P(k_q) - \varepsilon_j^F(k_q). \tag{3.39}$$

Here, j marks the band, the set of k_q values were defined in equation (3.24), and P and F mark the periodic and finite system, respectively. Then, according to equation (3.4),

$$\frac{d}{dk}\phi_j(k) = \frac{\Delta\varepsilon_j(k)}{E_{\mathrm{DC}}}, \tag{3.40}$$

from which we may calculate numerically $\phi_j(k)$,

$$\phi_j(k_q) \approx \sum_{i=1}^{q} \frac{\Delta\varepsilon_{ji}}{E_{\mathrm{DC}}}\Delta k = \frac{\pi}{(N+1)aE_{\mathrm{DC}}} \sum_{i=1}^{q} \Delta\varepsilon_{ji}. \tag{3.41}$$

An important quantity is the integral (sum) over the whole BZ. Using that $\Delta\varepsilon_j(k_q) = \Delta\varepsilon_j(-k_q)$, the total phase change of one band is

$$\Phi_j = 2 \cdot \phi_j\left(\frac{\pi}{a}\right) \approx \frac{2\pi}{(N+1)aE_{\mathrm{DC}}} \sum_{q=1}^{N} \Delta\varepsilon_{jq}, \tag{3.42}$$

which should be related to $\tilde{n}_j$ of equation (2.31),

$$\Phi_j = 2\pi \cdot \tilde{n}_j. \tag{3.43}$$

Thus, in our case with two doubly filled bands, the sum of $\tilde{n}_j$ over all filled bands equals

$$\tilde{n} = 2(\tilde{n}_1 + \tilde{n}_2) = \frac{1}{\pi}(\Phi_1 + \Phi_2). \tag{3.44}$$

As discussed elsewhere [21], this value can be interpreted as the total charge (in units of the elementary charge) accumulated at the terminations of the finite system.

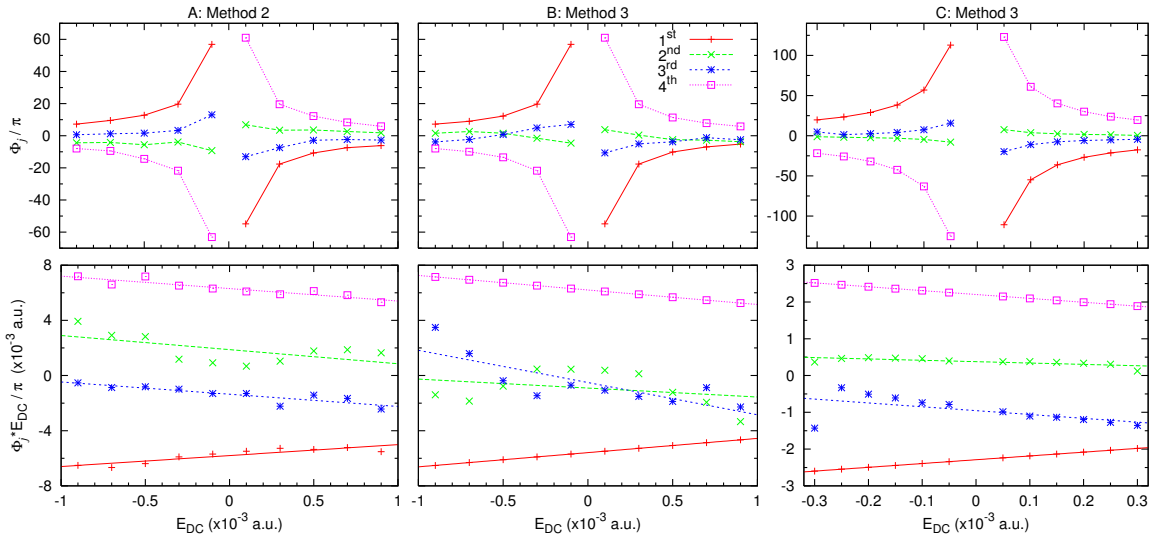

Figure 3.7: Results for Φ_j/π (upper panels) and $\Phi_j \cdot E_{\mathrm{DC}}/\pi$ (lower panels) calculated by Eqs. (3.42) and (3.45) for the four bands as a function of the external field using the second and third method in extracting the band structures. The right-most panels show the results for a smaller range of field strengths. The straight lines in the bottom panels represent linear fits.

The last equations above deserve some discussion. First, the numerical integral of equation (3.41) is defined only up to a constant that is not of importance here, because only the difference between $\phi_j(-\pi/a)$ and $\phi_j(\pi/a)$ defines Φ_j. Second, the problems related to the wavenumber assignment translate into small uncertainties in the energy differences, ε_{jq}, whereby Φ_j becomes more sensitive to those uncertainties when the field is weaker. Third, the energy differences are larger at the band edges, $k \to 0$ and $k \to \pi/a$, and in the k regions of the neighborhood of the HOMO and LUMO in the second and third band, respectively. Fourth, the difference at exactly $k = \pi/a$ is excluded in the sum in equation (3.42). For all these reasons one cannot expect to obtain an accurate but only an approximate value for Φ_j.

The results of figures 3.6 and 3.7 show that the three different methods for extracting the band structures yield similar, but not identical results. This does indeed

Band	A	B	C
1^{st}	0.895	1.031	1.030
2^{nd}	-1.024	-0.650	-0.370
3^{rd}	-0.888	-2.334	-1.046
4^{th}	-0.902	-1.053	-1.055
$\tilde{n}$	-0.129	0.381	0.660

Table 3.1: The slopes m_j of the lines plotted in bottom panels of figure 3.7 and the sum of the first two slopes.

suggest that it is not possible to determine uniquely the band structures for an infinite, periodic system in the presence of an electrostatic field, which is in agreement with the formalism for calculating the band structures. This issue becomes even more clear when attempting to determine $\tilde{n}$. Due to the small values of E_{DC}, $\tilde{n}$ tends to reach quite large values, as can be seen in the upper panels of figure 3.7. In particular for the smallest values of $|E_{\mathrm{DC}}|$, the calculated values of $\tilde{n}$ are very large, supporting that in this case, the application of equation (3.42) is connected with large numerical inaccuracies. The large values of $\tilde{n}$ must be considered unrealistic: $\tilde{n}$ can be interpreted as related to the number of elementary charges accumulated at the terminations of the large, finite systems, and from the way the model system has been constructed we know that this number should lie close to 0.

It turned out, however, that a higher numerical accuracy could be achieved by considering

$$\frac{\Phi_j(E_{\mathrm{DC}})}{\pi} E_{\mathrm{DC}} = \frac{2}{(N+1)a} \sum_{q=1}^{N} \Delta\varepsilon_{jq} = m_j \cdot E_{\mathrm{DC}} + a_j. \tag{3.45}$$

m_j is then related to $\tilde{n}_j$ and a_j quantifies the inaccuracy of the approach. This quantity, as a function of E_{DC} is shown in figure 3.7, too. As shown in the middle and right panels in the bottom row of this figure, in this case more stable results are found when concentrating on weaker fields. This is clearly in contrast to what we find when considering the equivalent panels in the upper row, and it is a promising finding that, numerically, the results for the weaker fields are more reliable than those for the stronger fields. We add that the values of the slopes m_j's do hardly change for different chain lengths, and in most of the cases they did not vary much when changing the method or the field range, whereas the y-intercept, a_j, was more arbitrary.

The obtained m_j slopes from the bottom panels of figure 3.7 are shown in Table 3.1. In most of the cases the value of m_j is between -2 and $+2$, and the sum of the

m_j over the occupied bands, is close to 0. This is satisfactorily, as it implies that no extra charge is accumulated at the terminations, in agreement with other results of the model calculations.

3.4 Conclusions

The purpose of this chapter was to explored whether it is possible to determine uniquely the band structures of an infinite, periodic system exposed to an electrostatic field. The Vector Potential Approach formalism for the treatment of such a situation does not offer a unique set of band structures but, instead, they depend on the phases of the orbitals and, in particular, their k dependence. As an alternative, we explored whether the results for large but finite systems exposed to the same field (for which the orbital energies are unique) could provide the desired information.

For this aim, first we need the band structure of both systems. However, it turned out that using the orbitals of the finite system exposed to an electrostatic field constitutes a particularly difficult case for extracting band structures from finite-system results. Therefore, we suggested and discussed three different approaches of which, at least for the present study, the third proposal was the better one in the sense that a larger set of finite-system orbitals could be assigned to a k value. Nevertheless, we cannot exclude that for other cases, other approaches may be better suited which is why we have chosen to present all three.

The constructed band structures were found to be very close to those calculated directly for the infinite and periodic system exposed to the electrostatic field using the Vector Potential Approach. We emphasize, however, that the changes in the finite-system band structures upon the inclusion of the field are very small. Nevertheless, the three approaches did not lead to identical band structures due to the distortion of the spatial distribution of the orbitals caused by the field. Without the electrostatic field, most of the orbitals are distributed over the complete system, but when the field is included, the largest part of the orbitals becomes more or less localized to one or the other end. This localization makes it difficult to assign a k value to them. On the other hand, the total electron distribution remains regular in a larger or smaller central region where the effects of the terminations are not felt.

The differences in the band structures extracted from the finite-system calculations and those of the periodic counterparts are related to additional phase factors in the periodic-system calculations. Ultimately, the total set of those additional phase factors

can be used (with a finite-difference approximation) to estimate charges accumulated at the terminations, and, here, we found that this approach could be numerically very unstable because very small energy differences have substantial effect in the calculated phase factors. A reformulation of the approach could stabilize it somewhat, but uncertainties remained.

The final conclusion of this chapter is that it is not possible to determine uniquely the band structure for an infinite, periodic system exposed to an electrostatic field. However, as it was mentioned at the beginning of this chapter, the integer $\tilde{n}$ associated with the phase factors can be used to simulate, in a crystal-orbital calculation, the charge transfer between the ends of a long chain. In that case, we can say that the correctness of $\tilde{n}$ is confirmed if the dipole moment per unit lies in the appropiate range.

Chapter 4

Studying the DFT Overestimation of the Responses

When focusing on responses to perturbing electric fields, the key quantity is the total dipole moment that, together with the field-induced contributions, i.e., the linear polarizability and the non-linear hyperpolarizabilities, contains all relevant information. A detailed understanding of how these properties depend on structure and composition of the materials has not yet been obtained. Thus, when attempting to optimize some of the responses for special purposes, one is forced to use, in part, a trial-and-error approach that may be both time-consuming and without guarantee of success. Theoretical studies of various properties are often useful in identifying adequate candidate systems and a similar approach can also be applied for the responses to electric fields. In that context, density- functional calculations are often used for determining the electronic properties of materials.

However, about 15 years ago, a significant overshoot of electric dipole properties calculated by density-functional theory (DFT) for polyacetylene chains of increasing size was found [24, 25] by comparing with the results of ab-initio calculations. This behavior was latter found for other quasilinear systems [26], as well and attributed to an incomplete screening of the external electric field within the DFT treatment. It has been suggested, among other things, that the overestimates can be alleviated by improving the exchange-energy functional [27, 28] or by including self-interaction corrections [29].

More specific, for regular systems (large systems that consist of a regularly repeated sequence of identical units with deviations from regularity only near the terminations) the linear and non-linear responses per repeat unit, in the thermodynamic limit, will

be independent of the system size. The DFT calculations predicted that this limit will be reached for much larger systems than what is found by the HF method and with much larger property values. Although the HF results are altered when correlation effects are included, this difference is small compared to the difference between HF and DFT calculations [30–32]. Therefore, it may be useful to completely ignore correlation effects which is what we shall do in the present work.

In order to understand this deficiency of DFT calculations, the resulting polarization and charge transfer along the chain have been analyzed [24, 26] and systems of higher dimension have also been studied [33]. However, accurate electronic structure calculations for large systems are computationally demanding and one may have to introduce approximations whose effects on the results are only approximately known. On the other hand, for smaller systems the thermodynamic limit will not be reached making it difficult to extract the desired information.

All of the cited studies have been carried out for finite systems, for which the calculation of the dipole moment is straightforward even in the presence of an electrostatic field. This situation is different when considering the system as being periodic and infinite. Although all real systems are finite, it is often of enormous advantage to calculate their properties by assuming they are infinite and periodic, whereby the thermodynamic limit is automatically reached. For that goal, here we use the VPA explained in the second chapter. It has been shown, through comparison with large finite systems, that the VPA can also account for effects due to terminations [19, 21, 22]. Even though, it has been rigorously established that the dipole moment per unit is a bulk property [12].

In this chapter we shall present results of model studies designed to obtain detailed information on the differences between HF and DFT descriptions of the responses of quasi-one-dimensional, extended systems (chains) to electrostatic fields. The model that will be employed has certain appealing features. First, it is so simple that even large (but finite) systems can be treated accurately without having to bother about errors due to truncations of various infinite summations in direct or reciprocal space. Second, we assume that an accurate description can be obtained when expanding the electronic orbitals in a particularly simple set of basis functions. This set is so constructed that gradient approximations within the DFT can be ignored. Third, with this basis set it becomes possible to separate the responses into atom- or unit cell-specific contributions. Finally, it is possible to use this approach within the VPA for the infinite and periodic system. In that case, additional information on the problems

behind the DFT overestimate can be obtained as we shall demonstrate.

4.1 Model II-A: The Finite Case

The model is very similar to that shown in figure 3.1. It describes a quasi-linear chain with two atoms per repeated unit. The positions of the two atoms are

$$\vec{R}_{pn} = \vec{R}_{p0} + n\,\vec{a}, \qquad n = -N, -N+1, \ldots, N-1, N. \tag{4.1}$$

Here, n labels the unit and p the atom. $\vec{R}_{p0}$ are the positions in the reference central (0th) unit. Moreover, $\vec{a}$ is the lattice vector that is supposed to be along the z axis. Accordingly,

$$\sum_{n=-N}^{N} z_{pn} = \sum_{n=-N}^{N} (z_{p0} + na) = (2N+1) z_{p0}. \tag{4.2}$$

If each unit has P atoms and $2B$ electrons, then the nuclear charges assumed to be,

$$Q = +\frac{2B}{P}, \tag{4.3}$$

in order to keep the whole system neutral. Ignoring the spin polarization, we will have $N_O = (2N+1)B$ doubly occupied molecular orbitals for the system. In presence of the electrostatic field $\vec{E} = (0, 0, E_{\mathrm{DC}})$, the single particle equations can be written as in equation (2.35),

$$\left(\hat{h} + E_{\mathrm{DC}}\,\hat{z}\right)\psi_i(\vec{r}) = \varepsilon_i \psi_i(\vec{r}), \tag{4.4}$$

where $\hat{h}$ is either the Fock operator,

$$\hat{F} = \hat{h}_1 + \hat{V}_{\mathrm{n}} + \sum_{j=1}^{N_O} \left(2\hat{J}_j - \hat{K}_j\right), \tag{4.5}$$

or the Kohn-Sham operator,

$$\hat{h}_{\mathrm{KS}} = \hat{h}_1 + \hat{V}_{\mathrm{n}} + \sum_{j=1}^{N_O} 2\hat{J}_j - \hat{V}_{\mathrm{x}}. \tag{4.6}$$

In both cases $\hat{h}_1$ contains the kinetic-energy operator and eventually other potentials, whereas $\hat{V}_{\mathrm{n}}$ is the potential from the nuclei and the core electrons; $\hat{J}_j$ and $\hat{K}_j$ are the Coulomb and exchange operators from the jth orbital, respectively. Finally, $\hat{V}_{\mathrm{x}}$ is the

exchange potential within density-functional theory.

We shall expand $\psi_j(\vec{r})$ in a set of basis functions,

$$\psi_j(\vec{r}) = \sum_{p,n} c_{pnj}\chi_{pn}(\vec{r}), \tag{4.7}$$

where $\chi_{pn}(\vec{r})$ is the pth basis function of the nth unit. We shall here make a particularly simple choice with just one basis function per atom given by

$$\chi_{pn}(\vec{r}) = \begin{cases} \left(\frac{4\pi}{3}R_p^3\right)^{-1/2} & |\vec{r} - \vec{R}_{pn}| < R_p \\ 0 & |\vec{r} - \vec{R}_{pn}| \geq R_p, \end{cases} \tag{4.8}$$

i.e., a constant within a sphere of radius R_p around the atom where the function is centered and otherwise 0. Although this basis set hardly can be considered as providing a good approximation to the true solutions to the single-particle equations, they are so simple that the calculations can be done fast. Moreover, they have the advantage that the density becomes piecewise constant, which may be an interesting aspect when studying DFT approaches: there should be no contributions from gradient corrections (except, maybe, from the surfaces of the spheres, but let us ignore those here).

With this basis set the single-particle equations can be written in matrix form,

$$\left\{\underline{\underline{h}} + E_{\mathrm{DC}}\,\underline{\underline{M}}\right\} \cdot \underline{c}_j = \varepsilon_j\,\underline{\underline{O}} \cdot \underline{c}_j. \tag{4.9}$$

where the elements of the overlap and dipole moment matrices in our model are simply

$$\begin{aligned} O_{pn}^{qm} &= \langle\chi_{pn}|\chi_{qm}\rangle = \delta_{pq}\delta_{nm} \equiv \delta_{pn}^{qm}{}^{1} \\ M_{pn}^{qm} &= \langle\chi_{pn}|z|\chi_{qm}\rangle = z_{pn}\,\delta_{pn}^{qm}. \end{aligned} \tag{4.10}$$

Equivalently, the field can be included by an additional term in the single-particle Hamiltonian, which contributes solely to the diagonal matrix elements,

$$\langle\chi_{pn}|\hat{h}_{\mathrm{DC}}|\chi_{qm}\rangle = E_{\mathrm{DC}}\,z\,\delta_{pn}^{qm}. \tag{4.11}$$

[1] This definition is used throughout the whole document

We shall now build the effective $\underline{\underline{h}}$ matrix. First, we assume that

$$\langle \chi_{pn}|\hat{h}_1|\chi_{qm}\rangle = h_1{}^{qm}_{pn} = \begin{cases} s_p & (p,n)=(q,m) \\ -te^{-bR^{qm}_{pn}} & (p,n)\neq(q,m) \text{ and } R^{qm}_{pn}<R_0 \\ 0 & \text{otherwise.} \end{cases} \tag{4.12}$$

Here, s_p (the on-site energies), t and R_0 are chosen constants, while $R^{qm}_{pn} = |\vec{R}_{pn} - \vec{R}_{qm}|$. We have chosen to have non-zero matrix elements $h_1{}^{qm}_{pn}$ for certain $(p,n) \neq (q,m)$ although the basis functions are non-ovelaping. This may be considered unrealistic but otherwise the model would hardly be able to describe chemical bonding, at least within the DFT.

For the two-electron integrals we have

$$\begin{aligned} \langle \chi_{pn}\chi_{p'n'}|\hat{h}_2|\chi_{qm}\chi_{q'm'}\rangle &= \iint \frac{1}{|\vec{r}-\vec{r}\,'|}\chi^*_{pn}(\vec{r})\chi^*_{p'n'}(\vec{r}\,')\chi_{qm}(\vec{r})\chi_{q'm'}(\vec{r}\,')\mathrm{d}\vec{r}\mathrm{d}\vec{r}\,' \\ &= U(p,n,p',n')\delta^{qm}_{pn}\delta^{q'm'}_{p'n'}. \end{aligned} \tag{4.13}$$

We calculate the quantity $U(p,n,p',n')$ by using the usual Coulomb potential of a sphere of charge uniformly distributed,

$$V_{pn}(\vec{r}) = \int \frac{\chi^*_{pn}(\vec{r}\,')\chi_{pn}(\vec{r}\,')}{|\vec{r}-\vec{r}\,'|}\mathrm{d}\vec{r}\,' = \begin{cases} \frac{3}{2R_p} - \frac{|\vec{r}-\vec{R}_{pn}|^2}{2R_p^3} & |\vec{r}-\vec{R}_{pn}|<R_p \\ \frac{1}{|\vec{r}-\vec{R}_{pn}|} & |\vec{r}-\vec{R}_{pn}|\geq R_p. \end{cases} \tag{4.14}$$

Then, for $(p,n)\neq(p',n')$

$$U(p,n,p',n') = \int_{|\vec{r}-\vec{R}_{p'n'}|\leq R_{p'}} \frac{|\chi_{p'n'}(\vec{r})|^2}{|\vec{r}-\vec{R}_{pn}|}d\vec{r}. \tag{4.15}$$

This can be calculated by expanding the function (potential) centered at $\vec{R}_{pn}$ around $\vec{R}_{p'n'}$ and keeping only the lowest order (spherically symmetric) term. Since $\chi_{p'n'}(\vec{r})$ is spherically symmetric, this is the only term that will contribute,

$$\frac{1}{|\vec{r}-\vec{R}_{pn}|} = \frac{1}{|\vec{R}_{p'n'}-\vec{R}_{pn}|} + \dots \tag{4.16}$$

Then

$$U(p,n,p',n') = \begin{cases} |\vec{R}_{p'n'}-\vec{R}_{pn}|^{-1} & (p,n)\neq(p',n') \\ \frac{6}{5R_p} & (p,n)=(p',n'). \end{cases} \tag{4.17}$$

Finally,

$$\langle\chi_{pn}|\hat{V}_{\rm n}|\chi_{qm}\rangle = Q\,\delta_{pn}^{qm}\sum_{p',n'}V_{\rm n}(p,n,p',n'), \tag{4.18}$$

but, substituting

$$V_{\rm n}(p,n,p',n') = \begin{cases} -|\vec{R}_{p'n'}-\vec{R}_{pn}|^{-1} = -U(p,n,p',n') & (p,n)\neq(p',n') \\ -\frac{3}{2R_p} = -\left[U(p,n,p,n)+\frac{3}{10R_p}\right] & (p,n)=(p',n'), \end{cases} \tag{4.19}$$

we obtain,

$$\langle\chi_{pn}|\hat{V}_{\rm n}|\chi_{qm}\rangle = -Q\,\delta_{pn}^{qm}\left[\sum_{p',n'}U(p,n,p',n')+\frac{3}{10R_p}\right]. \tag{4.20}$$

The density inside the (p,n)'th atom is

$$\rho_{pn} = \frac{3}{4\pi R_p^3}\sum_{j=1}^{N_O}2|c_{pnj}|^2 = \frac{3}{4\pi R_p^3}\,\eta_{pn}, \tag{4.21}$$

where η_{pn} is the number of electrons of the (p,n)'th atom (the Mulliken population).

Then, within DFT

$$\langle\chi_{pn}|\hat{V}_{\rm x}|\chi_{qm}\rangle = \delta_{pn}^{qm}V_{\rm x}[\rho_{pn}], \tag{4.22}$$

where $V_{\rm x}[\rho_{pn}]$ is an expresion for the exchange potential of the density ρ_{pn}.

Both within HF and within DFT, the sum over the occupied orbitals of the Coulomb matrix elements can be written as,

$$\begin{aligned}\sum_{j=1}^{N_O}2J_{j\,pn}^{qm} &= \sum_{j=1}^{N_O}\sum_{p',n'}\sum_{q',m'}2c_{p'n'j}^{*}c_{q'm'j}\left[\langle\chi_{pn}\chi_{p'n'}|\hat{h}_2|\chi_{qm}\chi_{q'm'}\rangle\right] \\ &= \sum_{j=1}^{N_O}\sum_{p',n'}\sum_{q',m'}2c_{p'n'j}^{*}c_{q'm'j}\left[U(p,n,p',n')\delta_{pn}^{qm}\delta_{p'q'}^{q'm'}\right] \\ &= \delta_{pn}^{qm}\sum_{p',n'}\sum_{j=1}^{N_O}2|c_{p'n'j}|^2U(p,n,p',n') \\ &= \delta_{pn}^{qm}\sum_{p',n'}\eta_{p'n'}U(p,n,p',n'),\end{aligned} \tag{4.23}$$

using equation (4.13). On the other hand, within HF, the sum over the occupied

orbitals of the exchange matrix elements are

$$\begin{aligned}\sum_{j=1}^{N_O} K_{j}{}_{pn}^{qm} &= \sum_{j=1}^{N_O}\sum_{p',n'}\sum_{q',m'} c^*_{p'n'j}c_{q'm'j}\left[\langle\chi_{pn}\chi_{p'n'}|\hat{h}_2|\chi_{q'm'}\chi_{qm}\rangle\right] \\ &= \sum_{j=1}^{N_O}\sum_{p',n'}\sum_{q',m'} c^*_{p'n'j}c_{q'm'j}\left[U(p,n,q,m)\delta_{pn}\delta_{q'm'}\delta_{p'n'}\delta_{qm}\right] \\ &= \sum_{j=1}^{N_O} c^*_{qmj}c_{pnj}U(p,n,q,m) \\ &= \tilde{c}^{qm}_{pn}U(p,n,q,m), \end{aligned} \tag{4.24}$$

where we have defined,

$$\tilde{c}^{qm}_{pn} = \sum_{j=1}^{N_O} c_{pnj}c_{qmj} = \tilde{c}^{pn}_{qm}, \tag{4.25}$$

using that, in this case, all the coefficients c_{pnj} are real. Moreover, the Mulliken populations are the double of the diagonal elements: $\eta_{pn} = 2\tilde{c}^{pn}_{pn}$.

Summarizing, the matrix elements of the operators $\hat{V}_{\rm n}$, $\hat{h}_{\rm DC}$, $\hat{J}_j$ and $\hat{V}_{\rm x}$ are diagonal, while only $\hat{h}_1$ and $\hat{K}_j$ lead to symmetric matrices with non-vanishing off-diagonal elements. In total, substituting the expressions (4.20-4.24) in equations (4.5) and (4.6) and then in (4.9), the elements of the effective Fock matrix become

$$F^{qm}_{pn} = \delta^{qm}_{pn}\left[\sum_{p'n'}(\eta_{p'n'}-Q)U(p,n,p',n') - \frac{3Q}{10R_p} + E_{\rm DC}\, z_{pn}\right] + {h_1}^{qm}_{pn} - \tilde{c}^{qm}_{pn}U(p,n,q,m), \tag{4.26}$$

whereas the elements of the effective Kohn-Sham matrix become

$$h_{\rm KS}{}^{qm}_{pn} = \delta^{qm}_{pn}\left[\sum_{p'n'}(\eta_{p'n'}-Q)U(p,n,p',n') - \frac{3Q}{10R_p} - V_{\rm x}[\rho_{pn}] + E_{\rm DC}\, z_{pn}\right] + {h_1}^{qm}_{pn}. \tag{4.27}$$

4.1.1 Energy and Dipole Moment

Once the eigenvalue problem (4.9) is solved self-consistently, we can calculate the total electronic energy that, within the HF method, is given as

$$E_e = 2\sum_{i=1}^{N_O}\langle\psi_i|\hat{h}_1 + \hat{V}_{\rm n} + \hat{h}_{\rm DC}|\psi_i\rangle + \sum_{i,j=1}^{N_O}\left(2\langle\psi_i\psi_j|\hat{h}_2|\psi_i\psi_j\rangle - \langle\psi_j\psi_i|\hat{h}_2|\psi_i\psi_j\rangle\right)$$

$$= 2\sum_{i=1}^{N_O} \varepsilon_i - \sum_{i,j=1}^{N_O} \big(2\langle\psi_i\psi_j|\hat{h}_2|\psi_i\psi_j\rangle - \langle\psi_j\psi_i|\hat{h}_2|\psi_i\psi_j\rangle\big), \tag{4.28}$$

and within the DFT method is

$$\begin{aligned} E_e &= 2\sum_{i=1}^{N_O}\langle\psi_i|\hat{h}_1 + \hat{V}_{\rm n} + \hat{h}_{\rm DC} - \hat{V}_{\rm x}|\psi_i\rangle + \sum_{i,j=1}^{N_O} 2\langle\psi_i\psi_j|\hat{h}_2|\psi_i\psi_j\rangle \\ &= 2\sum_{i=1}^{N_O}\varepsilon_i - \sum_{i,j=1}^{N_O} 2\langle\psi_i|E_{\rm x} - V_{\rm x}|\psi_i\rangle - \sum_{i,j=1}^{N_O} 2\langle\psi_i\psi_j|\hat{h}_2|\psi_i\psi_j\rangle. \end{aligned} \tag{4.29}$$

With the present model

$$\begin{aligned} \sum_{i,j=1}^{N_O} 2\langle\psi_i\psi_j|\hat{h}_2|\psi_i\psi_j\rangle &= \sum_{i,j=1}^{N_O}\sum_{p,n}\sum_{p',n'}\sum_{q,m}\sum_{q',m'} 2c^*_{pni}c^*_{p'n'j}c_{qmi}c_{q'm'j}\langle\chi_{pn}\chi_{p'n'}|\hat{h}_2|\chi_{qm}\chi_{q'm'}\rangle \\ &= \sum_{i,j=1}^{N_O}\sum_{p,n}\sum_{p',n'} 2c^*_{pni}c^*_{p'n'j}c_{pni}c_{p'n'j}U(p,n,p',n') \\ &= 2\sum_{p,n}\sum_{p',n'}\left[\sum_{i=1}^{N_O}|c_{pni}|^2\sum_{j=1}^{N_O}|c_{p'n'j}|^2\right]U(p,n,p',n') \\ &= \frac{1}{2}\sum_{p,n}\sum_{p',n'}\eta_{pn}\eta_{p'n'}U(p,n,p',n'), \end{aligned} \tag{4.30}$$

as well as

$$\begin{aligned} \sum_{i,j=1}^{N_O}\langle\psi_i\psi_j|\hat{h}_2|\psi_j\psi_i\rangle &= \sum_{i,j=1}^{N_O}\sum_{p,n}\sum_{p',n'}\sum_{q,m}\sum_{q',m'} c^*_{pni}c^*_{p'n'j}c_{q'm'j}c_{qmi}\langle\chi_{pn}\chi_{p'n'}|\hat{h}_2|\chi_{q'm'}\chi_{qm}\rangle \\ &= \sum_{p,n}\sum_{q,m}\left[\sum_{i=1}^{N_O}c^*_{pni}c_{qmi}\sum_{j=1}^{N_O}c^*_{qmj}c_{pnj}\right]U(p,n,q,m) \\ &= \sum_{p,n}\sum_{q,m}|\tilde{c}^{qm}_{pn}|^2U(p,n,q,m). \end{aligned} \tag{4.31}$$

Moreover,

$$\begin{aligned} \sum_{i=1}^{N_O} 2\langle\psi_i|E_{\rm x} - V_{\rm x}|\psi_i\rangle &= \sum_{i,j=1}^{N_O}\sum_{p,n}\sum_{q,m} 2c^*_{ipn}c_{qmi}\langle\chi_{pn}|E_{\rm x} - V_{\rm x}|\chi_{qm}\rangle \\ &= \sum_{i=1}^{N_O}\sum_{p,n}\sum_{q,m} 2c^*_{ipn}c_{qmi}\big(E_{\rm x}[\rho_{pn}] - V_{\rm x}[\rho_{pn}]\big)\delta^{qm}_{pn} \end{aligned}$$

$$= \sum_{p,n} \sum_{i=1}^{N_O} 2|c_{pni}|^2 \big(E_{\rm x}[\rho_{pn}] - V_{\rm x}[\rho_{pn}]\big)$$
$$= \sum_{p,n} \eta_{pn} \big(E_{\rm x}[\rho_{pn}] - V_{\rm x}[\rho_{pn}]\big). \tag{4.32}$$

In both cases we need to add the total energy contribution from the nuclei,

$$E_{\rm n} = \frac{Q^2}{2} \sum_{p,n} \sum_{q,m} \big(1 - \delta_{pn}^{qm}\big) U(p,n,q,m) - E_{\rm DC} Q \sum_{p,n} z_{pn}$$
$$= \frac{Q^2}{2} \left[\sum_{p,n} \sum_{q,m} U(p,n,q,m) - \sum_{p,n} U(p,n,p,n) \right] - E_{\rm DC} Q \sum_{p,n} z_{pn}$$
$$= \frac{Q^2}{2} \sum_{p,n} \sum_{q,m} U(p,n,q,m) - (2N+1) \sum_{p} \left[\frac{3Q^2}{5R_p} + E_{\rm DC} Q z_{p0} \right], \tag{4.33}$$

considering the definition of $U(p,n,q,m)$ in equation (4.17) and the expression (4.2).

By combining all terms of equations (4.28-4.33), we end up with the following total energy within the HF method,

$$E_T^{\rm HF} = 2 \sum_{i=1}^{N_O} \varepsilon_i - (2N+1) \sum_{p} \left[\frac{3Q^2}{5R_p} + E_{\rm DC} Q z_{p0} \right]$$
$$+ \frac{1}{2} \sum_{p,n} \sum_{q,m} \left[Q^2 - \eta_{pn}\eta_{qm} + 2|\tilde{c}_{pn}^{qm}|^2 \right] U(p,n,q,m), \tag{4.34}$$

and within the DFT method

$$E_T^{\rm KS} = 2 \sum_{i=1}^{N_O} \varepsilon_i - (2N+1) \sum_{p} \left[\frac{3Q^2}{5R_p} + E_{\rm DC} Q z_{p0} \right] - \sum_{p,n} \eta_{pn} \Big(E_{\rm x}[\rho_{pn}] - V_{\rm x}[\rho_{pn}] \Big)$$
$$+ \frac{1}{2} \sum_{p,n} \sum_{q,m} \left[Q^2 - \eta_{pn}\eta_{qm} \right] U(p,n,q,m). \tag{4.35}$$

In the case considered here, we use the expression (1.37) for the exchange potential and the corresponding energy,

$$V_{\rm x}[\rho] = \left(\frac{3}{\pi} \right)^{1/3} \rho^{1/3}$$
$$E_{\rm x}[\rho] = \frac{3}{4} \left(\frac{3}{\pi} \right)^{1/3} \rho^{4/3}. \tag{4.36}$$

On the other hand, we calculate the z component of the total dipole moment as

$$\begin{aligned}\mu &= \int z\rho_T(\vec{r})\mathrm{d}\vec{r} = \sum_{p,n}\int_{|\vec{r}+\vec{R}_{pn}|<R_p} z\rho_T(\vec{r})\mathrm{d}\vec{r} \\ &= \sum_{p,n}(Q-\eta_{pn})z_{pn} = -\sum_{p,n}\eta_{pn}z_{pn},\end{aligned} \tag{4.37}$$

and using the expansion in the field strength of equation 2.12, we obtain

$$\mu = \sum_{p,n}\mu_{pn} = \sum_{p,n}\left(\mu_{0pn} + \alpha_{pn}E_{\mathrm{DC}} + \frac{1}{2}\beta_{pn}E_{\mathrm{DC}}^2 + \frac{1}{6}\gamma_{pn}E_{\mathrm{DC}}^3 + \ldots\right), \tag{4.38}$$

i.e., we can define responses for the individual atoms. By comparing HF and DFT results it may be identified which atoms are responsible for the DFT catastrophe. We can imagine two scenarios, either the atoms in the central parts of the large chains show different behavior when comparing HF and DFT, or those at the terminations do. In the former case, DFT leads to a wrong charge distribution and a different (local or non-local) function of the density may be able to solve the problems. In the latter case, DFT again leads to a wrong charge distribution but remembering that when passing to the infinite, periodic chain, that part of the dipole moment for the finite chain that arises from the terminations is translated into a current contribution, it may be suggested that a pure (local or non-local) density function is not able to solve the problems, but instead, current contributions should be included.

4.2 Model II-B: The Periodic Case

We shall now tackle the case that the system is considered being infinite and periodic. When the electrostactic field is non-zero, we will use the vector-potential approach VPA (consistent with the MTP) and hence, solve the single-particle equations of the type

$$\left\{\underline{\underline{h}} + E_{\mathrm{DC}}\left[\underline{\underline{M}}(k) + i\underline{\underline{O}}(k)\frac{d}{dk}\right]\right\}\underline{C}_j(k) = \varepsilon_j(k)\underline{\underline{O}}(k)\underline{C}_j(k). \tag{4.39}$$

As already indicated, k is a good quantum number and we use, accordingly, a formulation whereby the atom-centered basis functions have been transformed into Bloch functions. We assume that we have $K = 2N + 1$ equidistant k points in the

interval $(-\pi/a, \pi/a)$,

$$k_n = \Delta k\, n = \frac{2\pi n}{a(2N+1)} \qquad \text{for} \quad n = -N, -N+1, \ldots, N \tag{4.40}$$

and that a summation of those replaces the integration over the first Brillouin zone. The orbitals are expanded in Bloch waves, which in turn, are formed from the atom-centered basis functions normalized within the BvK zone,

$$\begin{aligned} \psi_j(k, \vec{r}) &= \sum_p C_{pj}(k) \chi_p(k, \vec{r}) \\ \chi_p(k, \vec{r}) &= \frac{1}{\sqrt{K}} \sum_{n=-N}^{N} e^{ikan} \chi_{pn}(\vec{r}), \end{aligned} \tag{4.41}$$

with a being the lattice constant.

In order to carry through the calculations for the infinite and periodic chains, we need to represent all quantities in terms of the Bloch waves. For the calculation of the matrix elements for the Bloch waves we shall make use of the properties that our atom-centered basis functions satisfy and the general equation (1.49) will help us for simplifications. Firstly, they are orthonormal,

$$\begin{aligned} \langle \chi_p(k) | \chi_q(k) \rangle &= \frac{1}{K} \sum_{n,m} e^{ika(m-n)} \langle \chi_{pn} | \chi_{qm} \rangle \\ &= \frac{1}{K} \sum_{n,m} e^{ika(m-n)} \delta_{pq} \delta_{nm} \\ &= \frac{1}{K} \sum_{n} \delta_{pq} = \delta_{pq}. \end{aligned} \tag{4.42}$$

Thereby, considering that there are B doubly occupied bands, the electron density becomes

$$\begin{aligned} \rho(\vec{r}) &= 2 \sum_j \sum_k |\psi_j(k, \vec{r})|^2 \\ &= \frac{2}{K} \sum_j \sum_k \sum_{p,q} \sum_{n,m} C^*_{pj}(k) C_{qj}(k) e^{ika(m-n)} \chi_{pn}(\vec{r}) \chi_{qm}(\vec{r}) \\ &= \frac{2}{K} \sum_j \sum_k \sum_p \sum_n |C_{pj}(k)|^2 |\chi_{pn}(\vec{r})|^2. \end{aligned} \tag{4.43}$$

According to the definition (4.8), we have non-ovelaping spheres of radius R_p around

the (p,n)th atom, in which the electron density is constant,

$$\rho_p = \frac{3}{4\pi R_p^3}\,\eta_p, \tag{4.44}$$

defining η_p as its Mulliken population analogous to equation (4.21),

$$\eta_p = \frac{2}{K}\sum_{j}^{B}\sum_{k}^{K}|C_{pj}(k)|^2 \tag{4.45}$$

We have assumed that we have a gap between the occupied and unoccupied orbitals, i.e., that we have only completely filled and completely empty bands. Only in this case is it possible to include the external electrostatic field.

We shall now formulate the matrix elements that enter the equation (4.39) in terms of Bloch waves. Thus, we have

$$\begin{aligned}\langle\chi_p(k)|\hat{h}_1|\chi_q(k)\rangle &= \frac{1}{K}\sum_{n,m} e^{ika(m-n)}\langle\chi_{pn}|\hat{h}_1|\chi_{qm}\rangle \\ &= \sum_{n} e^{ikan}\langle\chi_{p0}|\hat{h}_1|\chi_{qn}\rangle,\end{aligned} \tag{4.46}$$

$$\begin{aligned}\langle\chi_p(k)|\hat{V}_{\mathrm{n}}|\chi_q(k)\rangle &= \sum_{n} e^{ikan}\langle\chi_{p0}|\hat{V}_{\mathrm{n}}|\chi_{qn}\rangle \\ &= \sum_{n} e^{ikan}\delta_{pq}\delta_{0n}Q\sum_{p',n'}V_{\mathrm{n}}(p,n,p',n') \\ &= -Q\delta_{pq}\left[\sum_{p',n'}U(p,0,p',n') + \frac{3}{10R_p}\right],\end{aligned} \tag{4.47}$$

where we have used equations (4.18) and (4.20), remembering that Q, defined in equation (4.3), is the nuclear charge of every atom. Then, for the DFT-exchange potential

$$\begin{aligned}\langle\chi_p(k)|\hat{V}_{\mathrm{x}}|\chi_q(k)\rangle &= \sum_{n} e^{ikan}\langle\chi_{p0}|\hat{V}_{\mathrm{x}}|\chi_{qn}\rangle \\ &= \sum_{n} e^{ikan}\delta_{pq}\delta_{0n}V_{\mathrm{x}}[\rho_p] \\ &= \delta_{pq}\,V_{\mathrm{x}}[\rho_p]\end{aligned} \tag{4.48}$$

with $V_{\mathrm{x}}[\rho_p]$ defined in equation (4.36).

For the two-electron matrix elements we have

$$\begin{aligned}\langle\chi_p(k)\chi_{p'}(k')|\hat{h}_2|\chi_q(k)\chi_{q'}(k')\rangle &= \frac{1}{K^2}\sum_{n,n',m,m'} e^{ika(m-n)}e^{ik'a(m'-n')}\langle\chi_{pn}\chi_{p'n'}|\hat{h}_2|\chi_{qm}\chi_{q'm'}\rangle \\ &= \frac{1}{K^2}\sum_{n,n'}\langle\chi_{pn}\chi_{p'n'}|\hat{h}_2|\chi_{pn}\chi_{p'n'}\rangle\delta_{pq}\delta_{p'q'} \\ &= \frac{1}{K}\sum_{n}\langle\chi_{p0}\chi_{p'n}|\hat{h}_2|\chi_{p0}\chi_{p'n}\rangle\delta_{pq}\delta_{p'q'}, \end{aligned} \tag{4.49}$$

as well as

$$\begin{aligned}\langle\chi_p(k)\chi_{p'}(k')|\hat{h}_2|\chi_{q'}(k')\chi_q(k)\rangle &= \frac{1}{K^2}\sum_{n,n',m,m'} e^{ika(m-n)}e^{ik'a(m'-n')}\langle\chi_{pn}\chi_{p'n'}|\hat{h}_2|\chi_{q'm'}\chi_{qm}\rangle \\ &= \frac{1}{K^2}\sum_{n,m} e^{ia(k-k')(m-n)}\langle\chi_{pn}\chi_{qm}|\hat{h}_2|\chi_{pn}\chi_{qm}\rangle\delta_{pq'}\delta_{p'q}\delta_{nm'}\delta_{n'm} \\ &= \frac{1}{K}\sum_{n} e^{ia(k-k')n}\langle\chi_{p0}\chi_{qn}|\hat{h}_2|\chi_{p0}\chi_{qn}\rangle\delta_{pq'}\delta_{p'q}. \end{aligned} \tag{4.50}$$

In equations (4.49) and (4.50) we have summations over the lattice characterized by a summation variable n. In principle, these summations run over the Born von Kármán zone and have, accordingly, the same number of terms as we have k points, i.e. $K = 2N + 1$. We may, however choose to let these summations run over considerably more unit cells, namely from $-N_s$ to N_s. Thereby, we may be able to converge to the infinite-chain limit for a smaller number of k points, what otherwise is required. However, it is very important to observe that the n summations in equation (4.49) describe the electrostatic potential felt by an electron sitting at the pth atom in the 0th unit cell arising from charges sitting regularly at the pth atom in all unit cells. This potential is no converging. Therefore, in a practical calculation we will truncate the n summation after a larger, finite number of terms. In parallel, the potential from the nuclei and the core electrons of equation (4.47) shall be truncated after the same number of terms.

Both within HF and DFT, the sum over occupied orbitals of the Coulomb matrix elements can be written as,

$$\sum_{j=1}^{B} 2J_{jpq}(k) = \sum_{j=1}^{B}\sum_{k'}\sum_{p',q'} C^*_{p'j}(k')C_{q'j}(k')\left[2\langle\chi_p(k)\chi_{p'}(k')|\hat{h}_2|\chi_q(k)\chi_{q'}(k')\rangle\right]$$

$$
\begin{aligned}
&= \sum_{j=1}^{B}\sum_{k'}\sum_{p',q'} C^*_{p'j}(k')C_{q'j}(k') \left[\frac{2}{K}\sum_{n}\langle\chi_{p0}\chi_{p'n}|\hat{h}_2|\chi_{p0}\chi_{p'n}\rangle\delta_{pq}\delta_{p'q'}\right] \\
&= \delta_{pq}\sum_{p',n}\left[\frac{2}{K}\sum_{j=1}^{B}\sum_{k'}|C_{p'j}(k')|^2\right]\langle\chi_{p0}\chi_{p'n}|\hat{h}_2|\chi_{p0}\chi_{p'n}\rangle \\
&= \delta_{pq}\sum_{p',n}\eta_{p'}U(p,0,p',n), \qquad (4.51)
\end{aligned}
$$

using the expresions (4.49),(4.45) and (4.13) successively. Then, the Coulomb matrix is diagonal and real. On the other hand, within HF, the sum over the occupied orbitals of the exchange matrix elements is

$$
\begin{aligned}
\sum_{j=1}^{B}K_{jpq}(k) &= \sum_{j=1}^{B}\sum_{k'}\sum_{p',q'} C^*_{p'j}(k')C_{q'j}(k')\left[\langle\chi_p(k)\chi_{p'}(k')|\hat{h}_2|\chi_{q'}(k')\chi_q(k)\rangle\right] \\
&= \sum_{j=1}^{B}\sum_{k'}\sum_{p',q'} C^*_{p'j}(k')C_{q'j}(k')\left[\frac{1}{K}\sum_{n}e^{ia(k-k')n}\langle\chi_{p0}\chi_{qn}|\hat{h}_2|\chi_{p0}\chi_{qn}\rangle\delta_{pq'}\delta_{p'q}\right] \\
&= \sum_{n}\sum_{k'}\left[\frac{1}{K}\sum_{j=1}^{B}C^*_{qj}(k')C_{pj}(k')\right]e^{ia(k-k')n}\langle\chi_{p0}\chi_{qn}|\hat{h}_2|\chi_{p0}\chi_{qn}\rangle \\
&= \sum_{n}\sum_{k'}\tilde{C}_{pq}(k')e^{ia(k-k')n}U(p,0,q,n) \equiv X_{pq}(k) \qquad (4.52)
\end{aligned}
$$

where we have defined,

$$
\tilde{C}_{pq}(k') = \frac{1}{K}\sum_{j=1}^{B}C^*_{qj}(k')C_{pj}(k'), \qquad (4.53)
$$

which, in fact, are real numbers and the diagonal elements are related to the Mulliken populations, $\eta_p = 2\tilde{C}_{pp}$.

We finally need

$$
\begin{aligned}
M_{pq}(k) &= \sum_{n}e^{ikan}\langle\chi_{p0}|z-na|\chi_{qn}\rangle \\
&= \sum_{n}e^{-ikan}\langle\chi_{pn}|z|\chi_{q0}\rangle = \langle\chi_{p0}|z|\chi_{q0}\rangle \\
&= \langle\chi_{p0}|z|\chi_{q0}\rangle = \delta_{pq}\,z_{p0}. \qquad (4.54)
\end{aligned}
$$

We are now ready to set up the matrix $\underline{\underline{h}}$ of equation (4.39). In the Hartree-Fock

case this becomes

$$F_{pq}(k) = \langle\chi_p(k)|\hat{h}_1|\chi_q(k)\rangle + \langle\chi_p(k)|\hat{V}_{\rm n}|\chi_q(k)\rangle + \sum_{j=1}^{B}\left[2J_{jpq}(k) - K_{jpq}(k)\right], \tag{4.55}$$

whereas in the DFT approach we have

$$h^{\rm KS}_{pq}(k) = \langle\chi_p(k)|\hat{h}_1|\chi_q(k)\rangle + \langle\chi_p(k)|\hat{V}_{\rm n}|\chi_q(k)\rangle - \langle\chi_p(k)|\hat{V}_{\rm x}|\chi_q(k)\rangle + \sum_{j=1}^{B} 2J_{jpq}(k). \tag{4.56}$$

The matrix elements of the operators $\hat{V}_{\rm n}$, $\hat{J}_j$ and $\hat{V}_{\rm x}$ are diagonal, while only $\hat{h}_1$ and $\hat{K}_j$ lead to Hermitan matrices with non-vanishing off-diagonal elements. In total, substituting (4.47), (4.48), (4.51) and (4.52) in (4.55) and (4.56), we have for the Fock operator,

$$\begin{aligned} F_{pq}(k) &= \delta_{pq}\left[-Q\sum_{p',n'}U(p,0,p',n') - \frac{3Q}{10R_p} + \sum_{p',n}\eta_{p'}U(p,0,p',n)\right] + h_{1pq} - X_{pq} \\ &= \delta_{pq}\left[\sum_{p'}(\eta_{p'} - Q)U_s(p,p') - \frac{3Q}{10R_p}\right] + h_{1pq} - X_{pq}, \end{aligned} \tag{4.57}$$

while for the Kohn-Sham operator,

$$\begin{aligned} h^{\rm KS}_{pq}(k) &= \delta_{pq}\left[-Q\sum_{p',n}U(p,0,p',n) - \frac{3Q}{10R_p} + \sum_{p',n}\eta_{p'}U(p,0,p',n) - V_{\rm x}[\rho_p]\right] + h_{1pq} \\ &= \delta_{pq}\left[\sum_{p'}(\eta_{p'} - Q)U_s(p,p') - \frac{3Q}{10R_p} - V_{\rm x}[\rho_p]\right] + h_{1pq}. \end{aligned} \tag{4.58}$$

In both equations we have simplified,

$$\sum_{n=-N_s}^{N_s} U(p,0,q,n) = U_s(p,q). \tag{4.59}$$

All the terms in equations (4.57) and (4.58) are real except for those due to the kinetic energy operator, $\hat{h}_1$, defined in (4.12) and (4.46), which can be split into real and imaginary parts,

$$\mathrm{Re}(h_{1pq}) = \sum_n \cos(kan)\langle\chi_{p0}|\hat{h}_1|\chi_{qn}\rangle \tag{4.60}$$

$$\mathrm{Im}(h_{1pq}) = \sum_n \sin(kan)\langle\chi_{p0}|\hat{h}_1|\chi_{qn}\rangle. \tag{4.61}$$

In practice, we do not use the equation (4.39) because it is not a standard matrix-eigenvalue problem. Instead, we use the expression (2.47) considering that, in our case, the overlap matrix is just the identity matrix, $\underline{\underline{O}} = \underline{\underline{1}}$. Then, it takes the form,

$$\left\{\underline{\underline{h}}(k) + E_{\mathrm{DC}}\left[\underline{\underline{M}}(k) + i\left(\frac{d}{dk}\underline{\underline{C}}(k)\right)\cdot\underline{\underline{C}}^{\dagger}(k)\right]\right\}\underline{C}_j(k) = \epsilon_j(k)\underline{C}_j(k). \tag{4.62}$$

The unit cell dipole matrix, $\underline{\underline{M}}(k)$, calculated in equation (4.54), is also a real diagonal matrix, and it will add the term $E_{\mathrm{DC}} z_{p0}\,\delta_{pq}$ to the expresions (4.57) and (4.58). Then, if we separate the term with the derivative of $\underline{\underline{C}}(k)$ into real and imaginary components,

$$\left(\frac{d}{dk}\underline{\underline{C}}(k)\right)\cdot\underline{\underline{C}}^{\dagger}(k) = \underline{\underline{A}} + i\underline{\underline{B}}, \tag{4.63}$$

the effective Hamiltonian (in curly brackets) for HF will be composed by the following matrix elements,

$$\begin{aligned} h^{\mathrm{eff}}_{pq} = \delta_{pq}&\left[\sum_{p'}(\eta_{p'} - Q)U_s(p,p') - \frac{3Q}{10R_p} + E_{\mathrm{DC}} z_{p0}\right] \\ &+ \mathrm{Re}(h_{1pq}) - X_{pq} - E_{\mathrm{DC}} B_{pq} + i\left[\mathrm{Im}(h_{1pq}) + E_{\mathrm{DC}} A_{pq}\right], \end{aligned} \tag{4.64}$$

while for the DFT are

$$\begin{aligned} h^{\mathrm{eff}}_{pq} = \delta_{pq}&\left[\sum_{p'}(\eta_{p'} - Q)U_s(p,p') - \frac{3Q}{10R_p} + E_{\mathrm{DC}} z_{p0} - V_{\mathrm{x}}[\rho_p]\right] \\ &+ \mathrm{Re}(h_{1pq}) - E_{\mathrm{DC}} B_{pq} + i\left[\mathrm{Im}(h_{1pq}) + E_{\mathrm{DC}} A_{pq}\right]. \end{aligned} \tag{4.65}$$

The equation (4.62) must to be solved for the eigenvectors self-consistently by including the smoothing procedure for the coefficients $C_{pj}(k)$ in order to be able to calculate their derivatives. To solve the Hermitian problem of the equation (4.62) we can convert it to real, symmetric one: Being $\underline{\underline{h}}^{\mathrm{eff}} = \underline{\underline{A}} + i\underline{\underline{B}}$ a Hermitian matrix, then the $n \times n$ complex eigenvalue problem

$$(\underline{\underline{A}} + i\underline{\underline{B}})\cdot(\underline{u} + i\underline{v}) = \lambda(\underline{u} + i\underline{v})$$

is equivalent to the $2n \times 2n$ real problem,

$$\begin{pmatrix} \underline{\underline{A}} & -\underline{\underline{B}} \\ \underline{\underline{B}} & \underline{\underline{A}} \end{pmatrix} \cdot \begin{pmatrix} \underline{u} \\ \underline{v} \end{pmatrix} = \lambda \begin{pmatrix} \underline{u} \\ \underline{v} \end{pmatrix}$$

Note that, because $\underline{\underline{h}}^{\text{eff}}$ is Hermitian, this $2n \times 2n$ matrix is real and symmetric: $\underline{\underline{A}}^T = \underline{\underline{A}}$ and $\underline{\underline{B}}^T = -\underline{\underline{B}}$.

Corresponding to a given eigenvalue λ with eigenvector $\underline{u} + i\underline{v}$, the vector $-\underline{v} + i\underline{u}$ is also an eigenvector. Thus each eigenvalue $\lambda_1, \lambda_2, \ldots, \lambda_n$ of $\underline{\underline{h}}^{\text{eff}}$ is repeated twice in the augmented problem and the corresponding eigenvectors are pairs of the form $\underline{u}_n + i\underline{v}_n$ and $i(\underline{u}_n + i\underline{v}_n)$.

In our case, $\underline{u}$ and $\underline{v}$ are the real and imaginary parts of the expansion coefficients $C_{pj}(k)$. Thus, it was checked if a smart selection between the two possible eigenvectors $C_{pj}(k)$ and $iC_{pj}(k)$ can smooth the coefficients as functions of k. It turned out that, despite some progress, we still need the smoothing procedure and, indeed, this selection has no effect on the smoothing procedure.

4.2.1 Energy and Polarization

Within the restricted HF method, the total electronic energy per unit is given as

$$\frac{1}{K}\sum_k E_e(k) = \frac{1}{K}\sum_k \left[2\sum_{i=1}^{B} \varepsilon_i(k) - \sum_{i,j=1}^{B} \left(2\langle \psi_i\psi_j|\hat{h}_2|\psi_i\psi_j\rangle - \langle \psi_j\psi_i|\hat{h}_2|\psi_i\psi_j\rangle \right) \right], \tag{4.66}$$

whereas for the DFT as

$$\frac{1}{K}\sum_k E_e(k) = \frac{2}{K}\sum_k \left[\sum_{i=1}^{B} \varepsilon_i(k) - \sum_{i=1}^{B} \langle \psi_i|E_{\text{x}} - V_{\text{x}}|\psi_i\rangle - \sum_{i,j=1}^{B} \langle \psi_i\psi_j|\hat{h}_2|\psi_i\psi_j\rangle \right], \tag{4.67}$$

With the present model, using equations (4.41), (4.45), (4.49) and (4.58), we have

$$\begin{aligned}
&\frac{2}{K}\sum_{i,j=1}^{B}\sum_k \langle \psi_i\psi_j|\hat{h}_2|\psi_i\psi_j\rangle \\
&= \frac{2}{K}\sum_{i,j=1}^{B}\sum_{k,k'}\sum_{p,p'}\sum_{q,q'} C^*_{pi}(k)C^*_{p'j}(k')C_{qi}(k)C_{q'j}(k') \left[\langle \chi_p(k)\chi_{p'}(k')|\hat{h}_2|\chi_q(k)\chi_{q'}(k')\rangle \right] \\
&= \frac{2}{K}\sum_{i,j=1}^{B}\sum_{k,k'}\sum_{p,p'}\sum_{q,q'} C^*_{pi}(k)C^*_{p'j}(k')C_{qi}(k)C_{q'j}(k') \left[\frac{1}{K}\sum_n \langle \chi_{p0}\chi_{p'n}|\hat{h}_2|\chi_{p0}\chi_{p'n}\rangle \delta_{pq}\delta_{p'q'} \right]
\end{aligned}$$

$$= \frac{1}{2}\sum_{p,p'}\left[\frac{2}{K}\sum_{i=1}^{B}\sum_{k}|C_{pi}(k)|^2\right]\left[\frac{2}{K}\sum_{j=1}^{B}\sum_{k'}|C_{p'j}(k')|^2\right]\sum_{n}U(p,0,p',n)$$
$$= \frac{1}{2}\sum_{p,p'}\eta_p\eta_{p'}U_s(p,p'), \tag{4.68}$$

as well as, using equations (4.41), (4.50), (4.52), (4.53) and (4.58),

$$\frac{1}{K}\sum_{i,j=1}^{B}\sum_{k}\langle\psi_j\psi_i|\hat{h}_2|\psi_i\psi_j\rangle$$
$$= \frac{1}{K}\sum_{i,j=1}^{B}\sum_{k,k'}\sum_{p,p'}\sum_{q,q'}C^*_{pi}(k)C^*_{p'j}(k')C_{q'j}(k')C_{qi}(k)\left[\langle\chi_p(k)\chi_{p'}(k')|\hat{h}_2|\chi_{q'}(k')\chi_q(k)\rangle\right]$$
$$= \frac{1}{K}\sum_{i,j=1}^{B}\sum_{k,k'}\sum_{p,p'}\sum_{q,q'}C^*_{pi}(k)C^*_{p'j}(k')C_{q'j}(k')C_{qi}(k)$$
$$\times\left[\frac{1}{K}\sum_{n}e^{ia(k-k')n}\langle\chi_{p0}\chi_{qn}|\hat{h}_2|\chi_{p0}\chi_{qn}\rangle\delta_{pq'}\delta_{p'q}\right]$$
$$= \sum_{p,q}\sum_{k}\left[\frac{1}{K}\sum_{i=1}^{B}C^*_{pi}(k)C_{qi}(k)\right]\sum_{n}\sum_{k'}\left[\frac{1}{K}\sum_{j=1}^{B}C^*_{qj}(k')C_{pj}(k')\right]e^{ia(k-k')n}U(p,0,q,n)$$
$$= \sum_{p,q}\sum_{k}\tilde{C}_{pq}(k)X_{pq}(k). \tag{4.69}$$

Moreover,

$$\frac{2}{K}\sum_{i=1}^{B}\sum_{k}\langle\psi_i|E_{\mathrm{x}}-V_{\mathrm{x}}|\psi_i\rangle = \frac{2}{K}\sum_{i=1}^{B}\sum_{k}\sum_{p,q}C^*_{pi}(k)C_{qi}(k)\Big(E_{\mathrm{x}}[\rho_p]-V_{\mathrm{x}}[\rho_p]\Big)\delta_{pq}$$
$$= \sum_{p}\left[\frac{2}{K}\sum_{i=1}^{B}\sum_{k}|C_{pi}(k)|^2\right]\Big(E_{\mathrm{x}}[\rho_p]-V_{\mathrm{x}}[\rho_p]\Big)$$
$$= \sum_{p}\eta_p\big(E_{\mathrm{x}}[\rho_p]-V_{\mathrm{x}}[\rho_p]\big). \tag{4.70}$$

In both cases we need to add the total energy contribution from the nuclei,

$$E_{\mathrm{n}} = \frac{Q^2}{2}\sum_{p,q}\sum_{m,n}\big(1-\delta^{qm}_{pn}\big)U(p,n,q,m) - E_{\mathrm{DC}}Q\sum_{p,n}z_{pn}. \tag{4.71}$$

In the periodic case we consider that we have an infinite number of units but the summation over m and n have to be truncated. Let say that we take into account only

the interaction between the atoms of the first N_s neighboring units. Thus, if we consider $2N_s+1$ units with $-N_s \leq n \leq N_s$, then m takes the values $-N_s+n \leq m \leq N_s+n$. So the summation over n gives $2N_s+1$ times the same value (for example that with $n=0$), but this factor is canceled when we divide by $2N_s+1$ to get the total energy per unit. The same happens with the last term using equation (4.2),

$$\begin{aligned}\frac{1}{2N_s+1}E_{\rm n} &= \frac{Q^2}{2}\sum_{p,q}\sum_{m=-N_s}^{N_s}\left(1-\delta_{p0}^{qm}\right)U(p,0,q,m) - E_{\rm DC}Q\sum_p z_{p0} \\ &= \frac{Q^2}{2}\sum_{p,q}\left[\sum_{m=-N_s}^{N_s}U(p,0,q,m) - \delta_{pq}U(p,0,p,0)\right] - E_{\rm DC}Q\sum_p z_{p0} \\ &= \frac{Q^2}{2}\sum_{p,q}U_s(p,q) - \sum_p\left[\frac{3Q^2}{10R_p} + E_{\rm DC}Qz_{p0}\right]. \end{aligned} \tag{4.72}$$

Here we are considering the same number of units of the truncation described below for the equations (4.47), (4.49) and (4.50). Thus, combining equations (4.66-4.72) the total energy per unit cell within HF is

$$\begin{aligned}E_{\rm cell} = &\frac{2}{K}\sum_{i=1}^{B}\sum_k \varepsilon_i(k) + \frac{1}{2}\sum_{p,q}\left[Q^2-\eta_p\eta_q\right]U_s(p,q) \\ &+\sum_{p,q}\sum_k \tilde{C}_{pq}(k)X_{pq}(k) - \sum_p\left[\frac{3Q^2}{10R_p} + E_{\rm DC}Qz_{p0}\right], \end{aligned} \tag{4.73}$$

whereas within the DFT it is

$$\begin{aligned}E_{\rm cell} = &\frac{2}{K}\sum_{i=1}^{B}\sum_k \varepsilon_i(k) + \frac{1}{2}\sum_{p,q}\left[Q^2-\eta_p\eta_q\right]U_s(p,q) \\ &-\sum_p\left[\frac{3Q^2}{10R_p} + E_{\rm DC}Qz_{p0} + \eta_p\Big(E_{\rm x}[\rho_p] - V_{\rm x}[\rho_p]\Big)\right]. \end{aligned} \tag{4.74}$$

In the present study we do not carry out any structure relaxation and all the nuclei have the same charge Q. This leads to $\sum_p Qz_{p0}=0$, and therefore, we can exclude the $E_{\rm DC}$-term in equations (4.73-4.74) and (4.34-4.35).

For the electronic dipole moment per unit, we use the expression (2.27),

$$\bar{\mu}_e = -\frac{2}{K}\sum_{j=1}^{B}\sum_k\sum_p\left[|C_{pj}(k)|^2 z_{p0} + iC_{pj}^*(k)\frac{dC_{pj}(k)}{dk}\right]$$

$$= -\sum_{p} \eta_p z_{p0} - \frac{2i}{K} \sum_{j=1}^{B} \sum_{k} \sum_{p} C^{*}_{pj}(k) \frac{dC_{pj}(k)}{dk} \tag{4.75}$$
$$= \bar{\mu}_Q + \bar{\mu}_I,$$

where $\bar{\mu}_Q$ and $\bar{\mu}_I$ are the charge and the current contributions respectively.

Including the dipole moment of the nuclei, we will have

$$\bar{\mu} = \bar{\mu}_{\mathrm{n}} + \bar{\mu}_e = Q \sum_{p} z_{p0} + \bar{\mu}_e = \bar{\mu}_e, \tag{4.76}$$

thereby, in the systems considered here, the nuclei do not contribute to the total dipole moment.

4.2.2 Analyzing the Effective Hamiltonian

Owing the simplicitity of our system, we can exhaustively analyze the differences between the HF and DFT expressions for the effective hamiltonian $h^{\mathrm{eff}}_{pq}(k)$, i.e., equations (4.64) and (4.65). First, we emphasize that the only k-dependent terms are h_{1pq}, A_{pq}, B_{pq} and X_{pq}, while the self-consistent and smooth coefficients affect η_p, $\tilde{C}_{pq}$ A_{pq}, B_{pq}, X_{pq} and ρ_p. On the other hand, only two terms are related to the truncation of the potential due to the electron-electron and electron-nucleus interactions. As mentioned previuosly, we consider the interactions with the $2N_s$ neighboring units and this summation affects only $U_s(p,q)$ and X_{pq} defined in equations 4.59 and 4.52 respectively. Champagne et al. [34] have shown how to remove the importance of this issue, but here we can calculate it analytically.

Considering, additionally, that the system is one-dimensional with two atoms per unit cell, one atom-centered basis function per atom and two electrons per unit, the k-dependent hamiltonian is the 2×2 complex matrix ($p, q = 1, 2$) given by equations (4.57) and (4.58),

$$\text{HF} \qquad h^{\mathrm{eff}}_{pq} = \delta_{pq} \left[\sum_{p'} (\eta_{p'} - Q) U_s(p,p') - \frac{3Q}{10R_p} \right] + h_{1pq} - X_{pq} \tag{4.77}$$

$$\text{DFT} \qquad h^{\mathrm{eff}}_{pq} = \delta_{pq} \left[\sum_{p'} (\eta_{p'} - Q) U_s(p,p') - \frac{3Q}{10R_p} - V_{\mathrm{x}}[\rho_p] \right] + h_{1pq} \tag{4.78}$$

Moreover, the populations fulfill $\eta_1 + \eta_2 = 2$ and the nuclear charge is $Q = 1$. Then,

the first terms of the diagonal elements are

$$\begin{aligned} p=1 \qquad \sum_{p'}(\eta_{p'}-Q)U_s(1,p') &= (\eta_1-1)U_s(1,1)+(\eta_2-1)U_s(1,2) \\ &= (\eta_1-1)[U_s(1,1)-U_s(1,2)] \\ &= (\eta_1-1)\Delta U_s \\ p=2 \qquad \sum_{p'}(\eta_{p'}-Q)U_s(2,p') &= (1-\eta_1)\Delta U_s. \end{aligned} \tag{4.79}$$

$U_s(p,q)$ does not converge for $N_s \to \infty$, but the difference, $\Delta U_s = U_s(1,1) - U_s(1,2)$, does as we can see in Appendix B.1. For this reason, within the present model, the DFT hamiltonian converges for $N_s \to \infty$. In fact, N_s has not to be very high to obtain a good approach to the infinite limit of ΔU_s. The HF hamiltonian has an additional term, X_{pq}, whose convergence for $N_s \to \infty$ was also confirmed.

Other term in which we truncate a summation is $h_{1pq}(k)$, but we also proved in Appendix B.2 that, as it is defined, it is possible to deduce analytic formulae for the convergence value considering an infinite number of units (or $R_0 \to \infty$). It would not be the case if the function in equation (4.12) was $-t/R$ (as we used in preliminary studies) instead of $-te^{-bR}$.

Something similar happens with the total energy, where the term,

$$\begin{aligned} \frac{1}{2}\sum_{p,q}(Q^2-\eta_p\eta_q)U_s(p,q) &= \frac{1}{2}\left[(2-\eta_1^2-\eta_2^2)U_s(1,1)+2(1-\eta_1\eta_2)U_s(1,2)\right] \\ &= \frac{1}{2}\left[(-2\eta_2^2+4\eta_1-2)U_s(1,1)+(2N_2^2-4\eta_1+2)U_s(1,2)\right] \\ &= -\Delta U_s(\eta_1-1)^2, \end{aligned} \tag{4.80}$$

is shared by both methods, but the HF expression has an additional one,

$$\sum_{p,q}\sum_{k}\tilde{C}_{pq}(k)X_{pq}(k) = \sum_{p,q}\sum_{k,k'}\sum_{n}\tilde{C}_{pq}(k)\tilde{C}_{pq}(k')e^{ia(k-k')n}U(p,0,q,n), \tag{4.81}$$

whose convergence for $N_s \to \infty$ is not straightforward and may be affected by truncation errors for a given N_s. Finally, after several test calculations for a fixed BvK-zone of size K and different N_s, we observed that the HF calculations were not improved with higher N_s. For that reason, we decided to include the inteactions with only the unit cells of the BVK zone, i.e., $K = 2N_s + 1$.

4.3 The Computer Program

A computer program for the finite model described in section 4.1 was constructed. It turns out to be a fairly small program that easily could be checked and made to work. Initiallly, the existing program code (`dftcat`) was modified and extended to include more atoms and electrons per unit. This also allow us to treat additional parallel chains. Later, a similar program code was made for the periodic treatment detailed in section 4.2 including the smoothing procedure. In figure 4.1, we can see the flow chart of this program.

First, using the atoms coordinates, the system is contructed and all the distances are calculated. Then, as initial guess for the matrix of expansion coefficients C in the field-free case, we use the identity matrix and run the self-consistent procedure (marked with the blue line in figure 4.1). The C-matrix is used to calculate the populations and the electron density. For the finite system, there is only one big effective Hamiltonian with $(2N+1)N_b$ eigenvalues, whereas for the periodic system, the Hamiltonian is k-dependent, so we have to solve the small (but complex) eigenvalue problem for each k in the BZ. In this manner we obtain the eigenvectors which form the output C-matrix. The new coefficients are then combined with the input coefficients by a simple linear mixing,

$$\begin{aligned} \tilde{C}^{\text{new}}_{pj}(k) &= (1-\tau)C^{\text{input}}_{pj}(k) + \tau\, C^{\text{output}}_{pj}(k) \\ C^{\text{new}}_{pj}(k) &= \mathcal{N}_j(k)\tilde{C}^{\text{new}}_{pj}(k), \\ \text{with} \qquad \mathcal{N}_j(k) &= \left[\sum_p |\tilde{C}^{\text{new}}_{pj}(k)|^2\right]^{-1/2}, \end{aligned} \tag{4.82}$$

so that, the new C-matrix used in the next iteration is obtained. Due to the mixing it is not automatically guaranteed that the orbitals are normalized, which is the reason for including the extra normalization step above. They may still not be orthogonal, but in the case of convergence that should be fulfilled and then also $\mathcal{N}_{pn} = 1$. Moreover, in the first iteration the mixing parameter is set $\tau = 1$.

The calculations are considered converged when a parameter,

$$W = \frac{1}{KN_b^2}\left[\sum_k \sum_{p,j} |C^{\text{output}}_{pj}(k)| - |C^{\text{input}}_{pj}(k)|^2\right]^{1/2} \tag{4.83}$$

is below a certain threshold value.

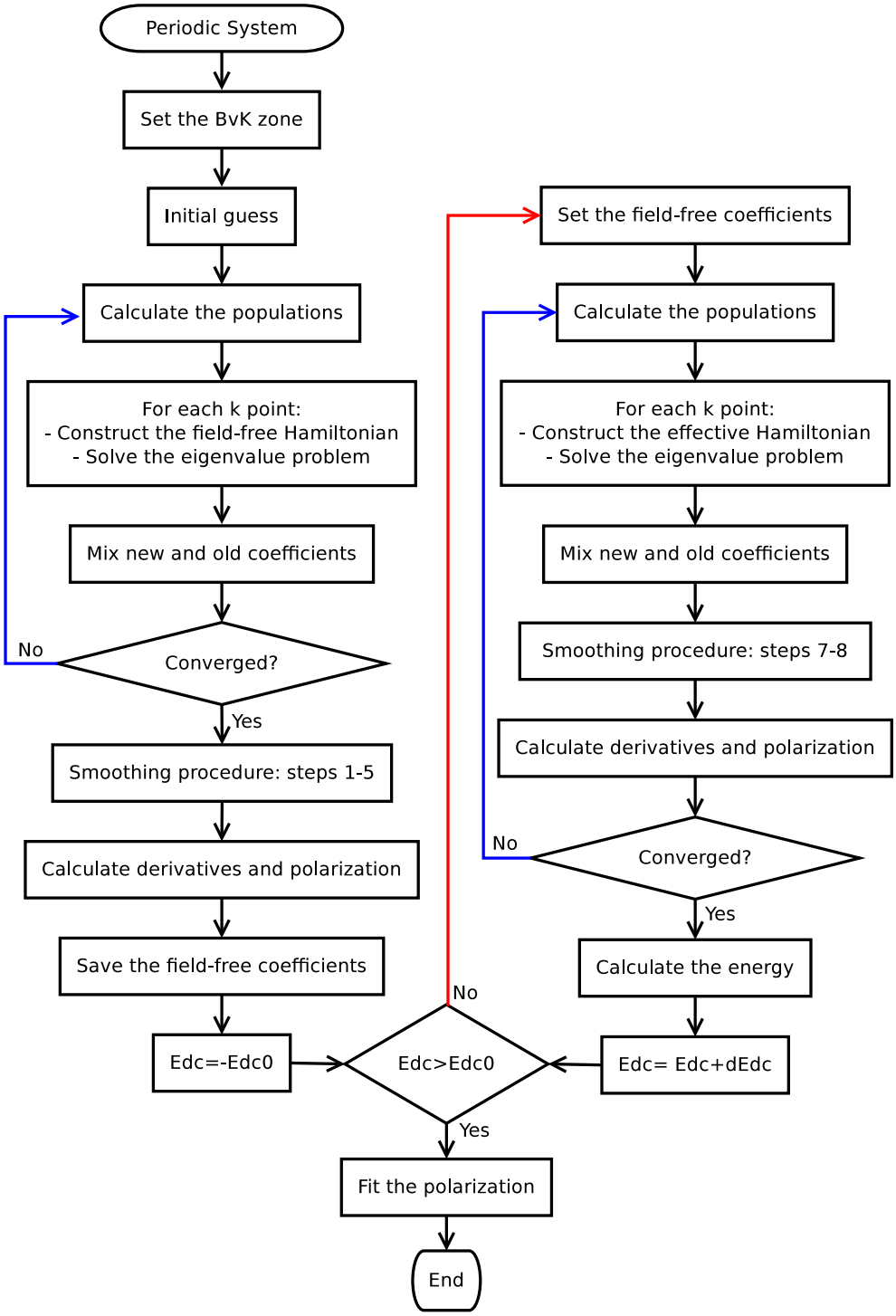

Figure 4.1: Flow chart of the program for the periodic system.

```
&inp alat=5.0, natom=2, nel=1, nmin0=1, nmax0=20,
t=5.16, b=0.3, r0=2000, edc0n=0.0020, dedcn=0.0002,
fdbck=1.00, conv=1.d-07, nitmax=50, ifit2=5 &end
&inpat xi0= 0.0, yi0=0.0, zi0=-1.10, ri=1.00, si=-0.5, &end
&inpat xi0= 0.0, yi0=0.0, zi0= 1.10, ri=1.00, si= 0.5, &end
```

Table 4.1: An input file for the program.

The first six steps of the smoothing procedure are carried out for the converged solution in the field-free case, while in the field-containing case, the steps 7 and 8 are inside the self-consistency, where we use as initial guess the converged solutions for the field-free case. The loop for all the field strengths is marked with the red line in figure 4.1. After that, the responses are obtained by fitting the dipole moment or the polarization with a power series of the field strength. The whole algoritm is done for both HF and DFT methods. In the finite case, we carry out the calculations for different chain lengths in order to find the infinite-chain limit.

4.3.1 The Input File

Table I shows the input file for the program. The parameters have the following meaning:

`alat:` a, the unit cell length.
`natom:` P, the number of atoms per unit cell.
`nel:` N_e, with $2N_e$ being the number of electrons per unit.
`nmin0,nmax0:` The range of N, being $2N+1$ the number of units.
`t,b,r0:` Parameters used in equation (4.12).
`edc0n,dedcn:` Maximum value of field strength, E_{DC}, and its increment.
`fdbck:` τ, parameter used in the linear mixing.
`conv:` The threshold value for W of equation (4.83).
`nitmax:` Maximal number of iterations.
`ifit2:` Number of chain lengths used to calculate the infinite-chain limit.
`xi0,yi0,zi0:` The three components of the vector $\vec{R}_{p0}$.
`ri:` The sphere radio R_p of equation (4.8).
`si:` The single-electron on-site energies of equation (4.12).

For the periodic system, `nmin0`, `nmax0` and `ifit2` are changed by:

`nn:` N, which defines the size of the BvK zone $K = 2N + 1$.

`nsum:` N_s, the number of neighboring units considered in equation (4.59).
`ndif:` N_D, used for the numerical derivatives of equation (2.55).
`qlam:` λ, parameter used in (2.53) to smooth the coefficients.
`iw:` flag, `iw=1` gives additional information to test some blocks.

In the first version of `dftcat`, the function used to define the single-electron hopping integrals in equation (4.12) was $-t'/R$, but the responses were not very stable when varying R_0, i.e., the maximum distance between basis functions which contribute to this term. For this reason we decided to use instead the exponential function, $-t\exp(-bR)$, with `t` and `b` chosen to obtain similar values of the hopping integrals for the nearest and next nearest neighbors. The exponential function is also used in modelling the effects of screening that otherwise are not included. With this definition, the solutions converge rapidly for increasing R_0 (see Appendix B.2) and the value $R_0 = 2000$ means that we consider the contribution from every pair of basis functions.

For the self-consistent procedure, it turned out that the simple mixing, $\tau = 1$ was the best choice. On the other hand, for the periodic treatment, we used the parameter λ in equation (2.53) to include the second-nearest-neighbor term to smooth the coefficients as functions of k. This term was added to improve the numerical stablity of the derivatives, however, in our case, it was found that this inclusion generates some fluctuations in the coefficients near to the boundaries of the BZ. These fluctuations affect mainly the derivatives with respect to k. On the other hand, by excluding this contribution (by setting $\lambda = 0$), the coefficients are pretty smooth and continuous along the whole band and its boundaries.

In the formula to calculate the derivatives numerically, equation (2.55), we use a higher-order finite-difference approximation, considering the coefficients at the N_D previuos and subsecuent k-values. Due to its weight, defined in equation (2.57), the contribution of the nth-nearest-neighbor term decays very fast for increasing n, while the difference between $N_D = 1$ and $N_D = 2$ is small but significant. We set for all the calculations $N_D = 5$.

As mentioned above, in the last step of the algorithm we fit the dipole moment or the polarization with a power series in the field strength to obtain μ_0, α, β and γ according to equation (4.38). We use both a 3^{rd} and a 5^{th} order expansion to estimate truncation errors. In the ideal case, the result should hardly differ, but in some cases, the values obtained with both fits differed substantially, specially for the higher order responses in the periodic treatment. For example, the ratio $\gamma(5^{th})/\gamma(3^{rd})$ was found to be very sensitive and sometimes arbitrary to the change of some parameters, but

it was by varying the range and the intervals of the field strength that we could get reliable results and make the ratio $\gamma(5^{th})/\gamma(3^{rd}) \sim 1$.

Finally, varying the size of the BvK zone, $K = 2N+1$, has a marginal effect on the responses when N has reached an appropriate value. In our case $N = 20$ is enough and allows us to make a bettter comparison between the results of the periodic system and those of a finite chain with $2N+1$ units. On the other hand, N_s, defined as the number of nearest neighbors considered for the Coulomb interaction, should be, in principle, equal to N, but we set it as an additional parameter trying to reach faster a converged value. As we mention in section 4.2.2, we did not find a clear improvement of the results by taking $N_s > N$. Thus, after several explorative calculations, we decided to keep $N_s = N$.

4.4 Results

Our model includes several parameters whose values can affect the results. In the present study, the most important ones are the difference in the on-site energies, Δs, as well as the bond-length-alternation (BLA) parameter [35], being the difference in the nearest-neighbor bond lengths. In order to obtain numerically significant results, it is useful to have large responses of the system to the external field. As a general rule, the more delocalized the electrons are, the larger are the responses. The delocalization is increased for smaller values of Δs or the BLA parameter, but simultaneously the band gap is reduced. A reduced band gap increases the probability for electron to tunnel from one end of the system to the other, implying that for systems with small band gaps only shorter chains and/or weaker fields can be treated. Weaker fields, on the other hand, implies that the changes in the dipole moment upon the inclusion of the field are smaller, whereby the calculation of the responses to the fields becomes numerically unstable. Thus, due to these aspects one has to make a compromise between the possible field strengths and the numerical accuracy of the responses.

Since our model has been developed with the aim of obtaining a phenomenological description but not as an approximation to existing systems, the units we are using can be considered arbitrary and may be omitted. In this sense, we used a lattice constant of a = 5 and an intramolecular bond of d = 2.2, so that the BLA parameter along the chain equals 0.6. Moreover, the radii of the spheres were set $R_p = 1$ length units.

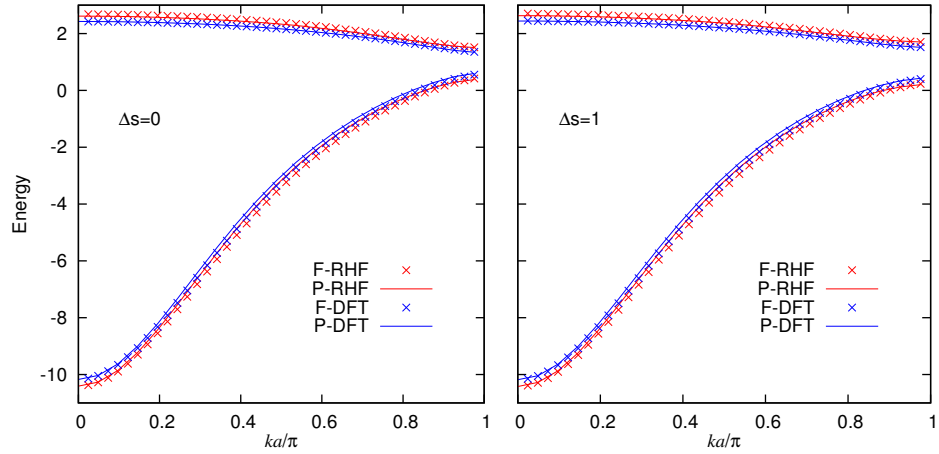

Figure 4.2: Band structures in absence of field for periodic (lines) and finite (crosses) systems, calculated within both RHF and DFT methods. The left one corresponds to a chain composed by identical atoms, while the right one belongs to a chain whose atoms have different on-site energies.

4.4.1 Band Structure

As shown in the previous chapter, it is possible to extract band structures for infinite periodic systems from the results for a sufficiently large finite system even in the presence of an electrostatic field although, in the latter case, only with some uncertainty. For our model, as it turns out, the band structures are barely affected by the electrostatic field, so that the field-free results contain the important information. The field-free band structures are shown in figure 4.2 for $\Delta s = 0$ and $\Delta s = 1$. Of the two bands, the lower one is filled, while the upper one is empty.

In general, the results for the periodic chains (lines) and those for the finite chains (crosses) lie almost on top of one another for both RHF and DFT. Only near the center of the valence band is a small difference found (the orbital energies for the finite-system occupied orbitals are slightly lower).

When comparing the band structures of the chain with identical atoms (i.e., $\Delta s = 0$) to those of the chain containing a permanent dipole moment (i.e., with $\Delta s \neq 0$) the differences are most noticeable in the region close to the bandgap. In agreement with expectations, the bandgap is smaller for $\Delta s = 0$.

It worth to mention that in the finite case, the chain length does not have an appreciable effect on the band structure, neither within the DFT nor the RHF methods, so far the system does not become metallic due to the electric field.

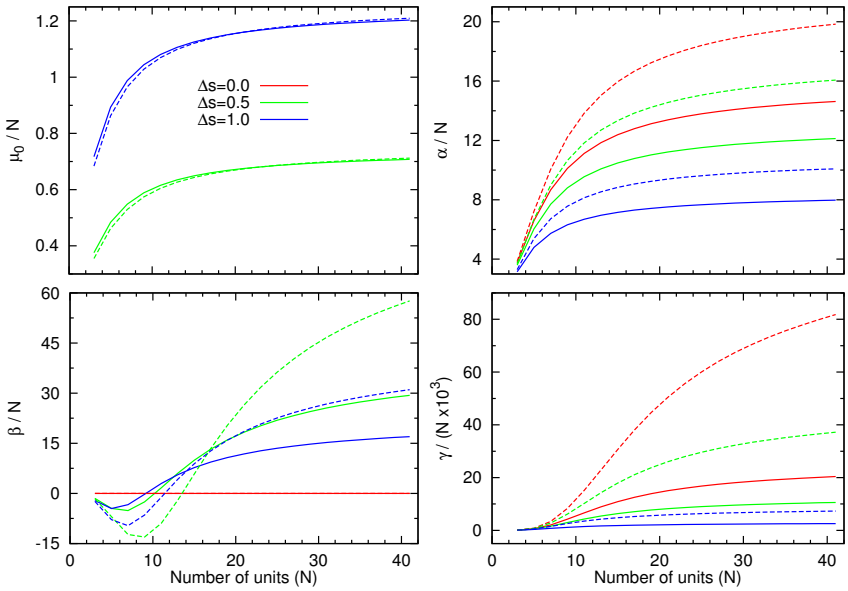

Figure 4.3: Responses divided by the number of units of a single chain as its size is increased. The different colors correspond to different on-site energies. The HF results are plotted in solid lines while the DFT ones in dashed lines.

4.4.2 Size Dependence

Regarding the finite system, in figure 4.3 we show the responses divided by the number of units, $R(N)/N$, as functions of the chain length for three values of Δs. The centrosymmetric chain exhibits the larger α and γ, but due to the symmetry, the values for μ_0 and β vanish. The responses from the DFT calculations are larger than those from the HF calculations, in particular for the higher-order responses. We can thus assume that our model is capable of grasping the problems related to the DFT overestimations.

In all the cases, to a larger or smaller degree, there is a tendency to converge towards a constant value, indicating that the infinite-chain limit can be identified. To this end, we assume that, for large N, any response $\vartheta(N)$ can be approximated as

$$\vartheta(N) = AN + B. \tag{4.84}$$

with $\bar{\vartheta} = A$ being the infinite-chain limit for the response per unit. This expression is consistent with that of equation (2.3), but instead of considering only two chain lengths, we found more stable to fit a whole set of results for different chain lengths: $N, N-\Delta N, N-2\Delta N, \ldots, N-(f-1)\Delta N$ to the expression (4.84). Here using $N = 41$, $\Delta N = 2$ and $f = 5$ we obtained converged values.

System	Method	Δs	gap	$\lvert q_0 \rvert$	$\bar{\mu}_0$	$\bar{\alpha}$	$\bar{\beta}$	$\bar{\gamma}$
Finite	RHF	1.0	1.389	0.2572	1.2483	8.4461	22.485	2989.3
	RHF	0.5	1.144	0.1290	0.7417	13.084	41.138	13087
	RHF	0.0	1.038	0.0000	0.0000	15.927	0.0000	25124
	DFT	1.0	1.025	0.2382	1.2618	10.813	44.355	8777.2
	DFT	0.5	0.826	0.1414	0.7520	17.655	91.413	49175
	DFT	0.0	0.740	0.0000	0.0000	22.111	0.0000	99379
Periodic	RHF	1.0	1.503	0.2524	1.1324	6.9749	17.439	1766.8
	RHF	0.5	1.232	0.1366	0.6484	9.9562	26.466	6400.0
	RHF	0.0	1.128	0.0000	0.0000	11.566	0.0010	12038
	DFT	1.0	1.090	0.2383	1.2619	10.814	44.656	8862.8
	DFT	0.5	0.840	0.1290	0.7521	17.649	90.240	45676
	DFT	0.0	0.744	0.0000	0.0000	22.076	0.0497	92234

Table 4.2: Results obtained for both systems and both methods varying the on-site-energy differences, $\Delta s = s_2 - s_1$. $|q_0|$ is the charge of the atoms in the central unit in absence of field.

4.4.3 The Responses per Unit and the Unit Contributions

In table 4.2 we list the calculated responses per unit for both the periodic and the finite systems. For the latter we used the procedure explained above, thereby the values of the table are the converged values of the figure 4.3, whereas for the periodic system, the dipole moment per unit is obtained through the equation (4.75) for different field strengths and subsequently fitted to a polynomial in the field strength (equation 2.12) similarly as we did for the finite system. In all cases we checked that, for the longest chains, the response properties obtained using a 3^{rd} order polynomial fit of μ in the field strength were close to those obtained by a 5^{th} order polynomial. For reliable values of the response properties, we found it was important to consider field strengths that were chosen so that the changes in the dipole moment per unit were neither too small nor too large as discussed earlier. In general, this meant that larger field strengths were employed for the RHF calculations because the RHF values, in general, were smaller than the corresponding DFT results. Since the RHF bandgaps are larger as well, it is possible to do so without having electrons tunnel from one end of the chain to the other.

In the table, we observe very good agreement (for the most part) between the DFT property values for the finite and the periodic system, whereas the agreement is not as good for RHF especially for the higher order response properties. The difference between the finite chain and infinite chain values for the gap, particularly for $\Delta s = 1$,

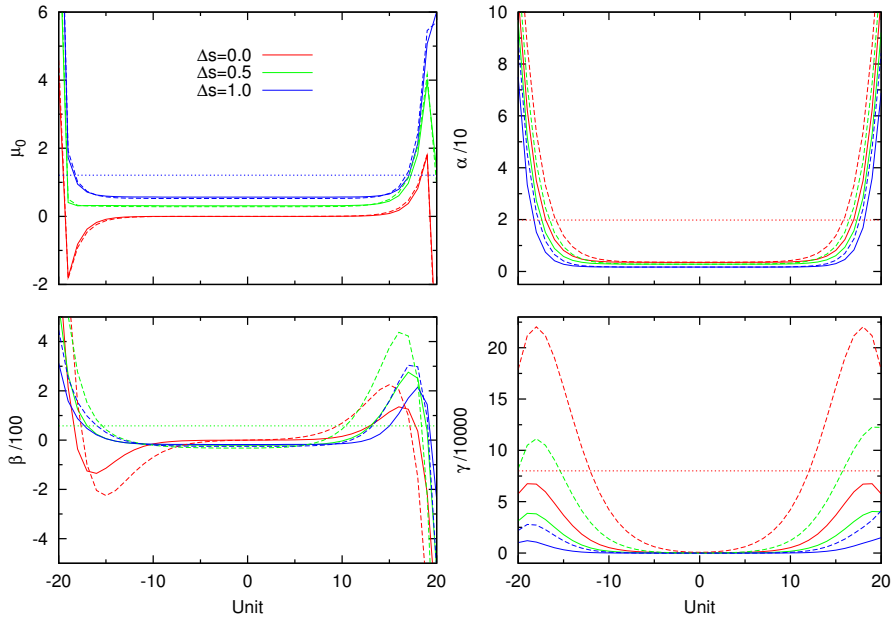

Figure 4.4: Unit contribution to the responses along the a finite chain of 41 units. The results for different on-site energies are plotted in different colors, RHF with solid line and DFT with dashed line. The horizontal dotted line is the total respose per unit (or the averange of the unit contribution), for the corresponding DFT calculation.

occurs because the energetically lowest unoccupied orbital is localized at the ends of the finite chain and accordingly has no analogue in the infinite periodic system. This leads to a reduction in the gap for both RHF and DFT, with the former being more strongly affected. As an example for the behavior of the response properties we may consider the γ values. In that case, within RHF the finite-system results are about twice those obtained for the periodic-system, whereas the DFT calculations show a much smaller effect. Since the two methods differ only in the treatment of exchange interactions, the latter must be responsible for the difference. In the RHF treatment, there are long-range exchange contributions that depend upon whether periodic boundary conditions are applied or not. On the other hand, in DFT the exchange contributions are purely local.

The expression (4.38) allows us to calculate the contribution from every atom of the finite chain to each response, but that leads to a zig-zagging line along the chain. Instead, we found the unit contribution more descriptive, which is just the sum of the two atomic contribution in each unit, $\vartheta_n = \sum_p \vartheta_{pn}$. This is what we see in figure 4.4 for the longest chain (41 units) considered in the previuos subsection. In red are the

System	Method	Δs	q_{intra}	μ_{0C}	α_C	β_C	γ_C
Finite	RHF	1.0	3.761	0.56596	1.6994	-17.745	-85.061
	RHF	0.5	6.252	0.31112	2.8034	-20.893	-19.253
	RHF	0.0	8.007	0.00000	3.5217	0.0000	324.25
	DFT	1.0	3.725	0.52411	1.7028	-25.271	-187.22
	DFT	0.5	6.251	0.28375	2.8320	-32.382	-94.329
	DFT	0.0	8.132	0.00000	3.5754	0.0000	682.81
		Δs	q_{intra}	$\bar{\mu}_{0Q}$	$\bar{\alpha}_Q$	$\bar{\beta}_Q$	$\bar{\gamma}_Q$
Periodic	RHF	1.0	3.748	0.55380	1.6798	-12.301	-34.313
	RHF	0.5	5.687	0.30059	2.5325	-12.293	57.112
	RHF	0.0	6.860	0.00000	3.0163	0.0000	1004.2
	DFT	1.0	3.424	0.52418	1.7027	-25.420	-196.88
	DFT	0.5	6.256	0.28383	2.8322	-31.970	151.45
	DFT	0.0	8.140	0.00000	3.5776	0.0264	2455.7

Table 4.3: For the finite system, the values correspond to the central unit contribution of a chain with 41 units, whereas for the periodic system correspond to the charge term contribution ($\bar{\mu}_Q$). The q_{intra} is the intramolecular charge transfer (multiplied by 10^3) in the central unit induced by a field strength of 0.005 a.u.

results for the centrosymmetric chain, which generates the highest values for α and γ, but vanish for μ_0 and β due to its symmetry, as we confirm with their unit components throughout the chain. There is a considerable contribution from the chain ends, but they cancel each other, while the effect of the asymmetry of the chain with $\Delta s = 0.5$ and $\Delta s = 1.0$ is clearly depicted in the left panels. In this regard, we observe that a central region, where the responses have almost a constant value, can also be identified. The extension of this central region is smaller for higher order responses and particularly with $\Delta s = 0$. In order to illustrate the contribution of the terminations versus the central region to the total DFT response, we plot with a dotted horizontal line the average value for the DFT calculation. This shows that the major contribution to the response values comes from the terminations. Additionally, for all field induced responses, and for all s, the DFT terminal values exceed the RHF ones.

On the other hand, in the expression (4.75) for the periodic chain we defined the charge ($\bar{\mu}_Q$) and the current ($\bar{\mu}_I$) contribution to the dipole moment. In an analogous way, we can calculate their contributions to each response. It has been proved [19] that the charge term corresponds to the contribution from the central part of the long finite chain. Therefore, in table 4.3 we compare the central values of the finite system with the charge term of the periodic system. Again, there is very good agreement between the finite and periodic calculations for the DFT treatment (except for γ, as discussed

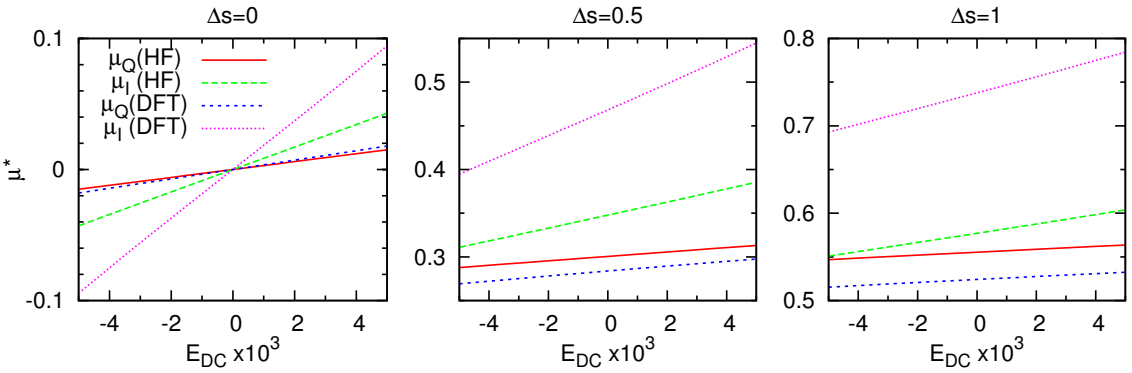

Figure 4.5: $\bar{\mu}_Q$ and $\bar{\mu}_I$ as functions of E_{DC} for infinite periodic chains calculated with different values of Δs using both RHF and DFT methods.

in the previous paragraphs), but larger differences are obtained for RHF. The fact that β from the charge term in the periodic LDA calculations is not zero for $s = 0$ can be ascribed to inaccuracies in fitting the responses with a third or fifth order power series. Hence, these values can be used as estimates of the accuracy in the fitting. Alternatively, we can use the differences between the results from the 3rd and the 5th order fit as estimates of the inaccuracies. Those differences were found to be below 5% (except for the vanishing μ_0 and β of the centrosymmetric chain).

It is interesting to analyze $\bar{\mu}_Q$ and $\bar{\mu}_I$ for the periodic chains as functions of the applied field. Their behavior is shown in figure 4.5 for both the RHF and the DFT calculations (notice that in these curves, the field strengths are so small that the non-linear responses can hardly be identified). $\bar{\mu}_I$ is the quantity that depends upon the phases of the single-particle orbitals. Since it determines the effects due to the terminations of a large finite system, $\bar{\mu}_I$ is an optimal quantity for analyzing long-range interactions. For DFT, the dependence of this quantity on the applied field is much stronger than that of $\bar{\mu}_Q$, which demonstrates that the overshoot arises primarily because the approximate DFT functional does not describe the long-range (exchange) interactions properly.

Comparing the tables 4.2 and 4.3 for the periodic system and using equation (2.27), we can analyze the relative contributions of the charge and the current terms for different response properties and different values of s. Independent of the value of s, both RHF and DFT predict that the current term is much larger than the charge term for all responses. (Only for μ_0 are they of similar magnitude.) For α the current contribution is roughly an order of magnitude larger. β is a special case because the charge and current contributions have opposite sign, but the latter clearly predominates. Finally,

we observe that γ is determined almost entirely by the current term both for DFT and for RHF in agreement with the greater weight of the terminal contributions in the finite system.

4.4.4 Charge Transfer

Now, we consider the induced intermolecular and intramolecular charge transfer[33] due to the presence of the external field, defined by

$$\begin{aligned} q_n^{\text{inter}} &= \Delta q_{1n} + \Delta q_{2n} \\ q_n^{\text{intra}} &= \frac{\Delta q_{1n} - \Delta q_{2n}}{2}, \end{aligned} \tag{4.85}$$

where $\Delta q_{pn} = q_{pn}(E_{DC}) - q_{pn}(0) = -\Delta N_{pn}$. Their values along a chain of 41 units are plotted in figure 4.6. We observe that the charge is transferred from one end of the chain to the other, and also that there is a central region of about 20 units with little charge transfer between them. We add that, per definition, units in the central region have to be neutral. In all instances the DFT calculations lead to a larger intercellular charge transfer than RHF. As opposed to the intercellular charge transfer, the charge transfer within the unit is largest, and almost constant, for the central region. Values calculated for the central unit of the finite chain are shown in Table 4.3. The largest such charge transfer occurs for the centrosymmetric case and decreases as Δs increases. For the intracellular charge transfer, the differences between RHF and DFT are negligible.

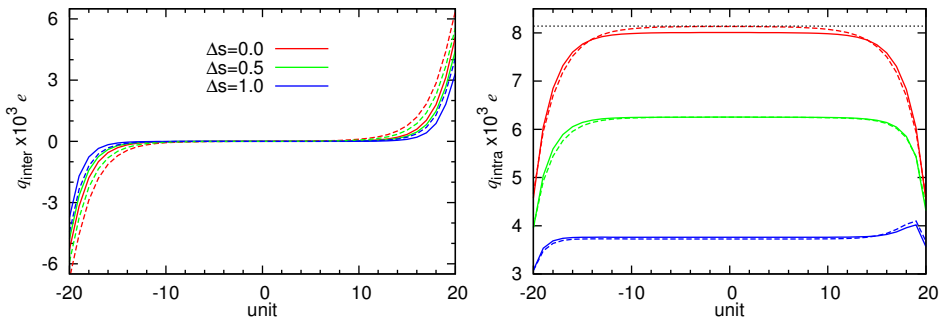

Figure 4.6: RHF (solid line) and DFT (dashed line) field-induced intermolecular and intramolecular charge transfer (multiplied by 10^3) for the chain of 41 units, obtained with a field strength of $E_{DC} = 0.005$ a.u. The dotted line corresponds to the calculated charge transfer in the unit cell of the periodic chain for $\Delta s = 0$ with the DFT method.

As in the case of the response properties, for the charge transfer within the central

unit there is very good agreement between the finite and infinite periodic chain DFT results (see Table 4.3). However, there are some differences for the RHF calculations, in particular for small values of Δs, which lead to large electron delocalization, whereby long-range effects become more important. Thus, this suggests that for exactly this property our system size has not reached the thermodynamic limit.

4.4.5 The System of Parallel Chains

We also studied arrays of 2, 3, and 4 parallel finite chains. The atoms of different chains were placed in perfect alignment so that they have the same z coordinate and the nearest neighbor interchain distance is 7 length units. Different realtive arrangements were tried as well but only small variations were found for any given number of parallel chains. Therefore, we discuss here only one set of results for each system size. For smaller values of the interchain distance, the band gap between occupied and unoccupied orbitals became so small that it was not possible to apply sufficiently strong fields for extracting numerical stable values for the responses and simultaneously to avoid an end-to-end charge transfer.

In Fig. 4.7 we show typical results for the responses per AB unit obtained for parallel chains. In the three-chains case ($M = 3$), they are arranged in a equilateral triangle with side $l = 7$ length units, whereas for $M = 4$, the tranversal section is a square with the same side length. These results show an essentially negligible dependence on the number of chains, with the one exception being β, in which case the magnitude increases modestly with the number of chains. Although the band gap is strongly affected by the number of chains (the systems ultimately become metallic for a sufficiently large number), the responses are hardly affected within our model.

The above result is in agreement with the results of Kirtman et al. [33] who also found that the DFT overestimate does not change substantially with dimensionality.

4.4.6 The Bond Length Alternation

Finally, we analyze the effect of varying the bond length alternation (BLA) on the responses. In all calculations whose results were reported so far, the BLA was fixed at $\Delta d = 0.6$, implying alternating bond lengths of $d_1 = 2.2$ and $d_2 = 2.8$ (the BLA is defined as $\Delta d = d_2 - d_1$). In this subsection Δd will be varied while keeping the lattice constant fixed at $a = 5$. We shall take d_1 as the length of the intra-unit-cell bond, whereas d_2 describes the bond length between atoms of neighboring unit cells.

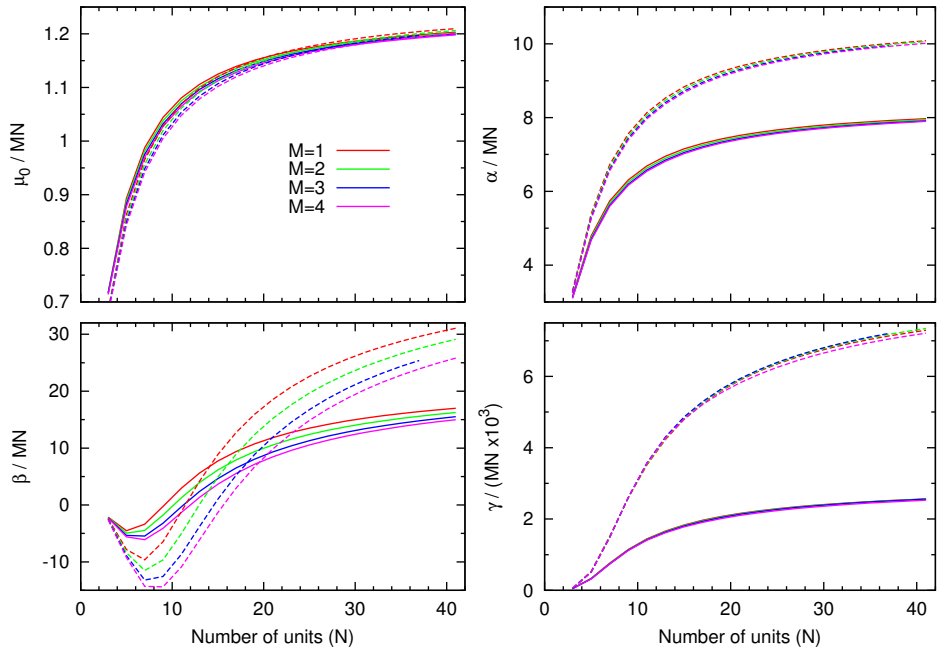

Figure 4.7: RHF (solid lines) and DFT (dashed lines) responses of arrays consisting of $M = 1 - 4$ parallel finite chains. The lattice constant is $a = 5$ and the interchain distance is $l = 7$. The on-site-energy difference between the A and B atoms is $\Delta s = 1.0$.

For $d_1 > 2.5$, the inter-unit-cell bond is shorter than the intra-unit-cell bond. For the infinite periodic chain, this is equivalent to switching the atoms in each unit (AB BA) and reorienting the chain in the opposite direction (due to the different on- site energies), which is equivalent to applying an electric field with opposite sign. As a result β will change sign, but α and γ will be left unchanged. The situation for μ_0 is slightly more complicated as will now be discussed. For the finite chain, the switch of atoms in each unit will create a non-bonded atom at each end giving rise to a diradical chain with dangling bonds. This will lead to an overall charge transfer from one end of the chain to the other (see further below) and an increase in the responses (because the electrons are more loosely bound for the diradical system). However, the effect is localized so that, for long chains, α and γ will tend to have very similar values for $d_1 = 2.5 + u$ and $d_1 = 2.5 - u$ as can be seen in figure 4.7, where the finite-chain results are obtained in the infinite-chain limit by the procedure explained in subsection 4.4.2.

As discussed above, upon changing $d_1 \to 5 - d_1$, β should change sign, while α and γ should remain unchanged. These predictions are satisfied in most of the cases.

with the RHF calculations for the periodic system being the only exception. The

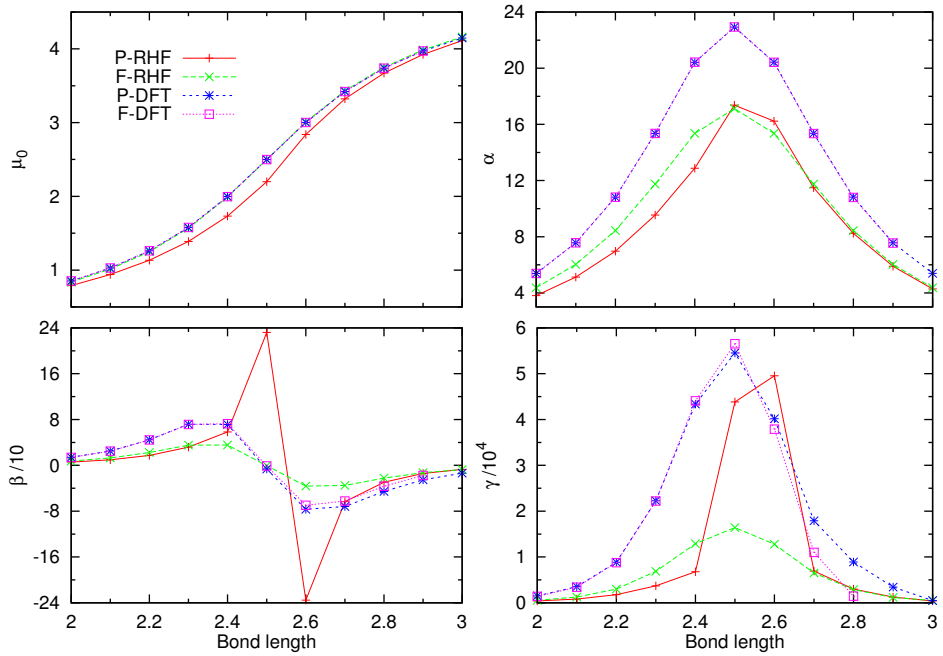

Figure 4.8: Infinite periodic (P-RHF, P-DFT) and inifite limit finite chain (F-RHF, F-DFT) responses per unit as function of d_1 for a chain with lattice constant $a = 5$ and on-site energy difference $\Delta s = 1.0$.

reason for the latter discrepancy is to be found in the previously mentioned problem with the convergence of the exchange summations. For μ_0 the situation is slightly different. Besides the change in sign, there is a charge transfer from one terminal region to the other that leads to an additional contribution of an integer times the lattice constant as we explained in the previous chapter. This prediction is satisfied as well with, again, the RHF calculations for the periodic system being the only exception.

There are two instances where the periodic RHF calculations do not satisfy this rule ($d_1 = 2.5$ and $d_1 = 2.6$), in particular for β and γ. These exceptions belong precisely to cases where the electrons are most delocalized and, therefore, more sensitive to the external field. The deviations seen for the finite DFT calculations of γ when $d_1 > 2.5$ are due to the dangling bonds on the first and last atom of the chain as can be seen by decomposing the response into atomic contributions (not shown). For μ_0 the situation is slightly different. Besides the change in sign, there is a charge transfer from one terminal region to the other that leads to an additional contribution of an integer (=1) times the lattice constant. This prediction is satisfied as well although, again, the RHF results for the periodic chain are slightly shifted.

4.5 Correcting the DFT Approach

Several suggestions have been proposed to reduce the DFT overshoot on the responses of large systems to electrostatic fields. One possibility, is to include the self-interaction correction proposed, e.g., by Pemmaraju et al. [36] and by Körzdörfer et al. [29]. Although these authors showed that it would improve the DFT results for the larger, finite systems, these corrections vanish for the periodic system when the electrons are occupying delocalized Bloch waves, as is the case here. Thus, this approach is not able to remove the DFT overestimates in all cases.

Alternatively, it has been suggested to include exact-exchange in the calculations. For instance, Mori-Sanchez et al. [37] and Champagne et al. [31] found significantly improved results for the polarizability of some smaller, finite chains. By including an exact description of exchange interactions, these are treated in an ultra-non-local way, in marked contrast to the treatment within a (semi-)local approximation within DFT. In agreement with earlier studies (see, e.g., [38]) our present results indicate that the DFT failures are related to long-range, non-local effects, in particular for the higher-order responses, the field-induced charge-density changes in the terminations are overestimated, leading to overestimates of the bulk responses. The results of Mori-Sanchez et al. [37] indicate also that the potential felt by the electrons contains an efficient screening of the external, electrostatic field. Unfortunately, however, the sizes of the systems in the referred studies [31, 37] are not sufficiently large to allow the identification of the thermodynamic limit or, equivalently, of a central region. Thus, it remains an open question whether such approaches will also be useful for infinite, periodic systems.

Instead, long-range corrected (LRC) density functionals have also been suggested as an useful approach for improving the DFT results for large, finite systems [39]. These functionals separate the exchange interactions into a short- and a long-range part, where the former is described by a DFT functional and the latter by an exact-exchange approach [40]. By analysing those approaches we can, accordingly, get information on the relative importance of an exact description of long- and short-ranged exchange interactions.

Within those approaches, the operator that describes the electron-electron interactions is rewritten, for the exchange terms, as

$$\frac{1}{r_{12}} = \frac{1-\mathrm{erf}(\nu r_{12})}{r_{12}} + \frac{\mathrm{erf}(\nu r_{12})}{r_{12}}, \tag{4.86}$$

where ν is a pre-chosen, positive parameter that determines the ratio of the partition and erf is the standard error function. The first term gives rise to the short-range exchange interactions. Many different formulations have been proposed, but here we shall use the simple one of Hirao and coworkers [41, 42], i.e.,

$$E_{\mathrm{x}}^{\mathrm{sr}} = G \int f[\rho(\vec{r})]\mathrm{d}\vec{r}, \tag{4.87}$$

with

$$f[\rho(\vec{r})] = \rho^{4/3} \left\{ 1 - \frac{4}{3} a \left[\sqrt{\pi}\, \mathrm{erf}\left(\frac{1}{a}\right) + ab - \frac{a + a^3 b}{2} \right] \right\}. \tag{4.88}$$

Here, a and b are functions of ρ,

$$\begin{aligned} a &= \frac{\nu\sqrt{G}}{3\sqrt{\pi}\rho^{1/3}} \\ b &= \exp\left(-\frac{1}{a^2}\right) - 1, \end{aligned} \tag{4.89}$$

whereas G is the constant we used in expression (4.36),

$$G = \frac{3}{4}\left(\frac{3}{\pi}\right)^{1/3}. \tag{4.90}$$

Then, we can calculate the short-range exchange potential as

$$V_{\mathrm{x}}^{\mathrm{sr}}[\rho] = \frac{\delta E_{\mathrm{x}}^{\mathrm{sr}}}{\delta\rho} = G f'(\rho). \tag{4.91}$$

Considering the expressions (4.88) and (4.89), the derivative is

$$f'[\rho] = \frac{4}{3}\rho^{1/3} \left\{ 1 - a \left[\sqrt{\pi}\, \mathrm{erf}\left(\frac{1}{a}\right) + ab \right] \right\}. \tag{4.92}$$

In our calculations we use the LCAO expansion of equation (4.7). Thus, due to the characteristics of the basis functions that we use, the DFT exchange potential is described by the diagonal matrix of the equation (4.22). Therefore, the short-range contribution will only determine the diagonal elements,

$$\langle \chi_{pn} | V_{\mathrm{x}}^{\mathrm{sr}} | \chi_{qm} \rangle = \delta_{pn}^{qm} V_{\mathrm{x}}^{\mathrm{sr}}[\rho_{pn}], \tag{4.93}$$

where, substituting equations (4.90) and (4.92) in equation (4.91), we have

$$V_{\mathrm{x}}^{\mathrm{sr}}[\rho_{pn}] = \left(\frac{3}{\pi}\right)^{1/3} \rho^{1/3} \left\{1 - a\left[\sqrt{\pi}\,\mathrm{erf}\left(\frac{1}{a}\right) + ab\right]\right\}. \tag{4.94}$$

The term in curly brackets in equation (4.94) (as well that of equation (4.88)) is a factor between 0 and 1 which takes into account the fact that part of the exchange interactions is not described within the local density approximation.

On the other hand, the long-range contribution is given by,

$$E_{\mathrm{x}}^{\mathrm{lr}} = \sum_{i,j} \left\langle \psi_j\psi_i \left| \frac{\mathrm{erf}(\nu r_{12})}{r_{12}} \right| \psi_i\psi_j \right\rangle. \tag{4.95}$$

Thus, using the LCAO expansion of equation (4.7), the matrix elements defined in equation (4.13) have to be recalculated,

$$\begin{aligned} W_{pn}^{qm} &= \delta_{pn}^{q'm'}\delta_{p'n'}^{qm}\langle\chi_{pn}\chi_{p'n'}|\hat{h}_2'|\chi_{q'm'}\chi_{qm}\rangle \\ &= \iint \frac{\mathrm{erf}(\nu|\vec{r}-\vec{r}\,'|)}{|\vec{r}-\vec{r}\,'|}|\chi_{pn}(\vec{r})|^2|\chi_{qm}(\vec{r}\,')|^2 d\vec{r}d\vec{r}\,'. \end{aligned} \tag{4.96}$$

This is done in Appendix C following the same idea as in section 4.1. Using the dimensionless parameter $v = \nu R_p$, the result is

$$\begin{aligned} W_{pn}^{pn} = \frac{1}{\sqrt{\pi}v^5R_p}&\left[\left(\frac{3v^4}{5} - \frac{9v^2}{20}\right)e^{-4v^2} + \frac{3v^2}{4} + \frac{3}{40}\left(e^{-4v^2} - 1\right)\right] \\ &+ \left(\frac{6}{5R_p} - \frac{3}{4vR_p}\right)\mathrm{erf}(2v), \end{aligned} \tag{4.97}$$

for the diagonal terms, whereas for the off-diagonal terms we considered the approximation

$$W_{pn}^{qm} \approx \frac{\mathrm{erf}(\nu R_{pn}^{qm})}{R_{pn}^{qm}}, \tag{4.98}$$

which is properly justified in Appendix C. Then, according to equation (4.24), the matrix elements of long-range exchange are

$$\langle\chi_{pn}|V_{\mathrm{x}}^{\mathrm{lr}}|\chi_{qm}\rangle = \tilde{c}_{pn}^{qm}\, W_{pn}^{qm}. \tag{4.99}$$

The sum of the matrices (4.93) and (4.99) forms the range-corrected exchange matrix. The normal DFT expressions are recovered for $\nu \to 0$, whereas the pure HF

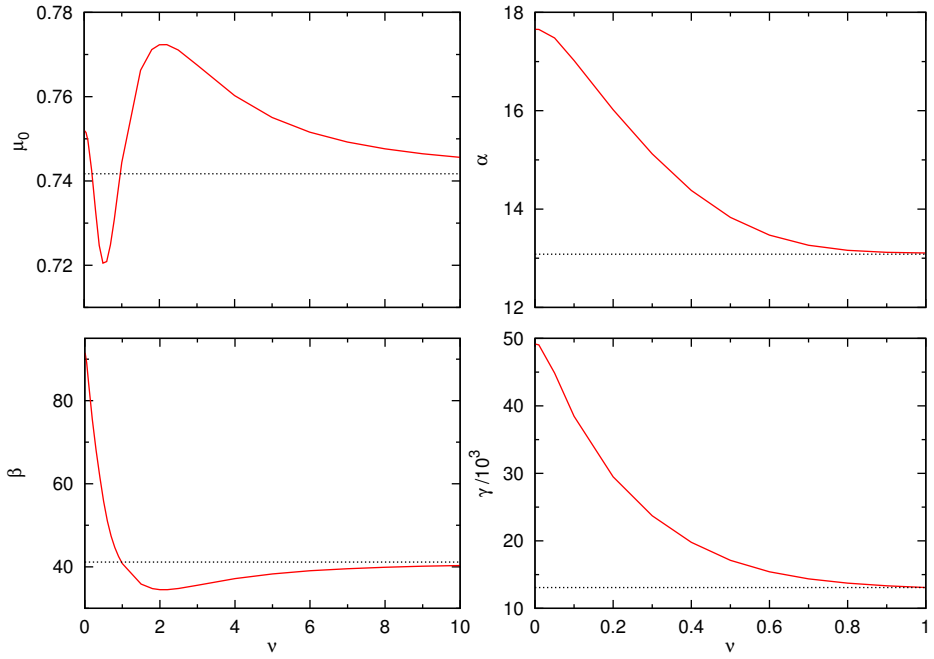

Figure 4.9: Responses per unit calculated with the long-range correction scheme as function of ν. The dashed line marks the HF value, whereas the DFT value is that obtained for $\nu = 0$.

exchange is obtained for $\nu \to \infty$ (see Appendix C for more details). The program code for the finite system was modified to implement this correction obtaining the following results.

Kamiya et al. [42] used the above LRC approach for some π-conjugated molecules of various lengths and found a significantly improved description of the polarizability and first hyperpolarizability. For computational reasons, however, this and others studies[39, 43–45] consider systems that might be too small to provide estimates for the performance in the thermodynamic limit, but using our simplified model it is possible to do so.

For the case $\Delta s = 0.5$, we varied the partition parameter ν and calculated the infinite chain limit using the approach described in section 4.4.2. The results are shown in figure 4.9. In the limit $\nu \to \infty$ all the responses converge towards the HF values, but α and γ do so rapidly, whereas μ_0 and β converge more slowly (they are plotted in a different range of ν). The permanent dipole moment even shows an oscillatory behavior. In fact, only α is strictly a monotonically decreasing function of ν, whereas β and γ have minima around $\nu = 2$ (not shown in the panel for γ).

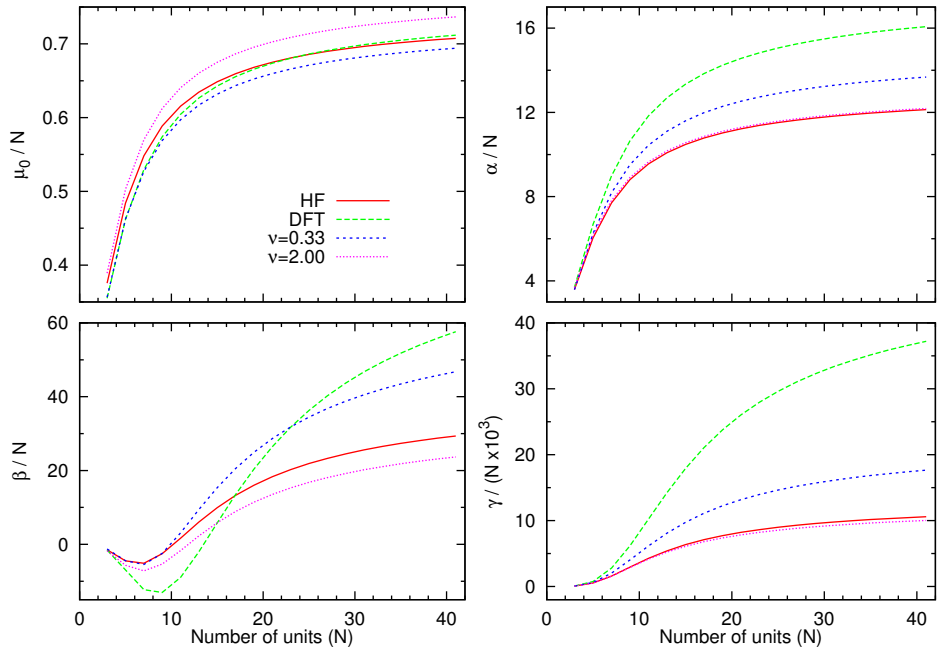

Figure 4.10: Responses divided by the number of units as functions of the chain size for $\Delta s = 0.5$ and $\nu = 1$.

The behavior of the extrapolated values for the response properties shown in figure 4.9 was confirmed by plotting the responses per unit as a function of chain length in comparison with RHF and DFT in figure 4.10. Clearly, the long-range corrected method significantly reduces the DFT overshoot, although the value used by Kamiya et al. [42] ($\nu = 0.33$) seems to be too small to provide accurate results, at least for the present study. A special case is $\nu = 1$ or, more properly, $\nu = 1/R_p$. This means making the partition parameter the inverse of the radius of the sphere where the basis functions are defined (equation 4.8). In that case all the responses calculated by the LRC method coincide with those obtained with the HF method, as it can be seen in figure 4.9 for $\nu = 1$, and this remains true varying the length of the chain giving results that if we plot them in figure 4.10 we get a line that mask the HF line. This result can be used in determining the appropiate ν for other system and basis set.

4.6 Conclusions

The use of a simple model had several advantages. At first, it allowed to treat large, finite systems without serious computational problems. Second, the model was so

designed that the electron density becomes piecewise constant, whereby gradient corrections within density-functional theory could be ignored. Third, the model allowed for separating the (linear and non-linear) responses to an electrostatic field into those of the individual atoms. And, finally, we could use our recently developed approach for treating infinite and periodic systems exposed to electrostatic fields for studying these systems, too.

Of course, a model may also suffer from limitations that occasionally can make it useless. Therefore, it was important to demonstrate first, that it does lead to a large overestimate of in particular the non-linear responses when using a density-functional approach. Subsequently, we could demonstrate the existence of a central region for systems of sufficiently large size. Inside the central region, the responses are independent of which unit cell is being analyzed. We found that the critical size above which the central region could be identified depends both on the order of the response that has been considered and on the computational approach. Thus, the DFT calculations tended to lead to larger critical sizes than the HF calculations. The above-mentioned DFT overestimates could thereby be related to electrons being more delocalized within that method leading to both larger responses in the terminations and in the central region. In particular the concept of intra- and intermolecular charge transfer were useful to identify this effect.

When comparing the results for the large, finite systems with those for the infinite, periodic systems, we found a good agreement in almost all cases when using the DFT method. In particular, we could clearly see how the central-unit contributions to the dipole moment per unit of the finite system corresponds to the so-called charge term for the periodic system and, equivalently, the contribution from the terminations of the finite system becomes the current contribution of the infinite system. For the RHF calculations, we found some deviations between the results for the infinite and for the finite chains which are related to the long range nature of the exchange interactions.

In some further calculations we found that the responses were only marginally affected by the presence of parallel neighboring chains. Finally we also studied the effects of changing the chemical composition (i.e., the differences in the on-site energies) or the structure of our chains. Thereby, we found that the largest differences between the RHF and the DFT values were found for systems with maximally delocalized electrons, i.e., systems of essentially identical atoms and with a small or vanishing bond-length alternation.

By comparing our results with other proposals to improve the performance of DFT

calculations we found that range-separated functionals could provide an useful approach for obtaining a more accurate description of the responses of large systems to electric fields. However, care should be taken in devising functionals that are computationally convenient and accurate for general application.

Appendix A

Steepest Descent Method

The crutial step of the smoothing procedure explained in 2.3.3 involves a minimization of the quantity defined in equation (2.53),

$$\begin{aligned} Q &= \sum_k \sum_p |C_p(k+\Delta k)e^{i\phi(k+\Delta k)} - C_p(k)e^{i\phi(k)}|^2 \\ &\quad +\lambda \sum_k \sum_p |C_p(k+2\Delta k)e^{i\phi(k+2\Delta k)} - C_p(k)e^{i\phi(k)}|^2, \end{aligned} \tag{A.1}$$

(suppresing the band index j) under the constraint,

$$\phi\left(-\frac{\pi}{a}\right) = \phi\left(\frac{\pi}{a}\right). \tag{A.2}$$

Here, we shall use the steepest descent method to carry out the minimization. In our case, we consider Q as a function of $\Phi = (\phi(k_{-N}), \phi(k_{-N+1}), \ldots, \phi(k_N))$, so Q descreases fastest when we go from an initial point Φ_0 in the direccion of the negative gradient of Q at Φ_0. It follows that, if

$$\Phi_1 = \Phi_0 - \tau \nabla Q(\Phi_0), \tag{A.3}$$

with τ being a small enough number, then $Q(\Phi_0) \geq Q(\Phi_1)$. And repeating the procedure m times with,

$$\Phi_m = \Phi_{m-1} - \tau \nabla Q(\Phi_{m-1}), \tag{A.4}$$

we may obtain, $Q(\Phi_0) \geq Q(\Phi_1) \geq \cdots \geq Q(\Phi_m)$, until $\Delta Q_m = Q(\Phi_{m-1}) - Q(\Phi_m)$

becomes below a convergence threshold. For this aim we need to calculate the gradient,

$$\nabla Q(\Phi) = \left(\frac{\partial Q}{\partial \phi_{-N}}, \frac{\partial Q}{\partial \phi_{-N+1}}, \ldots, \frac{\partial Q}{\partial \phi_N} \right), \tag{A.5}$$

where we have simplified,

$$\phi(k) = \phi(i\Delta k) = \phi(k_i) = \phi_i \qquad \text{with} \quad \Delta k = \frac{2\pi}{(2N+1)a}. \tag{A.6}$$

Then, the partial derivative respect to ϕ_i is

$$\begin{aligned} \frac{\partial Q}{\partial \phi_i} &= \frac{\partial}{\partial \phi_i} \left\{ \sum_p \left[C_p(k_i) e^{i\phi_i} - C_p(k_{i-1}) e^{i\phi_{i-1}} \right]^2 + \sum_p \left[C_p(k_{i+1}) e^{i\phi_{i+1}} - C_p(k_i) e^{i\phi_i} \right]^2 \right. \\ &\left. + \lambda \sum_p \left[C_p(k_i) e^{i\phi_i} - C_p(k_{i-2}) e^{i\phi_{i-2}} \right]^2 + \lambda \sum_p \left[C_p(k_{i+2}) e^{i\phi_{i+2}} - C_p(k_i) e^{i\phi_i} \right]^2 \right\} \end{aligned}$$

Every term in square braquets in this equation is the norm of a complex number. It can be proved (done below) that if $C_p(k_i) = C'_p(k_i) + iC''_p(k_i)$, with $C'_p(k_i)$ and $C''_p(k_i)$ real numbers, the above derivative is

$$\frac{\partial}{\partial \phi_i} \sum_p \left[C_p(k_i) e^{i\phi_i} - C_p(k_{i-1}) e^{i\phi_{i-1}} \right]^2 = a_{i-1} \sin(\phi_i - \phi_{i-1}) - b_{i-1} \cos(\phi_i - \phi_{i-1}), \tag{A.7}$$

defining

$$\begin{aligned} a_{i-1} &= 2 \sum_p \left[C'_p(k_i) C'_p(k_{i-1}) + C''_p(k_i) C''_p(k_{i-1}) \right] \\ b_{i-1} &= 2 \sum_p \left[C'_p(k_i) C''_p(k_{i-1}) - C''_p(k_i) C'_p(k_{i-1}) \right]. \end{aligned}$$

Therefore, using the same notation,

$$\begin{aligned} \frac{\partial Q}{\partial \phi_i} &= a_{i-1} \sin(\phi_i - \phi_{i-1}) - b_{i-1} \cos(\phi_i - \phi_{i-1}) \\ &+ a_{i+1} \sin(\phi_i - \phi_{i+1}) - b_{i+1} \cos(\phi_i - \phi_{i+1}) \\ &+ \lambda \big[a_{i-2} \sin(\phi_i - \phi_{i-2}) - b_{i-2} \cos(\phi_i - \phi_{i-2}) \\ &+ a_{i+2} \sin(\phi_i - \phi_{i+2}) - b_{i+2} \cos(\phi_i - \phi_{i+2}) \big], \end{aligned} \tag{A.8}$$

for $i = -N, -N+1, \ldots, N$. And this is iteratively subtituted in equation (A.4) keeping

the constraint (A.2) in order to obtain the final phases Φ_m and with them we calculate the smooth coefficients of the field-free case,

$$\tilde{C}^0_{pj}(k) = C_{pj}(k)e^{i\phi_m(k)}, \tag{A.9}$$

for every j band.

A.1 A Complex Derivative

Let z_1 and z_2 be complex numbers decomposed as

$$\begin{aligned} z_1 &= x_1 + iy_1 \\ z_2 &= x_2 + iy_2. \end{aligned} \tag{A.10}$$

If we multiply each number by a different phase factor, we would have

$$\begin{aligned} z_1 e^{i\phi_1} &= x_1\cos\phi_1 - y_1\sin\phi_1 + i(x_1\sin\phi_1 + y_1\cos\phi_1) \\ z_2 e^{i\phi_2} &= x_2\cos\phi_2 - y_2\sin\phi_2 + i(x_2\sin\phi_2 + y_2\cos\phi_2). \end{aligned} \tag{A.11}$$

Then, we can write,

$$z_1 e^{i\phi_1} - z_2 e^{i\phi_2} = Z = X + iY, \tag{A.12}$$

with

$$\begin{aligned} X &= x_1\cos\phi_1 - y_1\sin\phi_1 - x_2\cos\phi_2 + y_2\sin\phi_2 \\ Y &= x_1\sin\phi_1 + y_1\cos\phi_1 - x_2\sin\phi_2 - y_2\cos\phi_2 \end{aligned} \tag{A.13}$$

Now, calculating the partial derivative

$$\frac{\partial}{\partial\phi_1}|z_1 e^{i\phi_1} - z_2 e^{i\phi_2}|^2 = \frac{\partial}{\partial\phi_1}Z^*Z = 2\left[X\frac{\partial X}{\partial\phi_1} + Y\frac{\partial Y}{\partial\phi_1}\right], \tag{A.14}$$

where

$$\begin{aligned} \frac{\partial X}{\partial\phi_1} &= -x_1\sin\phi_1 - y_1\cos\phi_1 \\ \frac{\partial Y}{\partial\phi_1} &= x_1\cos\phi_1 - y_1\sin\phi_1. \end{aligned} \tag{A.15}$$

Substituting in (A.14), we have

$$\begin{aligned}\frac{1}{2}\frac{\partial}{\partial\phi_1}|Z|^2 &= x_1x_2\sin\phi_1\cos\phi_2 - x_1y_2\sin\phi_1\sin\phi_2 + y_1x_2\cos\phi_1\cos\phi_2 \\ &\quad - y_1y_2\cos\phi_1\sin\phi_2 - x_1x_2\cos\phi_1\sin\phi_2 - x_1y_2\cos\phi_1\cos\phi_2 \\ &\quad + y_1x_2\sin\phi_1\sin\phi_2 + y_1y_2\sin\phi_1\cos\phi_2 \\ &= (x_1x_2 + y_1y_2)(\sin\phi_1\cos\phi_2 - \cos\phi_1\sin\phi_2) \\ &\quad - (x_1y_2 - x_2y_1)(\cos\phi_1\cos\phi_2 + \sin\phi_1\sin\phi_2) \\ &= (x_1x_2 + y_1y_2)\sin(\phi_1 - \phi_2) - (x_1y_2 - y_1x_2)\cos(\phi_1 - \phi_2). \qquad \text{(A.16)}\end{aligned}$$

Similarly,

$$\frac{1}{2}\frac{\partial}{\partial\phi_2}|Z|^2 = (x_1x_2 + y_1y_2)\sin(\phi_2 - \phi_1) - (y_1x_2 - x_1y_2)\cos(\phi_2 - \phi_1). \qquad \text{(A.17)}$$

Appendix B

Some Analytic Formulae

Because of the simplicity of our linear system, it is possible to deduce analitycal formulae for some terms of equation (4.57) and (4.58). The position of the atoms are described by equation (4.1) being a the lattice constant. Then, considering just 2 atoms per unit separate each other a distance d, the distances between the pth atom of the central unit and the qth atom of the nth unit are

$$|\vec{R}_{p0}^{qn}| = |\vec{R}_{qn} - \vec{R}_{p0}| = \begin{cases} |na| & p = q \\ |na + d| & p \neq q \end{cases} \tag{B.1}$$

B.1 Regarding the Coulomb Interaction

Considering the electron-electron and electron-nucleus interactions within our model appears the quantity $U_s(p, q)$, defined in equations (4.17) and (4.59). Here, we can easily calculate it and find the limit when $N_s \to \infty$,

$$U_s(1,1) = U_s(2,2) = \frac{3}{5R_p} + 2\sum_{n=1}^{N_s} \frac{1}{na} \xrightarrow{N_s \to \infty} \frac{3}{5R_p} + \frac{2}{a}[\ln(N_s) + \gamma], \tag{B.2}$$

where γ is the *Gauss-Mascheroni* constant $\gamma \approx 0.577216$. Similarly,

$$\begin{aligned} U_s(1,2) = U_s(2,1) \quad &= \quad \frac{1}{d} + \frac{1}{a}\sum_{n=1}^{N_s} \frac{1}{n + \frac{d}{a}} + \frac{1}{a}\sum_{n=1}^{N_s} \frac{1}{n - \frac{d}{a}} \\ &\xrightarrow{N_s \to \infty} \quad \frac{1}{d} + \frac{1}{a}[\ln(N_s) + \alpha] + \frac{1}{a}[\ln(N_s) + \beta] \\ &\xrightarrow{N_s \to \infty} \quad \frac{1}{d} + \frac{2}{a}[\ln(N_s) + \gamma'], \end{aligned} \tag{B.3}$$

where α and β have similar definitions as γ but depend on d/a. Here, for $d/a = 0.44$, we have redefined $\gamma' = (\alpha + \beta)/2 \approx 0.857861$. The summation over n is exactly the summation of equations (4.47), (4.49) and (4.50), which should run from $-N$ to N, but with $N_s > N$ we try to obtain the infinite limit. We observe that these summations are no converging and have to be truncated after N_s terms. However, considering together the electron-electron and the electron-nucleus Coulomb interactions, the contribution to the hamiltonian will depend only on the difference ΔU_s, as we see in equations (4.79), and this converges for $N_s \to \infty$,

$$\Delta U_s = U_s(1,1) - U_s(1,2) \xrightarrow{N_s\to\infty} \frac{3}{5R_p} - \frac{1}{d} - \frac{2}{a}(\gamma' - \gamma). \tag{B.4}$$

B.2 Regarding the Kinetic-Energy Operator

The matrix associated with the operator $\hat{h}_1(k)$ can also be calcualted analytically from the definitions (4.12) and (4.46),

$$h_{1pp}(k) = s_p - t\sum_{n\neq 0} e^{ikan} e^{-b|\vec{R}^{pn}_{p0}|}, \tag{B.5}$$

where the summation can be written as,

$$\begin{aligned}
\sum_{n=1}^{N_s} e^{ikan}e^{-ban} + \sum_{n=1}^{N_s} e^{-ikan}e^{-ban} &= \sum_{n=1}^{N_s}\left[e^{-a(b-ika)}\right]^n + \sum_{n=1}^{N_s}\left[e^{-a(b+ika)}\right]^n \\
\xrightarrow{N_s\to\infty}\ \frac{1}{1-e^{-a(b-ik)}} + \frac{1}{1-e^{-a(b+ik)}} - 2 &= \frac{2 - e^{-ba}(e^{ikan}+e^{-ikan})}{1 - e^{-ba}(e^{ikan}+e^{-ikan}) + e^{-2ba}} - 2 \\
= 2\left(\frac{1-e^{-ba}\cos(ka)}{1-2e^{-ba}\cos(ka)+e^{-2ba}} - 1\right) &= 2e^{-ba}\left(\frac{\cos(ka) - e^{-ba}}{1-2e^{-ba}\cos(ka)+e^{-2ba}}\right).
\end{aligned}$$

Then, defining,

$$\zeta(k) = \frac{2e^{-ba}}{1 - 2e^{-ba}\cos(ka) + e^{-2ba}}, \tag{B.6}$$

the diagonal elements become

$$h_{1pp}(k) \xrightarrow{N_s\to\infty} s_p - t\zeta(k)\left[\cos(ka) - e^{-ba}\right], \tag{B.7}$$

i.e., real numbers. Similarly, for the non-diagonal terms we have,

$$h_{1pq}(k) = -t \sum_{n=-N_s}^{N_s} e^{ikan} e^{-b|\vec{R}^{qn}_{p0}|}, \tag{B.8}$$

in this case, with $p \neq q$, the summation is

$$\begin{aligned}
\sum_{n=-N_s}^{N_s} e^{ikan} e^{-b|\vec{R}^{qn}_{p0}|} &= e^{-bd} + \sum_{n=1}^{N_s} e^{ikan} e^{-b(na+d)} + \sum_{n=1}^{N_s} e^{-ikan} e^{-b(na-d)} \\
&= e^{-bd} + e^{-bd} \sum_{n=1}^{N_s} \left[e^{-a(b-ik)}\right]^n + e^{bd} \sum_{n=1}^{N_s} \left[e^{-a(b+ik)}\right]^n \qquad \text{(B.9)} \\
&\xrightarrow{N_s\to\infty} e^{-bd} + e^{-bd}\left(\frac{1}{1-e^{-a(b-ik)}} - 1\right) + e^{bd}\left(\frac{1}{1-e^{-a(b+ik)}} - 1\right),
\end{aligned}$$

the terms in parenthesis are

$$\begin{aligned}
\frac{1}{1-e^{-a(b-ik)}} - 1 &= \left(\frac{e^{-a(b-ik)}}{1-e^{-a(b-ik)}}\right)\left(\frac{1-e^{-a(b+ik)}}{1-e^{-a(b+ik)}}\right) \\
&= \frac{e^{-a(b-ik)} - e^{-2ba}}{1 - 2e^{-ba}\cos(ka) + e^{-2ba}} \\
&= \frac{\zeta(k)}{2}\left[e^{ika} - e^{-ba}\right] \\
&= \frac{\zeta(k)}{2}\big[\cos(ka) - e^{-ba} + i\sin(ka)\big], \\
\frac{1}{1-e^{-a(b+ik)}} - 1 &= \frac{\zeta(k)}{2}\big[\cos(ka) - e^{-ba} - i\sin(ka)\big].
\end{aligned}$$

Substituting in equations (B.9) and (B.8), we can separate the real and the imaginary parts as,

$$\begin{aligned}
\mathrm{Re}[h_{112}(k)] &\xrightarrow{N_s\to\infty} -te^{-bd} - t\cosh(bd)\zeta(k)\left[\cos(ka) - e^{-ba}\right] \\
\mathrm{Im}[h_{112}(k)] &\xrightarrow{N_s\to\infty} t\sinh(bd)\zeta(k)\sin(ka).
\end{aligned} \tag{B.10}$$

It can also be proved that $h_1(k)$ is an hermitian matrix, so that $h_{112}(k) = h^*_{121}(k)$.

In all the deductions we have used the geometric series formula,

$$\lim_{N\to\infty} \sum_{n=0}^{N} z^n = \lim_{N\to\infty} \frac{1-z^{N+1}}{1-z} = \frac{1}{1-z}. \tag{B.11}$$

In our case $|z| = |e^{-a(b\pm ik)}| < 1$, and $z^{N_s+1} \ll 1$ even for a not so large N_s. Therefore, the $h_1(k)$-matrix elements, calculated through equations (B.7) and (B.10) are the infinite limit values.

Appendix C

The Integration of the LRC Exchange

In the long-range correction (LRC) scheme described in section 4.5 the long-range contribution for the exchange interaction is calculated by equation (4.95),

$$E_{\mathrm{x}}^{\mathrm{lr}} = \sum_{i,j}^{N_O} \left\langle \psi_j \psi_i \left| \frac{\mathrm{erf}(\nu r_{12})}{r_{12}} \right| \psi_i \psi_j \right\rangle . \tag{C.1}$$

In our model, we use the LCAO expansion of equation (4.7),

$$\psi_j(\vec{r}) = \sum_{p,n} c_{pnj} \chi_{pn}(\vec{r}), \tag{C.2}$$

where χ_{pn} is the pth basis function of the nth unit. Additionally, the basis functions are given by equation (4.8),

$$\chi_{pn}(\vec{r}) = \begin{cases} \left(\frac{4\pi}{3} R_p^3\right)^{-1/2} & |\vec{r} - \vec{R}_{pn}| < R_p \\ 0 & |\vec{r} - \vec{R}_{pn}| \geq R_p, \end{cases} \tag{C.3}$$

That means that the electrons form an uniform sphere of charge with radius R_p around the p^{th} atom.

Now, to calculate the elements of the exchange matrix we used the expression (4.24),

$$\langle \chi_{pn} | \hat{V}_{\mathrm{x}}^{\mathrm{lr}} | \chi_{qm} \rangle = \sum_{j=1}^{N_O} \sum_{p',n'} \sum_{q',m'} c_{p'n'j}^* c_{q'm'j} \left[\langle \chi_{pn} \chi_{p'n'} | \hat{h}_2' | \chi_{q'm'} \chi_{qm} \rangle \right]. \tag{C.4}$$

But here the two-electron operator is

$$\hat{h}_2' = \frac{\mathrm{erf}(\nu|\vec{r}-\vec{r}'|)}{|\vec{r}-\vec{r}'|}. \tag{C.5}$$

Moreover, we keep only the elements with $(p,n) = (q',m')$ and $(p',n') = (q,m)$,

$$\begin{aligned} W_{pn}^{qm} &= \delta_{pn}^{q'm'}\delta_{p'n'}^{qm}\langle\chi_{pn}\chi_{p'n'}|\hat{h}_2'|\chi_{q'm'}\chi_{qm}\rangle \\ &= \iint \frac{\mathrm{erf}(\nu|\vec{r}-\vec{r}'|)}{|\vec{r}-\vec{r}'|}|\chi_{pn}(\vec{r})|^2|\chi_{qm}(\vec{r}')|^2 d\vec{r}d\vec{r}'. \end{aligned} \tag{C.6}$$

This is a double volume integral or a sextuple integral and the presence of the error function makes it non-straightforward to calculate. The error function is already defined as an integral,

$$\mathrm{erf}(x) = \frac{2}{\sqrt{\pi}}\int_0^x e^{-t^2}dt, \tag{C.7}$$

so that, its derivative is

$$\frac{d}{dx}\mathrm{erf}(u) = \frac{2}{\sqrt{\pi}}e^{-u^2}\frac{du}{dx}. \tag{C.8}$$

It is clear that the error function is odd and $\mathrm{erf}(0) = 0$. Additionally, in the derivation below the following formulae are very useful:

$$\begin{aligned} \int e^{-c^2x^2}dx &= \frac{\sqrt{\pi}}{2c}\mathrm{erf}(cx) \\ \int xe^{-c^2x^2}dx &= -\frac{1}{2c^2}e^{-c^2x^2} \\ \int x^2e^{-c^2x^2}dx &= -\frac{x}{2c^2}e^{-c^2x^2} + \frac{\sqrt{\pi}}{4c^3}\mathrm{erf}(cx) \\ \int x^3e^{-c^2x^2}dx &= -\frac{x^2}{2c^2}e^{-c^2x^2} - \frac{1}{2c^4}e^{-c^2x^2} \\ \int x^4e^{-c^2x^2}dx &= -\frac{x^3}{2c^2}e^{-c^2x^2} - \frac{3x}{4c^4}e^{-c^2x^2} + \frac{3\sqrt{\pi}}{8c^5}\mathrm{erf}(cx) \\ \int x^5e^{-c^2x^2}dx &= -\frac{x^4}{2c^2}e^{-c^2x^2} - \frac{x^2}{c^4}e^{-c^2x^2} - \frac{1}{c^6}e^{-c^2x^2}, \end{aligned}$$

as well as,

$$\int \mathrm{erf}(u)f'(x)dx = f(x)\mathrm{erf}(u) - \frac{2}{\sqrt{\pi}}\int \frac{du}{dx}f(x)e^{-u^2}dx.$$

To calculate the integral of equation (C.6) we use the same strategy as in section 4.1. We calculate the screened Coulomb potential generated by the $(q,m)^{th}$ occupied

orbital at the position $\vec{r}$,

$$V_{qm}(\vec{r}) = \int \frac{\mathrm{erf}(\nu|\vec{r}-\vec{r}\,'|)}{|\vec{r}-\vec{r}\,'|}|\chi_{qm}(\vec{r}\,')|^2 d\vec{r}\,'. \tag{C.9}$$

To simplify the notation, first we consider that the $(q,m)^{th}$ occupied orbital is a unifrom sphere of charge $(Q=1)$ with radius R centered at the origin and we calculate the potential at the position $\vec{r}=(0,0,z)$ so that the distances,

$$|\vec{r}-\vec{R}_{qm}| = z \tag{C.10}$$

and

$$|\vec{r}-\vec{r}\,'| = \sqrt{z^2+r'^2-2zr'\cos\phi} = u(r',\phi) = \begin{cases} |z-r'| & \text{for} \quad \phi=0 \\ |z+r'| & \text{for} \quad \phi=\pi. \end{cases} \tag{C.11}$$

Subsecuently,

$$\begin{aligned} V(z) &= \frac{3}{4\pi R^3}\int_0^{2\pi}\int_0^{\pi}\int_0^{R}\frac{\mathrm{erf}(\nu u)r'^2\sin\phi}{u}dr'd\phi d\theta \\ &= \frac{3}{2R^3}\int_0^{\pi}\int_0^{R}\frac{\mathrm{erf}(\nu u)r'^2\sin\phi}{u}dr'd\phi \\ &= \frac{3}{2R^3}\int_0^{R}\left[\frac{r'u}{z}\mathrm{erf}(\nu u)+\frac{r'}{\sqrt{\pi}\nu z}e^{-\nu^2u^2}\right]_{\phi=0}^{\phi=\pi}dr' \\ &= \frac{3}{2zR^3}\int_0^{R}\Big\{r'(r'+z)\mathrm{erf}[\nu(r'+z)]-r'(r'-z)\mathrm{erf}[\nu(r'-z)] \\ &\qquad +\frac{r'}{\sqrt{\pi}\nu}\left[e^{-\nu^2(r+z)^2}-e^{-\nu^2(r-z)^2}\right]\Big\}dr'. \end{aligned} \tag{C.12}$$

And after many further steps we get,

$$\begin{aligned} V(z)\,R^3 &= \left(\frac{3R^2}{4}-\frac{z^2}{4}-\frac{3}{8\nu^2}\right)\Big\{\mathrm{erf}[\nu(R+z)]+\mathrm{erf}[\nu(R-z)]\Big\} \\ &\quad +\frac{R^3}{2z}\Big\{\mathrm{erf}[\nu(R+z)]-\mathrm{erf}[\nu(R-z)]\Big\} \\ &\quad +\frac{1}{\nu\sqrt{\pi}}\left\{\frac{R}{4}\left[e^{-\nu^2(R+z)^2}+e^{-\nu^2(R-z)^2}\right]\right. \\ &\quad \left.+\left(\frac{R^2}{2z}-\frac{z}{4}-\frac{1}{4\nu^2z}\right)\left[e^{-\nu^2(R+z)^2}-e^{-\nu^2(R-z)^2}\right]\right\} \\ &= T_1+T_2+T_3+T_4. \end{aligned} \tag{C.13}$$

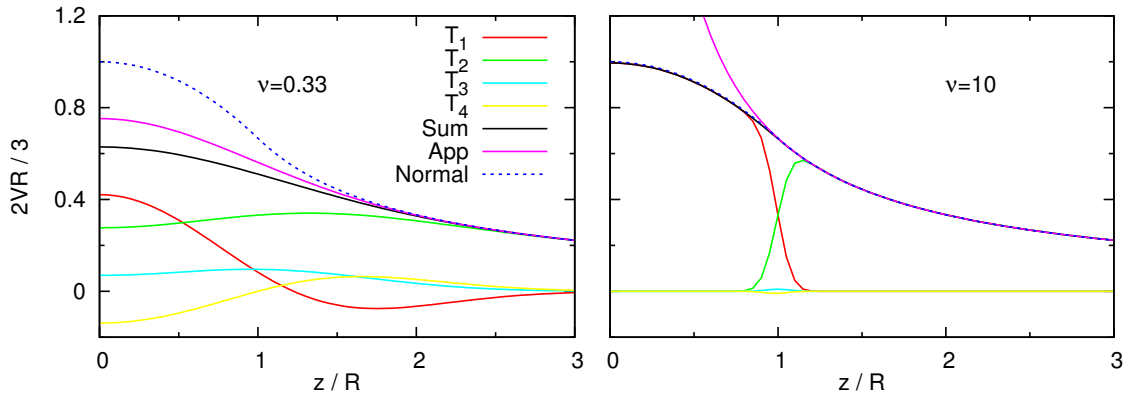

Figure C.1: The four terms and the their sum of the exact Coulomb attenuated potential of a uniform sphere of charge, equation (C.13). The approximation (App) of equation (C.15) and the normal Coulomb potential, equation (C.14), are also shown for two values of the partition parameter, $\nu = 0.33$ (left) and $\nu = 10$ (right).

This expression is valid both inside ($z < R$) and outside ($z > R$) the sphere. In figure C.1, every single term and the total sum are plotted as functions of z for two values of the partition parameter ν. The first two terms, T_1 and T_2, are the most important. In fact, for $\nu = 10$ (right panel) it is clearly seen that T_1 describes the potential inside, while T_2 do it outside the sphere. The reason is that inside, $\mathrm{erf}[\nu(R \pm z)]$ is always positive, but outside it changes its sign. Thus, we confirm that,

$$\lim_{\nu\to\infty} V(z) = \begin{cases} \frac{3}{2R} - \frac{z^2}{2} & \text{for} \quad z < R \\ \frac{1}{z} & \text{for} \quad z \geq R, \end{cases} \tag{C.14}$$

i.e., we recover the expression for the normal Coulomb potential of equation (4.14). This is plotted in figure C.1 with the blue dashed line.

The other limit can also be confirmed, $\lim_{\nu\to 0} V(z) = 0$. Additionally, we plot the function $\mathrm{erf}(\nu z)/z$ in figure C.1 with a magenta line. One can observe that this function fits very well with the exact potential very near outside the sphere. Therefore, we can approximate the potential,

$$V(z) \approx \frac{\mathrm{erf}(\nu z)}{z} \quad \text{for} \quad z > R. \tag{C.15}$$

Even inside, the difference between these functions is not so big whenever ν remains small. Moreover, $\mathrm{erf}(\nu r)/r$ was our starting point of the integral in equation (C.9).

The next step is to calculate the matrix elements W_{pn}^{qm} of equation (C.6) by inte-

grating the obtained potential,

$$W_{pn}^{qm} = \int V_{qm}(\vec{r})|\chi_{pn}(\vec{r})|^2 d\vec{r}. \tag{C.16}$$

For $(p,n) = (q,m)$, the integral with respect to $\vec{r}$ is over the same sphere of radius R_p, so we can calculate the interaction with a spherical shell of radius z and thickness dz. In that case, the charge of the shell would be $4\pi\rho z^2 dz = 3z^2 dz/R_p^3$. Thus,

$$W_{pn}^{pn} = \frac{3}{R_p^3}\int_0^{R_p} z^2 V(z) dz. \tag{C.17}$$

Substituting $V(z)$ from equation (C.13) and using the dimensionless quantity $v = \nu R_p$, we finally obtain

$$\begin{aligned} W_{pn}^{pn} = \frac{1}{\sqrt{\pi} v^5 R_p}\left[\left(\frac{3v^4}{5} - \frac{9v^2}{20}\right)e^{-4v^2} + \frac{3v^2}{4} + \frac{3}{40}\left(e^{-4v^2} - 1\right)\right] \\ + \left(\frac{6}{5R_p} - \frac{3}{4vR_p}\right)\mathrm{erf}(2v). \end{aligned} \tag{C.18}$$

Similarly as the expression for the potential, W_{pn}^{pn} tends to the value obtained with the normal Coulomb potential in equation (4.17),

$$\lim_{\nu\to\infty} W_{pn}^{pn} = \frac{6}{5R_p}, \tag{C.19}$$

and it tends to zero for $\nu \to 0$.

As we have mentioned, our basis functions do not overlap, therefore for the off-diagonal terms, $(p,n) \neq (q,m)$, we use twice the approximation of expression (C.15),

$$\begin{aligned} W_{pn}^{qm} &\approx \int \frac{\mathrm{erf}\left(\nu|\vec{r} - \vec{R}_{qm}|\right)}{|\vec{r} - \vec{R}_{qm}|}|\chi_{pn}(\vec{r})|^2 d\vec{r} \\ &\approx \frac{\mathrm{erf}\left(\nu|\vec{R}_{pn} - \vec{R}_{qm}|\right)}{|\vec{R}_{pn} - \vec{R}_{qm}|}. \end{aligned} \tag{C.20}$$

Finally, to check the limiting behavior of expressions (C.13) and (C.18) when $\nu \to 0$, it is useful to take the series expansion of the error function,

$$\mathrm{erf}(x) = \frac{2}{\sqrt{\pi}}\left(x - \frac{x^3}{3} + \frac{x^5}{10} - \frac{x^7}{42} + \dots\right). \tag{C.21}$$

Bibliography

[1] B. Kirtman, F. L. Gu, and D. M. Bishop, The Journal of Chemical Physics **113**, 1294 (2000).

[2] M. Springborg and B. Kirtman, The Journal of Chemical Physics **126**, 104107 (2007).

[3] M. Springborg and B. Kirtman, Phys. Rev. B **77**, 045102 (2008).

[4] R. D. King-Smith and D. Vanderbilt, Phys. Rev. B **47**, 1651 (1993).

[5] R. Resta, Rev. Mod. Phys. **66**, 899 (1994).

[6] I. Souza, J. Íñiguez, and D. Vanderbilt, Phys. Rev. Lett. **89**, 117602 (2002).

[7] P. Umari and A. Pasquarello, Phys. Rev. Lett. **89**, 157602 (2002).

[8] D. M. Bishop, F. L. Gu, and B. Kirtman, The Journal of Chemical Physics **114**, 7633 (2001).

[9] M. Springborg, *Methods of Electronic-Structure Calculations*, Wiley series in Theoretical Chemistry (John Wiley & Sons, Ltd., 2000).

[10] J. C. Slater, Phys. Rev. **81**, 385 (1951).

[11] M. Springborg and B. Kirtman, Chem. Phys. Lett. **454**, 105 (2008).

[12] D. Vanderbilt and R. D. King-Smith, Phys. Rev. B **48**, 4442 (1993).

[13] M. Springborg and B. Kirtman, Canadian Journal of Chemistry **87**, 984 (2009).

[14] K. N. Kudin, R. Car, and R. Resta, The Journal of Chemical Physics **127**, 194902 (2007).

[15] G. Ortiz and R. M. Martin, Phys. Rev. B **49**, 14202 (1994).

[16] M. Stengel and N. A. Spaldin, Phys. Rev. B **75**, 205121 (2007).

[17] E. Blount, in *Formalisms of Band Theory*, edited by F. Seitz and D. Turnbull (Academic Press, 1962), vol. 13 of *Solid State Physics*, pp. 305 – 373.

[18] M. Springborg, B. Kirtman, and Y. Dong, Chemical Physics Letters **396**, 404 (2004).

[19] M. Springborg and B. Kirtman, Theoretical Chemistry Accounts **130**, 687 (2011).

[20] M. Dvornikov, ArXiv Mathematics e-prints (2003), arXiv:math/0306092.

[21] M. Springborg, V. Tevekeliyska, and B. Kirtman, Phys. Rev. B **82**, 165442 (2010).

[22] J. Vargas and M. Springborg, The Journal of Chemical Physics **137**, 144108 (2012).

[23] A. Pomogaeva, M. Springborg, B. Kirtman, F. L. Gu, and Y. Aoki, The Journal of Chemical Physics **130**, 194106 (2009).

[24] B. Champagne, E. A. Perpète, S. J. A. van Gisbergen, E.-J. Baerends, J. G. Snijders, C. Soubra-Ghaoui, K. A. Robins, and B. Kirtman, The Journal of Chemical Physics **109**, 10489 (1998).

[25] S. J. A. van Gisbergen, P. R. T. Schipper, O. V. Gritsenko, E. J. Baerends, J. G. Snijders, B. Champagne, and B. Kirtman, Phys. Rev. Lett. **83**, 694 (1999).

[26] B. Champagne, E. A. Perpète, D. Jacquemin, S. J. A. van Gisbergen, E.-J. Baerends, C. Soubra-Ghaoui, K. A. Robins, and B. Kirtman, The Journal of Physical Chemistry A **104**, 4755 (2000).

[27] M. van Faassen, P. L. de Boeij, R. van Leeuwen, J. A. Berger, and J. G. Snijders, Phys. Rev. Lett. **88**, 186401 (2002).

[28] F. A. Bulat, A. Toro-Labbe, B. Champagne, B. Kirtman, and W. Yang, The Journal of Chemical Physics **123**, 014319 (2005).

[29] T. Körzdörfer, M. Mundt, and S. Kümmel, Phys. Rev. Lett. **100**, 133004 (2008).

[30] D. Jacquemin, J.-M. Andre, and E. A. Perpète, The Journal of Chemical Physics **121**, 4389 (2004).

[31] B. Champagne, F. A. Bulat, W. Yang, S. Bonness, and B. Kirtman, The Journal of Chemical Physics **125**, 194114 (2006).

[32] J. R. Hammond, N. Govind, K. Kowalski, J. Autschbach, and S. S. Xantheas, The Journal of Chemical Physics **131**, 214103 (2009).

[33] B. Kirtman, V. Lacivita, R. Dovesi, and H. Reis, The Journal of Chemical Physics **135**, 154101 (2011).

[34] B. Champagne, D. Jacquemin, F. L. Gu, Y. Aoki, B. Kirtman, and D. M. Bishop, Chemical Physics Letters **373**, 539 (2003).

[35] B. Champagne and E. A. Perpète, International Journal of Quantum Chemistry **75**, 441 (1999).

[36] C. D. Pemmaraju, S. Sanvito, and K. Burke, Phys. Rev. B **77**, 121204 (2008).

[37] P. Mori-Sanchez, Q. Wu, and W. Yang, The Journal of Chemical Physics **119**, 11001 (2003).

[38] N. T. Maitra and M. van Faassen, The Journal of Chemical Physics **126**, 191106 (2007).

[39] D. Jacquemin, E. A. Perpète, M. Medved', G. Scalmani, M. J. Frisch, R. Kobayashi, and C. Adamo, The Journal of Chemical Physics **126**, 191108 (2007).

[40] H. Iikura, T. Tsuneda, T. Yanai, and K. Hirao, The Journal of Chemical Physics **115**, 3540 (2001).

[41] Y. Tawada, T. Tsuneda, S. Yanagisawa, T. Yanai, and K. Hirao, The Journal of Chemical Physics **120**, 8425 (2004).

[42] M. Kamiya, H. Sekino, T. Tsuneda, and K. Hirao, The Journal of Chemical Physics **122**, 234111 (2005).

[43] P. A. Limacher, K. V. Mikkelsen, and H. P. Lüthi, The Journal of Chemical Physics **130**, 194114 (2009).

[44] M. Medved, imon Budzk, and T. Pluta, Chemical Physics Letters **515**, 78 (2011).

[45] A. J. Garza, G. E. Scuseria, S. B. Khan, and A. M. Asiri, Chemical Physics Letters **575**, 122 (2013), ISSN 0009-2614.

Index